

# **EXPERIMENTAL AND NUMERICAL INVESTIGATION OF RUBBER WHETHER STRIP EXTRUSION**

A Dissertation

by

Nayyef Ahmed Talib

Submitted to the

Graduate School of Sciences and Engineering

In Partial Fulfillment of the Requirements for

the Degree of

Doctor of Philosophy

in the

Department of Mechanical Engineering

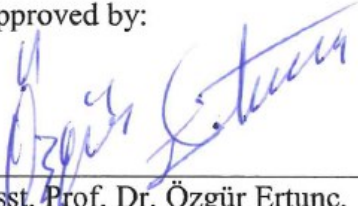
Özyeğin University

3 / January / 2019

Copyright © 2019 by Nayyef Ahmed Talib

# EXPERIMENTAL AND NUMERICAL INVESTIGATION OF RUBBER WHEATHER STRIP EXTRUSION

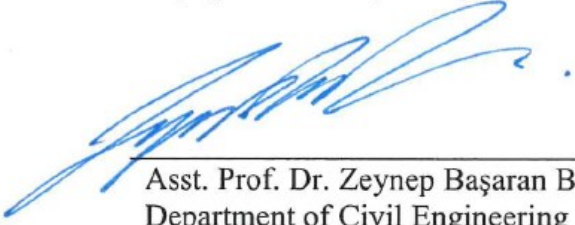
Approved by:



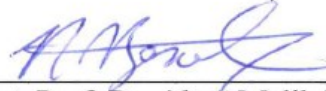
Asst. Prof. Dr. Özgür Ertunç,  
Department of Mechanical Engineering  
*Özyeğin University*



Professor. Dr. Kadir Kırkköprü,  
Department of Mechanical Engineering  
*Istanbul Technical University*



Asst. Prof. Dr. Zeynep Başaran Bundur,  
Department of Civil Engineering  
*Özyeğin University*



Asst. Prof. Dr. Altuğ Melik Başol,  
Department of Mechanical Engineering  
*Özyeğin University*



Assoc. Prof. Dr. Onuralp Uluer,  
Department of Manufacturing Engineering  
*Gazi University*

Date Approved: 3 /1/ 2019

*This dissertation is dedicated to the souls of*

*My mother and My father.*

*& My wife and my sons (Lana, Fatimah. Sajjad and Ahmed)*

*& My brothers and sisters*

## **ABSTRACT**

Extrusion is the main method used to produce rubber weather strips in automotive industries. The product quality is dependent on many factors, which include the design parameters of the die, the processing variables, and the rheological behaviour of the used material. On the other hand, the flow of the rubber compound is complex due to both the shear thinning behaviour and the high viscoelastic character of this material. Therefore, the inclusion of many factors, which have an influence on product quality during the extrusion process, cause the relationship between the die design and the flow field to be not-intuitive. The current conventional die design employs trial-error process during which the manufactured die is reworked in several trials to guarantee the required product quality. Therefore, converting the running-in experiment into a virtual one by adopting numerical modelling is a powerful method leading to a reduction in waste material and time. In addition, it can also be used for the in-depth analysis of the rheological material variables in combination with the die design parameters to evaluate their effect on product quality.

In extrusion process of high reactive material such as rubber, it is important to find less reactive conditions. This because of the time course of heating is very important factor in controlling the peroxide' degradation or scorching inside the die. Therefore, estimation of the residence time and temperature of the material for a specific die design play an important role for products quality control.

In the first part of the investigations, a special extrusion die instrumented with a special sensor was designed in an industrial scale size. Extrusion experiments were conducted in an extrusion line and flow rate, temperature and pressures were measured for

different extruder speeds. The rheological properties of the filled rubber compound were characterized using a capillary rheometer (Rosand) at different temperatures to evaluate the required material parameters for the numerical simulation. The curing characteristics were investigated using a rubber process analyser (RPA-2000) to construct a curing curve at different temperatures. A three-dimensional model was established for modelling the non-isothermal viscous flow of the ethylene propylene diene monomer (EPDM) rubber melts. A purely inelastic model was assumed through a power law model and a mixed finite element method to solve the complex flow in the extrusion die domain. The pressure-stabilized Petrov–Galerkin (PSPG) method and streamline upwind/Petrov–Galerkin numerical scheme were employed to solve the flow equations and increase numerical stability. The results confirmed that for the EPDM rubber compound, the screw speed exerted a remarkable effect on the temperature rise and pressure drop in the extrusion die. The impact of the viscous dissipation on the thermal behaviour and pressure drop prediction was also discussed. The obtained scorch time was compared with the estimated residence time in the flow domain to elucidate the influence of the extruder speed on the curing characteristic. The results suggested that there is neither premature vulcanisation nor the start of the scorching inside the flow domain within the studied extruder speed range. The velocity uniformity index and streamline were evaluated at the die exit and the entire flow domain, respectively. The analyses of the results obtained confirmed the ability of the proposed die design to produce a defect free product without the risk of the circulation or appearance of a large distortion. The validity of the model prediction was verified by the comparison between the simulation and the experimental results.

The second part of the investigations was devoted to studying the swelling phenomenon which occurred during the extrusion of the rubber. Extrudate swell is an important phenomenon occurring when high viscoelastic materials, such as rubber and rubber compounds, are extruded. In this work, the effects of the relaxation time and the relaxation mode on the swell predictions using a nonlinear differential viscoelastic model, that is, the Giesekus model, were studied systematically for the Styrene-Butadiene rubber (SBR) extrusion in the capillary die. The corresponding 3D, steady-state finite element simulation for the predictions of the swelling was presented and compared with the experimental data for the validation. The velocity distribution, pressure drop and circulation flow in the die were analysed and discussed through the simulation. The results of the swell prediction revealed that the three-relaxation mode of the Giesekus model with a wide range of relaxation time reproduced the experimental data. In addition, the number of relaxation mode and range of relaxation time had a remarkable effect on the circulation flow at the die corner and some effect on the other field variables.

After the validation of the proposed model, the same model was implemented on the capillary extrusion of the EPDM rubber, which is mainly used in the weather strip in automotive industries. The swelling of the EPDM rubber was compared with the swelling of the SBR. The results obtained showed that the swell ratio of the EPDM was less than the swell ratio of the SBR for all the studied parameters. This finding approved the ability of the invoke purely inelastic model in modelling this kind of material when a viscous effect is predominant. The influence of the die design parameter such as the die length and slippage at die wall on the swell was also discussed and analysed.

Finally, viscoelastic simulation based Giesekus viscoelastic model was applied for modelling of extrudate swelling in an industrial scale extrusion die. The predicted extrudate profile was compared with basic profile at die exit. The results obtained show very slight deviation in extrudate profile from basic geometry at die exit which validate the proposed die design to produce the precise extrudate dimension without necessary to make die correction. The three dimensional stress field at die exit were discussed and analysed to evaluate their effect on the evolution of some defects such as melt fracture or surface defects.

## ÖZETÇE

Ekstrüzyon, otomotiv endüstrisinde kauçuk sızdırmazlık profilleri üretmek için kullanılan ana yöntemdir. Ürün kalitesi, kalıbın ölçülerine, süreç değişkenlerini ve kullanılan malzemenin reolojik davranışını içeren birçok faktöre bağlıdır. Öte yandan, kauçuk bileşiminin akışı, hem bu malzemenin viskozitesinin kayma incelmeye, hem de yüksek viskoelastik karakteri birlikte sergilemesi nedeniyle karmaşıktır. Bu nedenle, ekstrüzyon işlemi sırasında ürün kalitesi üzerinde etkili olan birçok faktörün dahil edilmesi, kalıp tasarımı ile akış alanı arasındaki ilişkinin sezgisel olarak tahmin edilememesine yol açmaktadır. Mevcut konvansiyonel kalıp tasarımı bir deneme yanılma sürecinden oluşur. Kalıp, istenen ürün kalitesi sağlanana kadar deneme yanılmaya bağlı olarak yeniden işlenir. Bu nedenle, sayısal simülasyonlarla, denemeyi sanal bir hale dönüştürmek, atık malzeme ve zamanın azalmasına yol açan güçlü bir tasarım yöntemidir. Kalıp tasarımına ek olarak, simülasyonlar, reolojik parametrelerin ürün kalitesi üzerindeki etkilerini değerlendirmek için derinlemesine incelenebilir.

Kauçuk gibi yüksek reaktif malzemelerin, ekstrüzyon sürecinde daha az reaktif olacakları koşullarda bulunmaları önemlidir. Bu nedenle, malzemenin kalıp içinde kalma süresi, malzemenin viskoz ısınma ile ya da kalıptan akan ısıya maruz kalma süresini etkiler ve sonuç olarak peroksitin bozunması, polimerin bozunması veya jelleşmesi gibi fenomenler ortaya çıkabilir. Bu nedenle, sürecin termal kontrolü, ürün kalite kontrolünün anahtarıdır.

Araştırmanın ilk kısmında, endüstriyel ölçekte tasarlanmış özel bir test kalıbı, basınç ve sıcaklık sensörleri ile donatılarak ekstrüzyon deneyleri yapılmıştır. Ekstrüzyon deneyleri bir ekstrüzyon hattında, farklı ekstruder hızları için debi, sıcaklık ve basınç değişkenleri



ölçülerek yapılmıştır. Doldurulmuş kauçuk bileşiğinin reolojik özellikleri, sayısal simülasyon için gerekli malzeme parametrelerini elde etmek için farklı sıcaklıklarda bir kapiler reometre (Rosand) kullanılarak karakterize edilmiştir. Kauçuğun kurlenme özellikleri, farklı sıcaklıklarda sertleşme eğrilerinin, bir kauçuk işlem analiz cihazı (RPA-2000) kullanılarak tespit edilmiştir. Etilen propilen dien monomeri (EPDM) kauçuk eriyiklerinin izotermal olmayan viskoz akışının modellenmesi için üç boyutlu bir model oluşturulmuştur. Elastiklik içermeyen, Newtonian olmayan akışların viskozitesi güç yasası modeli (power law model) kullanılarak ekstrüzyon kalıbı içindeki akış karma sonlu elemanlar yöntemi ile çözülmüştür. Basınç-dengelenmiş Petrov-Galerkin (PSPG) ve akış çizgisi upwind/Petrov-Galerkin yöntemi akış denklemlerini dengeli bir şekilde çözmek için kullanıldı. Sonuçlar, EPDM kauçuk bileşiği için, ekstrüder hızının ekstrüzyon kalıbındaki sıcaklık artışı ve basınç düşüşü üzerinde kayda değer bir etki verdiğini doğrulamıştır. Viskoz enerji kayıplarının termal davranış ve basınç düşüşü tahmini üzerindeki etkisi de tartışılmıştır. Elde edilen kurlenme (ve sonrasındaki kavrulma) süresi, kauçuğun kalıp içinde tahmini kalma süresi ile kıyaslanarak nihai ürün üstüne etkisi incelenmiştir. Sonuçlar, çalışılan ekstrüder hız aralığında, erken vulkanizasyon ya da akış alanının içinde kavrulmanın olmadığını göstermiştir.. Hız dağılım endeksi ve akış çizgileri, sırasıyla kalıp çıkışında ve tüm akış alanında değerlendirildi. Elde edilen sonuçların analizi, önerilen kalıbın içinde, akış kopması, girdap oluşumu veya büyük bir distorsiyon olmadığını ve bu kalıbın hatasız bir ürün üretme kabiliyeti olduğunu doğrulamıştır. Simulasyonlarla yapılan tahmininin geçerliliği, deney sonuçları arasındaki karşılaştırma ile doğrulanmıştır.

Araştırmanın ikinci bölümü, kauçuğun ekstrüzyonu sırasında meydana gelen şişme olayını incelemeye ayrılmıştır. Ekstrüdat şişmesi, kauçuk ve kauçuk bileşikleri gibi yüksek viskoelastik malzemeler ekstrüde edildiğinde ortaya çıkan ürünün şeklini değiştiren önemli bir olgudur. Bu çalışmada, nonlinear diferansiyel viskoelastik model olan Giesekus modeli kullanılarak gevşeme zamanının ve gevşeme modunun şişme tahminleri üzerindeki etkileri kapiler kalıpta Stiren-Butadien kauçuk (SBR) ekstrüzyonu için sistematik olarak incelenmiştir. 3 boyutlu, kararlı akış, şişme simülasyonları sonlu elemanlar yöntemi ile yapılmış ve deneysel veriler ile doğrulanmıştır. Hız dağılımı, basınç düşüşü ve girdap oluşumu simülasyon sonuçlarının analizi ile tartışılmıştır. Şişme simülasyonlarının sonuçları, Giesekus modelinin geniş bir gevşeme aralığında kullanılan üç gevşeme moduyla deney verilerini yeniden üretebildiğini ortaya çıkarmıştır. Ayrıca, gevşeme modunun sayısının ve gevşeme süresinin, kalıp köşesindeki girdaplı akış üzerinde önemli bir etkisi ve diğer alan değişkenleri üzerinde de etkileri olduğunu ortaya koymuştur.

Önerilen fiziksel ve sayısal modelin doğrulunun ispat edilmesinden sonra, aynı model, otomotiv endüstrisinde sızdırmazlık profillerinde kullanılan EPDM kauçuğunun kapiler ekstrüzyonuna uygulanmıştır. EPDM kauçuğun şişmesi, SBR kauçuğunun şişmesi ile karşılaştırılmıştır.. Elde edilen sonuçlar, EPDM'nin şişme oranının, incelenen tüm parametreler için SBR kauçuğun şişme oranından daha az olduğunu göstermiştir. Bu bulgu, viskoz bir etki baskın olduğunda bu tür materyalin modellenmesinde elastik olmayan bir viskoz modelin kullanılabileceğini ortaya koymuştur. Kalıp uzunluğu ve kalıp duvarındaki kaymanın, ekstrüzyon ve ürün üzerine etkisi de simülasyonlar yardımı ile incelenmiştir.

Son olarak, endüstriyel ölçekte bir ekstrüzyon kalıbında ekstrüdat şişmesinin modellenmesinde viskoelastik simülasyon bazlı Giesekus viskoelastik modeli uygulanmıştır. Tahmini ekstrüdat profili, kalıp çıkışındaki temel profille karşılaştırıldığında, ekstrüdat profilinde çok hafif bir sapma gözlemlenmiş ve kalıbın istenilen profil için uygun olduğu tespit edilmiştir. Kalıp çıkışındaki üç boyutlu gerilme alanı incelenmiş ve eriyik kırılması ya da yüzey kusurları gibi bazı kusurların evrimi üzerindeki etkileri tartışılmıştır.

## ACKNOWLEDGMENTS

This thesis is the successful end of my long journey in obtaining my PhD degree in Mechanical Engineering. Fortunately, there are many people who made this work easier and support me to overcome all challenging.

Firstly, I would like to thank God Almighty for giving me the strength and determination to complete my Ph.D. thesis. Secondly, I am deeply indebted to my advisor, Assistant Professor Dr. Ozgur Ertunc whose constant help me to overcome all obstacle and his encouragement helped me in all phases of my research work. I have been found Dr. Ozgur Ertunc as the most admirable and respectful person. I owe him lots of gratitude for shown me the right way for doing research work and working hard until get the fruitful results. I would like to thank my thesis committee members Dr. Ilknur Erucar, Dr. Zeynep Basaran and Dr. Altug Melik Basol for their suggestions and guidance during monitoring my progress in research work as well as for taking effort in reading and provide me with valuable support. I am really glad that I have come to know him in my life. I would like to thank the external thesis defence members Professor Dr. Kadir Kırkköprü from Istanbul Technical University and Assoc.Prof. Dr. Onuralp Uluer from Gazi University for taking effort to come to my thesis defence and accept to be members in my thesis defence committee. I would also like to express my sincere appreciation for the standard profile company team especially Tarik Turkistanli Extrusion Simulation Team Leader, Dr. Ali Erkin Kutlu and Dr. Müfit Çağlayan Group research and development (R&D) Director, Erdem Aydın Rubber Process Development Team Leader, Isa Çolakoğlu, Emre Ayrıl, Arif Çavuş, Aydın Suler and all

other members who give me a wonderful support to complete my experimental work in standard profile company.

Special thanks go to Dr. Mustafa Pınar Mengüç the head of department for his furtherly support and assistance to all Iraqi students. Sincere appreciation also goes to Dr. Altug Melik Başol who has made a valuable support during my work on high performance computer (HPC) of Özyegin university. I would also like to express my sincere appreciation to Assoc.Prof. Dr. Ahmet Zafer Şenalp from Gebze Teknik University for his responsive and warm-hearted help, during additional course study in Gebze Teknik University, and provides me with valuable course of Finite Element analysis which has a big contribution to this project. I wish to acknowledge University of Diyala for its financial support for this study. Without this funding this work will not possible. Additionally, I am thankful to all my friends especially Dr. Thamer Khalif Salem and all other support which help me survive through many hard time and made this journey a memorable experience.

I would like to express my deepest gratitude to professor Dilhan M. Kalyon Director of Highly Filled Materials Institute / Stevens Institute of Technology and professor P. M. Coelho for them big support during this work. Also, my great gratitude to professor H. Winter, Dr. Sarath chandran, Dr. Johan T. Padding, for him great support during this study.

Finally, I highly appreciate my beloved family, specially my wife who dedicated their lives to support me during all year of study and deeply thank to all my sons Lana, Fatima, Sajjad and finally my lovely and part of my heart the smallest son Ahmed. Also, my gratitude to all my brothers and sisters for them encouragement and support during this study.

## TABLE OF CONTENTS

ABSTRACT .....	iv
ÖZETÇE .....	viii
ACKNOWLEDGMENTS.....	xii
TABLE OF CONTENTS.....	xiv
LIST OF TABLES .....	xviii
LIST OF FIGURES.....	xix
NOMENCLATURE.....	xxv
CHAPTER I .....	1
1 INTRODUCTION .....	1
<b>1.1 Background</b> .....	<b>1</b>
<b>1.2 Modelling polymer flow</b> .....	<b>4</b>
1.2.1 Characterization of material parameters .....	4
1.2.2 Numerical methods .....	8
1.2.3 Extrusion swelling.....	10
1.2.4 Die design.....	13
1.2.5 Non-isothermal modelling.....	14
<b>1.3 Novelty aspect</b> .....	<b>19</b>
<b>1.4 Objective</b> .....	<b>23</b>
<b>1.5 Methodology</b> .....	<b>26</b>
<b>1.6 Thesis organization</b> .....	<b>30</b>
CHAPTER II.....	34
2 THEORETICAL MODEL.....	34
<b>2.1 Newtonian Fluids</b> .....	<b>34</b>
<b>2.2 Non-Newtonian Fluids</b> .....	<b>35</b>
<b>2.3 Viscosity model</b> .....	<b>37</b>
2.3.1 Power law model.....	38
2.3.2 Cross model.....	39

2.3.3	Carreau-Yassuda model .....	40
<b>2.4</b>	<b><i>Temperature dependency</i></b> .....	<b>41</b>
<b>2.5</b>	<b><i>Viscoelastic fluid</i></b> .....	<b>42</b>
<b>2.6</b>	<b><i>Constitutive equations for viscoelastic fluid</i></b> .....	<b>46</b>
2.6.1	Maxwell Model .....	48
2.6.2	Oldroyd-B Model .....	50
2.6.3	Phan-Thien Tanner model.....	52
2.6.4	Giesekus Model.....	52
2.6.5	Pom-Pom model.....	55
<b>2.7</b>	<b><i>Oscillatory Shear Flow</i></b> .....	<b>57</b>
<b>2.8</b>	<b><i>Characteristic values</i></b> .....	<b>61</b>
<b>2.9</b>	<b><i>Conservation equations</i></b> .....	<b>62</b>
<b>2.10</b>	<b><i>Finite element formulation</i></b> .....	<b>63</b>
2.10.1	Elastic-Viscous-Split-Stress (EVSS) Formulation.....	64
2.10.2	Computational formulations.....	65
2.10.3	Newton’s Linearization Method.....	68
<b>CHAPTER III</b>	.....	<b>70</b>
<b>3</b>	<b>EXPERIMENTAL SET UP</b> .....	<b>70</b>
<b>3.1</b>	<b><i>Introduction</i></b> .....	<b>70</b>
<b>3.2</b>	<b><i>Die design</i></b> .....	<b>70</b>
<b>3.3</b>	<b><i>Extrusion experiments</i></b> .....	<b>73</b>
<b>3.4</b>	<b><i>Material and rheological testing</i></b> .....	<b>76</b>
<b>3.5</b>	<b><i>Rubber process analyser tests</i></b> .....	<b>78</b>
3.5.1	Viscoelastic properties .....	81
3.5.2	Curing test .....	85
<b>CHAPTER IV</b>	.....	<b>87</b>
<b>4</b>	<b>NUMERICAL SIMULATION SET UP</b> .....	<b>87</b>
<b>4.1</b>	<b><i>Introduction</i></b> .....	<b>87</b>
<b>4.2</b>	<b><i>Finite volume simulation</i></b> .....	<b>93</b>
<b>4.3</b>	<b><i>Finite element mesh of extrusion die</i></b> .....	<b>98</b>

4.4	<i>Viscoelastic simulation</i> .....	103
4.5	<i>Geometry and boundary conditions</i> .....	105
4.6	<i>Finite element mesh of capillary die</i> .....	107
4.7	<i>Modelling mesh motion</i> .....	110
4.8	<i>Method of numerical solution</i> .....	111
4.9	<i>Determination of relaxation time</i> .....	113
4.10	<i>Relaxation time and relaxation mode</i> .....	116
4.11	<i>Modelling swell in complex geometry</i> .....	117
CHAPTER V .....		119
5 RESULTS OF VISCOUS MODELLING .....		119
5.1	<i>Introduction</i> .....	119
5.2	<i>Temperature field</i> .....	119
5.3	<i>Pressure field</i> .....	121
5.4	<i>Velocity field</i> .....	123
5.5	<i>Residence time</i> .....	125
5.6	<i>Streamline</i> .....	128
CHAPTER VI .....		130
6 RESULTS OF VISCOELASTIC MODELLING .....		130
6.1	<i>Introduction</i> .....	130
6.2	<i>Extrudate swell of rubber compound</i> .....	130
6.3	<i>Velocity and pressure field</i> .....	132
6.4	<i>Shear rate and dynamic viscosity</i> .....	134
6.5	<i>Circulation flows</i> .....	135
6.6	<i>Swelling of EPDM rubber in capillary die</i> .....	139
6.7	<i>Stress evolution in capillary die</i> .....	141
6.8	<i>Effect of design parameters</i> .....	143



<b>6.9</b>	<b><i>Effect of slip</i></b> .....	<b>144</b>
<b>6.10</b>	<b><i>Swelling of EPDM rubber in complex geometry</i></b> .....	<b>146</b>
<b>6.11</b>	<b><i>Stress evolution in complex geometry</i></b> .....	<b>146</b>
CHAPTER VII .....		149
7 CONCLUSION AND FUTURE WORK .....		149
<b>7.1</b>	<b><i>Conclusions</i></b> .....	<b>149</b>
<b>7.2</b>	<b><i>Future Work</i></b> .....	<b>152</b>
APPENDIX .....		154
References .....		161

## LIST OF TABLES

<b>Table 1-1:</b> Mechanical properties of vulcanized EPDM rubber [2]. .....	2
<b>Table 3-1:</b> Formulation of the EPD Rubber/Carbon Black Compounds. ....	77
<b>Table 3-2:</b> Physical and rheological properties of the EPDM rubber compound. ....	78
<b>Table 3-3:</b> Giesekus model parameters for EPDM rubber extracted from numerical fitting. .....	84
<b>Table 4-1:</b> Flow and thermal boundary conditions. ....	90
<b>Table 4-2:</b> Properties of FVM mesh. ....	95
<b>Table 4-3:</b> Properties of FEM mesh for extrusion die. ....	99
<b>Table 4-4:</b> Mesh refinement properties for capillary die. ....	109
<b>Table 4-5:</b> Parameters of Giesekus model for various relaxation time and relaxation mode. .....	117

## LIST OF FIGURES

<b>Figure 1.1:</b> Typical schematic diagram of single extruder machine [45].	15
<b>Figure 1.2:</b> Conventional design procedure for rubber extrusion dies.	24
<b>Figure 1.3:</b> Flow chart of the first stage experimental methodology.	26
<b>Figure 1.4:</b> Flow chart of the second stage of experimental methodology.	27
<b>Figure 1.5:</b> Flow chart of FEM simulation strategies.	29
<b>Figure 1.6:</b> Flow chart of frame work for viscoelastic modelling.	30
<b>Figure 2.1:</b> Shear stress verse shear rate for different class of fluids [71].	36
<b>Figure 2.2:</b> Characteristic velocity profile in a pipe flow for a- Newtonian.	37
<b>Figure 2.3:</b> Typical viscosity curve vs shear rate fitted to Carreau- Yassuda Model (reproduce from style of [71]).	40
<b>Figure 2.4:</b> Response of stress after step strain for different material. ( reproduced from Macosko [76] ).	43
<b>Figure 2.5:</b> Weissenberg (rod climbing) effect [77].	44
<b>Figure 2.6:</b> Die swell a-Newtonian fluid, b- Viscoelastic fluid (from style of Bird [78]).	45
<b>Figure 2.7:</b> Open siphon for Newtonian and viscoelastic fluid [74].	46
<b>Figure 2.8:</b> Maxwell element (reproduce from style of Pauli [88]).	48
<b>Figure 2.9:</b> Configuration of Oldroyd-B model (reproduce from style of Pauli [88])	50
<b>Figure 2.10:</b> The structure of the idealised pom-pom molecule under various degrees of stretch. (From style of McLeish and Larson [96]).	56
<b>Figure 2.11:</b> The sinusoidal imposed strain and the out-of-phase output stress response for linear viscoelastic fluid [63].	57

<b>Figure 3.1:</b> Schematic isometric view of the assembled extrusion die (with permission and courtesy of Standard Profil A.S./Düzce). .....	72
<b>Figure 3.2:</b> Extrusion die mounted on a single-screw extruder in an industrial extrusion line. ....	74
<b>Figure 3.3:</b> Measured signal of temperature and pressure from sensors (R10-extruder speed10, R15-extruder speed15,R20-extruder speed=20 rev/min). ....	75
<b>Figure 3.4:</b> Portable surface temperature measurement instrument. ....	76
<b>Figure 3.5:</b> Viscosity against the shear rate of the rubber compound at 60°C, 80°C and 100 °C .....	78
<b>Figure 3.6:</b> Biconical die configuration for RPA 2000 [110].....	79
<b>Figure 3.7:</b> Preparation test specimen using rubber process analyser [110].....	81
<b>Figure 3.8:</b> Discrete Fourier Transformation to access the real elastic and imaginary viscous phase[110].....	82
<b>Figure 3.9:</b> Shear modulus in strain sweep at 100 °C to find linear and No-linear domain. ....	83
<b>Figure 3.10:</b> Frequency sweep at constant temperature (100°C) and strain amplitude. ....	84
<b>Figure 3.11:</b> Fitting experimental data of EPDM rubber to Giesekus rheological model. .	85
<b>Figure 3.12:</b> Cure curves obtained from the RPA2000 for the rubber compound at 120 °C, 130 °C, 140 °C, and 150 °C.....	86
<b>Figure 4.1:</b> Geometry and boundary conditions of the flow domain. (all dimension in mm). ....	88
<b>Figure 4.2:</b> Mass flow rate and temperature at extruder head versus extruder speed. ....	89
<b>Figure 4.3:</b> External thermal boundaries of the steel die and interface boundary. ....	90

<b>Figure 4.4:</b> Side view of hot cylinder with boundary layer flow due to natural convection. .....	91
<b>Figure 4.5:</b> Variation of convective heat transfer coefficient at boundaries BS2 and BS4 and heat flux across the interface boundary (B2). .....	92
<b>Figure 4.6:</b> Chart of physical model adopted by STAR CCM++ for control volume method a-Liquid phase b-solid phase. ....	93
<b>Figure 4.7:</b> Generated finite volume mesh elements for both liquid and solid phase at section plane.....	94
<b>Figure 4.8:</b> Predicted heat flow over boundary adopting F.V. simulation for extruder speed 10 rev/min. ....	95
<b>Figure 4.9:</b> Predicted heat flow across thermal boundaries adopting F.V. simulation for extruder speed 15 rev/min.....	96
<b>Figure 4.10:</b> Predicted heat flow over boundary adopting F.V. simulation for extruder speed 20 rev/ min. ....	96
<b>Figure 4.11:</b> Comparison of total heat calculated by Empirical Equations and predicted by F.V.M at different extruder speed.....	97
<b>Figure 4.12:</b> Contour of temperature distribution adopting F.V.M simulation for extruder speed 10 rev/min. ....	97
<b>Figure 4.13:</b> Generated finite element mesh of the flow domain with zoom picture in the local surface area to demonstrate mesh elements. ....	99
<b>Figure 4.14:</b> Predicted temperature versus the number of elements for an extruder speed of 10 rev/min. ....	100
<b>Figure 4.15:</b> Cell volume distribution on section plane of extrusion die (for M2).....	101

<b>Figure 4.16:</b> Tetrahedral mesh element (reproduce from style of [71]).	102
<b>Figure 4.17:</b> Chart of physical model adopted by STAR CCM++ software.	103
<b>Figure 4.18:</b> Geometry of typical capillary die.	105
<b>Figure 4.19:</b> Boundary conditions imposed on capillary die.	106
<b>Figure 4.20:</b> Section plane show finite element mesh of capillary die (M2).	107
<b>Figure 4.21:</b> Predicted swelling ratio vs number of element adopting 3 relaxation mode of Giesekus model.	108
<b>Figure 4.22:</b> Calculated cell diameter distribution for M2 in capillary die section plane.	109
<b>Figure 4.23:</b> Physical model for viscoelastic flow in capillary die.	110
<b>Figure 4.24:</b> Shear viscosity, storage and loss moduli of rubber compound. Reproduced from reference [37] under permission from publisher ©Carl Hanser Verlag GmbH & Co.KG.	114
<b>Figure 4.25:</b> Countor of shear rate distribution in the middle die section for Non-Newtonian simulation.	115
<b>Figure 4.26:</b> Extrude Finite elements directed mesh technique.	118
<b>Figure 5.1:</b> Measured and predicted temperatures versus extruder speed.	120
<b>Figure 5.2:</b> Contours of temperature distribution in the entire flow domain for different extruder speeds: (a) 10 (b) 15, and (c) 20 rev/min.	120
<b>Figure 5.3:</b> Measured and predicted pressure versus the extruder speed.	121
<b>Figure 5.4:</b> Contours of predicted pressure distribution in the entire flow domain for different extruder speeds: (a) 10, (b) 15, and (c) 20 rev/min.	122
<b>Figure 5.5:</b> Contours of velocity distribution at exit section of die for different extruder speeds: (a) 10, (b) 15, and (c) 20 rev/min.	123
<b>Figure 5.6:</b> Velocity vector at die exit at extruder speed 10 rev/min.	125

<b>Figure 5.7:</b> Contour of residence time distribution at various extrusion speeds: a. 10, b. 15, and c. 20 rev/min .....	126
<b>Figure 5.8:</b> Variation of maximum residence time with extruder speed. ....	127
<b>Figure 5.9:</b> Variation of scorch time versus temperature for EPDM rubber compound. .	128
<b>Figure 5.10:</b> Streamline in the three dimension flow domain for extruder speed 20 rev/min. ....	129
<b>Figure 6.1:</b> Comparison of predicted die swell adopting various relaxation time and relaxation mode with experimental data given by Choi and Lyu [37]. ....	131
<b>Figure 6.2:</b> Velocity distributions (m/s) in a capillary die for three relaxation mode simulation and constant flow rate =0.011 cm <sup>3</sup> /s. a) $\lambda = \lambda b/4 - \lambda b x^4$ , b) $\lambda = \lambda b/5 - \lambda b x^5$ . ....	133
<b>Figure 6.3:</b> Contour of pressure distributions in a capillary die for three relaxation mode simulation and constant flow rate=0.011cm <sup>3</sup> /s .a) $\lambda = \lambda b/4 - \lambda b x^4$ ,b) $\lambda = \lambda b/5 - \lambda b x^5$ . ....	134
<b>Figure 6.4:</b> Contour of a- Shear rate distribution b-Dynamic viscosity distributions in a capillary die for three relaxation mode simulation case2, $\lambda = \lambda b/5 - \lambda b x^5$ . ....	135
<b>Figure 6.5:</b> Core vortices at the corner of reservoir for three relaxation mode, a) Case1 $\lambda = \lambda b/4 - \lambda b x^4$ , b) Case2 $\lambda = \lambda b/5 - \lambda b x^5$ .(Flowrate=0.011 cm <sup>3</sup> /s). ....	136
<b>Figure 6.6:</b> Core vortices at the corner of reservoir for various relaxation modes, a) One relaxation mode simulation case1 $\lambda = \lambda b/2$ , b) Two relaxation modes case1 $\lambda = \lambda b/4 - \lambda b x^4$ , c) Three relaxation modes simulation case2 $\lambda = \lambda b/5 - \lambda b x^5$ (Flowrate=0.011 cm <sup>3</sup> /s).....	137

<b>Figure 6.7:</b> Core vortices at the corner for various flowrate adopting three relaxation mode simulation case2: $\lambda = \lambda b/5 - \lambda b x 5$ a) Flowrate=0.01 cm <sup>3</sup> /s, b) flowrate=0.035 cm <sup>3</sup> /s). ...	139
<b>Figure 6.8:</b> Comparison of swelling for Styrene-Butadiene rubber and EPDM rubber. .	140
<b>Figure 6.9:</b> Stress vectors evolution at die exit and middle die section from the first mode in x-direction. ....	141
<b>Figure 6.10:</b> Stress vectors evolution at die exit and middle section plan from the first mode in y-direction. ....	142
<b>Figure 6.11:</b> Stress vectors evolution at die exit and middle section plan from the first mode in Z-direction. ....	142
<b>Figure 6.12:</b> Swell ratio versus different die length of die for EPDM rubber compound. ....	144
<b>Figure 6.13:</b> Swell ratio of EPDM rubber for various slip conditions. ....	145
<b>Figure 6.14:</b> Die exit profile and final predicted extrude profile in complex geometry ...	146
<b>Figure 6.15:</b> Evolution of stress vector at die exit from third elastic mode a.x-direction component, b.y-direction component, c.z- direction component. ....	147
<b>Figure 7.1:</b> a-3-D View of internal channel with external steel die. b. 2-D View of internal channel with steel die with imposed thermal boundary conditions. ....	154
<b>Figure 7.2:</b> Vertical hot plat ( $T_{BS3}$ is the surface temperature at boundary BS3, $T_{\infty}$ is surrounding air temperature, D diameter of cylinder). ....	157
<b>Figure 7.3:</b> Section view of fluid-solid interface domain. ....	160



## NOMENCLATURE

$a$	Shape parameter Carreau-Yassuda model	[-]
$a_T$	Shift factor	[-]
$A_f$	Area of individual face of node element	[m <sup>2</sup> ]
$C_p$	Heat capacity	[J.kg <sup>-1</sup> .K <sup>-1</sup> ]
$C_1, C_2$	Williams-Landel-Ferry models constant	[-]
$D$	Rate of deformation tensor	[1/s]
$De$	Deborah numbers	[-]
$E_a$	Activation energy	[J.kmol <sup>-1</sup> ]
$f$	Frequency of oscillation Hz	[Hz]
$f_b$	Body forces per unit volume	[N]
$F_u^k$	Jacobian matrix at step $k$	[-]
$G$	Shear modulus	[Pa]
$G^*$	Complex shear modulus	[Pa]
$G'$	Storage shear modulus	[Pa]
$G''$	Loss shear modulus	[Pa]
$G(t, \varepsilon)$	Relaxation modulus	[Pa]
$I$	Unit tensor	[-]
$K$	Consistency index	[Pa.s <sup><math>n</math></sup> ]
$m$	Cross rate constant of Cross model	[-]
MH	Maximum torque	[dN.m]
ML	Minimum torque	[dN.m]
$n$	Power law index	[-]
$N$	Number of mode	[-]
$N_1$	First normal stress difference	[Pa]
$N_2$	Second normal stress difference	[Pa]
$p$	Hydraulic pressure	[Pa]
$q$	Number of arms on the polymer molecule	[-]
$R$	Universal gas constant= 8.314	[J/mol.K]
$S^*$	Complex torque	[dN.m]
$t$	Time	[s]
$\tilde{t}$	Characteristic time of observation	[s]
$t_{res}$	Residence time	[s]
$\dot{T}$	Material time derivative	[-]
$\hat{T}$	Temperature	[K]
$T^\nabla$	Upper-convected time derivative of stress	[Pa]
$T_{average}$	Average temperature	[K]
$T_2$	Newtonian or viscous stress	[Pa]
$T_f$	Extra stress tensor	[Pa]
$T_D$	Stress in the damper element	[Pa]
$T_g$	Glass transition temperature	[K]
$T_o$	Reference temperature	[K]

$T_s$	Stress-in the spring element	[Pa]
TS2	Scorch time	[s]
$T(t, \varepsilon)$	Stress	[Pa]
$T_{total}$	Total stress	[Pa]
$u(x, t)$	Vector of field variables	[-]
$\bar{V}$	Average velocity at capillary die	[m/s]
$\bar{V}$	Average velocity at outlet surface	[m/s]
$V_f$	Velocity at individual node	[m/s]
$V_u$	Velocity uniformity index	[-]
$W_i$	Weissenberg number	[-]
$w_p$	Weighting functions corresponding to pressure field	[-]
$w_m$	Weighting functions corresponding to moment	[-]
$x$	Position vector	[mm]

### ***Greek Symbols***

$\alpha$	Anisotropic mobility factor of Giesekus model	[-]
$\alpha_p$	Anisotropic parameter of Pom-Pom model	
$\beta$	Ratio of retardation time to relaxation time	[-]
$\gamma$	Strain in elastic material	[-]
$\dot{\gamma}$	Shear rate	[1/s]
$\dot{\gamma}_c$	Critical shear strain-rate	[1/s]
$\gamma_o$	Strain amplitude	[-]
$\Gamma$	Boundary of computational domain	[-]
$\varepsilon$	Strain	[-]
$\varepsilon_{total}$	The total strain	[-]
$\epsilon$	Extensional parameter of PTT model	[-]
$\eta$	Total viscosity	[Pa.s]
$\eta_o$	Zero shear viscosity	[Pa.s]
$\eta_1$	Polymeric viscosity	[Pa.s]
$\eta_2$	Solvent viscosity	[Pa.s]
$\eta_a$	Apparent viscosity, or non-Newtonian viscosity	[Pa.s]
$\eta(\dot{\gamma}, T)$	Shear rate and temperature dependent viscosity	[Pa.s]
$\eta_\infty$	Infinite-shear viscosity	[Pa.s]
$\theta$	Biconical angle of RPA =0.1251	[rad]
$\kappa$	Thermal conductivity	[W/m.K]
$\lambda$	Relaxation time	[s]
$\lambda_b$	Relaxation time of the backbone tube orientation	[s]
$\lambda_s$	Relaxation time of the backbone stretch	[s]
$\Lambda$	Stretch factor of pom-pom model	[-]
$\mu$	Newtonian constant viscosity	[Pa.s]
$\xi$	Shear parameter of PTT model	[-]
$\rho$	Density	[kg/m <sup>3</sup> ]
$\sigma$	Total stress tensor	[Pa]
$\sigma_o$	Stress amplitude	[Pa]

$\tau$	Viscous stress tensor	[Pa]
$\tau_1$	Polymeric stress	[Pa]
$\tau_{1i}$	Viscoelastic stress of $i^{th}$ mode	[Pa]
$\tau_1^{\nabla}$	Upper convective time derivative of stress	[Pa]
$\tau_f$	Total extra stress for Newtonian fluid	[Pa]
$\varphi$	Phase angle between strain and stress	[rad]
$\phi$	Oscillation angle of RPA	[rad]
$\psi$	Viscous dissipation term	[watt]
$\omega$	Angular frequency in RPA	[rad/s]
$\Omega$	Computational domain	[-]

### ***ABBREVIATIONS***

ALE	Arbitrary lagrangian-eulerian formulation
BC	Boundary condition
CAD	Computer aided design
DEVSS	Discrete elastic-viscous stress splitting
EDM	Electric discharge machining
EPDM	Ethylene propylene diene monomer
EVSS	Elastic-viscous stress splitting
FEM	Finite element method
FVM	Finite volume method
GNF	Generalized Newtonian fluid
HWNP	High Weissenberg number
K-BKZ	Kaye and Bernstein integral model
LAOS	Large amplitude oscillatory shear
LDPE	Low density polyethylene
MFEM	Mixed finite elements method
PDE	Partial differential equation
PSPG	Pressure-stabilized Petrov–Galerkin
PTT	Phan-Thien-Tanner model
RPA	Rubber process analyser
SAS	Semi-analytical solutions
SBR	Styrene-butadiene rubber
SCR	Stress-controlled sliding cylinder rheometer
SU	Streamline-up winding
SUPG	Stream-upwinding-Petrov-Galerkin
WLF	Williams-Landel-Ferry model
XPP	Extended Pom-Pom model

# CHAPTER I

## INTRODUCTION

### ***1.1 Background***

EPDM (ethylene propylene diene monomer) rubber has been widely used in polymeric sealant applications in the automotive weather seal industry for many years. Since the commercial introduction of this industrial material in the early 1960, the worldwide production capacity has grown to approximately 920,000 metric tons per year [1]. Different technologies have been used to provide the ability to design polymers for specific applications and processing requirements. Synthetic rubber is highly durable against weather conditions, sun exposure, ozone, heat, oxidation, and polar solvents such as acids, alcohol and alkalis. Adaptability in polymer design and exceptional performance has brought about the expansive use in automotive weather-stripping and seals, radiator, rubber mechanical goods, glass-run channel, belts, tubing, roofing, plastic impact modification, motor oil additive applications, and electrical insulation. These polymers offer good compatibility with high filler loading, which is made from them economical compounds by developing high tensile and tear properties, better immunity to oil swell, as well as perfect abrasion resistance [2]. A summary of the mechanical properties of the vulcanized EPDM rubber is shown in Table 1-1. This property can be extended by proper compounding.

**Table 1-1:** Mechanical properties of vulcanized EPDM rubber [2].

<b>Hardness, shore A Durometer</b>	30 A to 95A
<b>Tensile strength, MPa</b>	7 to 21
<b>Elongation, %</b>	100 to 600
<b>Tear resistance</b>	Fair to good
<b>Abrasion resistance</b>	Good to Excellent
<b>Resiliency</b>	Fair to good
<b>Wear resistance</b>	good

The addition of the high amount of silica and carbon black as reinforcing fillers will introduce additional complexities in the rheological behaviour of these material which undergo a Thermo-mechanochemical reaction during processing. Moreover, the strong interaction between the filler particles and elastomer will impart the modification in the viscoelastic behaviour and complex flow of the uncured filled rubber [3]. During the extrusion of the rubber compound, the complex flow will generate two types of stresses: elastic and viscous stress. These stresses, which define the viscoelastic behaviour under the applied deformation, will affect the processing behaviour, which in turn affect the final properties of the products [4].

The processing parameters include the inlet temperature and pressure, the mass flow rate, and in addition the die design, which play an important role in the dimensional tolerance of the final profile and extrudate properties. On the other hand, the viscoelastic properties of the rubber melts in the flow domain, which includes the pressure, the temperature, the residence time, and field velocity, significantly depend on the processing variable. Both the controlling of the processing parameters and the viscoelastic behaviour of the complex

polymer system make producing the irregular shape with the filled rubber extrusion a very difficult task [5].

Other important factors that must be taken into consideration during the rubber extrusion, mostly related to the high viscoelastic nature of the rubber melt, are the extrudate-swell and stretching by the pulling system on the exit profile. These post extrusion phenomena will have a great influence on the final shape dimensions; therefore, their effect must be accounted for at the die design stage [6].

Due to all the above mentioned factors, the rheological phenomena occurring in the filled rubber extrusion requires more understanding in order to manage and understand the melt processing to evaluate their effect on the final property of the automotive rubber sealing products.

For many years, the research of non-Newtonian fluid has been carried out in different areas such as the food industry, pharmacology, the lacquer and paint industry, oil drilling, and polymer processing. The non-Newtonian behaviour of elastomer is largely determined because of the presence of the long chain macromolecules in the rubber structure [7].

With the increase in competition between the companies around the world in terms of finding cost effective techniques in product development, the computational modelling of filled rubber extrusion is becoming an important tool in the die design process as well as in the setting up of the optimum processing parameters for the production line of the extrusion process.

## ***1.2 Modelling polymer flow***

The diverse disciplines in studying the rheology of polymer have attracted researchers from various fields such as mechanical engineers, polymer scientists, chemical engineers, chemists, and physicist. For several years, researchers have spent a lot of time and effort on the development of various numerical methods and constitutive equations based on both microscopic and macroscopic approaches.

In the macroscopic based models, the description of a viscoelastic fluid expresses the stress generated during flow by the fluid element in terms of the deformation history experienced by that element, whereas in the microscopic based models the description of viscoelastic fluid is by a number of microscopic levels description, namely: atomistic modelling, the kinetic theory and quantum mechanics [8]. Recently, the development of the hybrid approach, which couples both a smaller scale and full scale level size (macro-micro) approach to the continuum mechanics and kinetic theory, has generally been utilised by the application of the finite element and stochastic reproduction technique [9].

Thus, relating to the modelling and simulation of the viscoelastic polymeric material extrusion, different groups of literature surveys, which have been documented and developed in an integrated manner in this production process is required to present and review as follows.

### **1.2.1 Characterization of material parameters**

In order to mimic the polymeric material behaviour through extrusion simulation: firstly, one should characterize the material parameters accurately for the suitable constitutive

equation, which will enable the capture of the rheological behaviour of the complex flow. Here is a summary of the most important and recent research performed in the characterization and the modelling of viscoelastic material such as polymer melt.

There was an early attempt to model the shear viscosity of the rubber-carbon black compound by L.White et al. [10]. They found that the shear viscosity decreases with the increase of the shear rate at a high shear rate regime. However, in the low shear rates regime, they found unbounded increasing shear viscosity, which indicated a yield value. In their experimental work they used the old version of a sandwich rheometer at low shear rates and a capillary rheometer at a high shear regime. The concept of the viscoelastic behaviour was not mature, which was one of the limitations of their work at that time.

C. Barre's et al. [11] investigated the viscoelastic properties of filled elastomers with two specially designed rheometers. Both torsional strain-controlled, rubber process analyser (RPA), and stress-controlled sliding cylinder rheometer (SCR) were used for the characterization of the complex system. The shear modulus (expressed by  $G'$  and  $G''$ ) and relaxation modulus were measured by the first rheometer, while the creep compliance was measured by the SCR. In this study, the cross-check method of the material function was used for the validation the results in both the linear and nonlinear viscoelastic domain. Also, three batches of the materials dependent on the filler volume fraction were used and the characteristic viscoelastic functions were extracted by two test modes to evaluate both the effect of the filler and the deformation mode. They used the time dependent viscoelastic model namely, the K-BKZ model, which was first proposed by Kaye and Bernstein [12] . The results of this investigation revealed that quantitative agreement was validated for all the



three batches in the linear domain, whereas the agreement between the experiment and K-BKZ model prediction was limited to only pure elastomer in the nonlinear viscoelastic domain.

Kwang Soo Cho et al.[13] proposed a new powerful method for analysing large amplitude oscillatory shear (LAOS) flow data based on a geometrical approach, which gave a more sensitive and significant physical interpretation of the stress response through the LAOS tests. Although previous methods, such as Fourier transform analysis FT [14], which depends on the intensities of the higher harmonics as a measure of nonlinearity and the Lissajous plot, involve the graphical representation of the nonlinear behaviour, it is trivial to extract a physical meaning beyond the linear viscoelastic limit regime by using both of these methods. In those studies, a new measure of elastic stress contribution, namely the generalized storage modulus and viscous contribution, associated with the generalized loss modulus, were introduced based on mathematical and physical foundations. The proposed method offers a greater physical significance for the both elastic and viscous stress contribution even in the nonlinear regime in addition to the extract results with higher accuracy and simple analysis of output LAOS data without using integral Fourier transformation or being dependent on any constitutive equation.

Jean L. Leblanc [15] introduced a technique, which was so-called harmonic or dynamic testing, to both linear and non-linear viscoelastic behaviour of complex fluid such as polymer material based on Fourier transform (FT) rheometry. This test procedure can promptly be applied to complex polymer frameworks, for example, filled rubber compounds, whose behaviour can be largely described by intrinsic non-linear viscoelasticity. They

described this new technique based on suitable test protocols and recorded the output signal, utilising a commercial purposely modified rotational harmonic rheometer RPA® (Alpha Technologies.UK), which allows for the full tracing of the viscoelastic domain. The effect of the reinforcing fillers as carbon black filled compound on the viscoelastic properties were discussed. The results revealed that the qualification amongst the intrinsic and extrinsic non-linear characters was effortlessly made when considering the single number  $Q1/Q2$ , which was extracted from the experimental data.

Andreea Calina et al.[16] presented a novel method to extract the non-linear parameter (mobility factor) of the Giesekus model, which describes the fluid rheology for the polyacrylamide solutions by the implementation of large amplitude oscillatory shear technique (LAOS). In those studies, the non-linear parameters of the n-mode Giesekus differential equation ( $\alpha_i$ ) were computed by considering the third harmonic in the Fourier spectrum of the shear stress acquired signal, instead of using the classical method, which described the non-linearity effect in terms of the shear-thinning viscosity. In this approach, the shear rate dependent viscosity was fitted by using a more sensitive and accurate non-linear data by application of (LAOS). In their second investigation [17], they also determined a set of three parameters including relaxation times ( $\lambda_i$ ), viscosity coefficients ( $\eta_i$ ) and the mobility factor ( $\alpha_i$ ) for each mode of the Giesekus model by implementing the same former procedure. The main inadequacy in the proposed procedure is the limited concentration and molecular weight that can be analogized by using this approach, in other words, at high polymer concentrations and high mass, the obtainment of the free noise signal becomes a difficult task.

Bae and Cho [18] suggested a semi-analytical approach in characterising the non-linear parameters of the viscoelastic constitutive equations that describe the complex flow. The main shortcoming in the Numerical Solutions lies in the complex procedures that require both accurate nonlinear data and fitting numerical solutions of the complex differential equations to the non-linear experimental data. Since the analytical solution is impossible for a higher order than the fifth, the authors presented semi-analytical solutions (SAS), which were based on significant quantities of LAOS. The results of their work demonstrated the success of the method for both Giesekus and Phan-Thien-Tanner (PTT) models for any strain amplitude with  $De < 1$ .

### 1.2.2 Numerical methods

The early progression of experimental research, which concentrated on the contraction flow in the late 70 s [19] and in the 80 s [20], was exceptionally influential in a portion of the early advancements in the numerical procedures adopted at that time. The basic target of the numerical methods proposed by Cable et al. and Evans et al. [19, 20] was to reproduce the experimental flow feature. The vast majority of these constitutive equations are confounded by the nearness of the improvements dependent on the finite element technique. The efforts were driven towards expanding the domain of the *Weissenberg number* ( $Wi$ ), which is a measure of the elasticity of the material, over which a stable solution can exist. The hyperbolic form of the viscoelastic peculiarity in the stream geometry has been distinguished as the primary driver of the loss of convergence of the numerical methods. In addition to the increased memory requirements and the variable to be solved, the *high Weissenberg number* (HWNP) is considered to be the greatest challenge in the simulation

of the viscoelastic fluid [21]. In this regard, a lot of researchers have devoted their time and effort to deal with this problem by adopting several approaches. One of these approaches includes using elastic-viscous stress splitting (EVSS) by introducing elliptic terms into the momentum equation [22] and by employing higher order differencing schemes [23], or by using discrete elastic-viscous stress splitting (DEVSS) first proposed by Guenette and Fortin [24].

The numerical study of Crochet and Marchall was one of the leading pieces of research that paved the way for creating the convergence computational scheme for viscoelastic complex flow problems. In their first work [25], the velocity field was modelled by a new function named the Hermitian shape function. This proposed approach guaranteed that the stress field estimation spaces could represent the velocity gradient and reduce the effect of peak oscillations due to the stress field gradient and step velocity. This oscillation normally happens at a moderately low  $Wi$ , consequently expanding the domain of the  $Wi$  over which a united arrangement could be obtained. In their second investigation [26], they proposed another mixed finite element strategy, which utilised a couple of bilinear sub-element configurations for the stress field and streamline-up winding (SU) for the constitutive equation. With the improvement of the calculation capacity by utilising the high memory PC, some of these numerical procedures were further developed over numerous years and made accessible in different available commercial software, for instance, ANSYS and STAR CCM+. This commercial software has been utilised broadly to model complex physical problems including mass, momentum, and heat transfer, as well as modelling the complex flow in the extrusion of polymeric material.

### 1.2.3 Extrusion swelling

Pioneering experimental and theoretical studies on die swell phenomena for several polymeric materials have been conducted by many researchers [27–31]. Sombatsompop and Sergsiri [32] studied the effects of the shear rate, the die temperature, and the reservoir diameter on the die swell ratio of the polystyrene melt. They found that the overall die swell ratio decreases with the increase in the die temperature; by contrast, this ratio increases in the range of 1.5–1.9 with the increase in the shear rate for all the barrel sizes in the study. The increase in the barrel diameter (contraction ratio) resulted in an increase in the overall die swell; thereby, contributing to the amount of elastic energy stored in the material; the amount of this energy depends on the contraction ratio in the flow domain. In addition, the residence time, which depends on the die length and extrusion speed (mass flow rate), plays an important role in the die swell. Increasing the residence time causes a decrease in the die swelling because the material has a considerable amount of time to relax (decaying memory) through the long path before it emerges from the die lip. The effect of the die length in the capillary extrusion-based polypropylene resin on the swelling ratio at different temperature ranges has been widely explored [33,34]. A high die swell ratio is observed for small die lengths through all the studied temperature ranges. An empirical equation was derived by Mullner et al. [35] to identify one new material parameter and consequently assess and compare the die swell of different materials with the consideration of the dependency of the swelling on the melt temperature and the shear rate rather than the geometry of the capillary dies. According to the viewpoint of the rheological properties of the materials, the capillary extrusion of the high-density polyethylene blending with a range of carbon fibers was investigated by using different entrance angles in the capillary dies [36].

The applications of the Phan–Thien and Tanner model under different relaxation times and relaxation modes in the capillary extrusion of rubber compound by utilising the PolyFlow software package were investigated [37]. The experiments were conducted using the Capillary Fluidity Tester instrument, in addition the Rubber Process Analyzer (RPA 2000) was used to measure the viscosity, storage, and loss modulus. The results revealed that the three and two relaxation modes most suitably described the swelling in the capillary die's application. They discussed two methods to extract the appropriate relaxation time, which were required for the PTT model simulation, and they used the reciprocal number of the average shear rate as a basis of the relaxation time for the different relaxation mode. They concluded that there was no difference in the die swell by using two or three relaxation modes, which shows a closer result to the experimental measurement, and those show a higher value in the die swell when compared to using one relaxation mode. In addition, a large circulation flow was predicted by implementing the two and three relaxation modes, as compared with one relaxation mode. Kim and Lyu [38] studied the swell of a rubber compound by utilizing different rheological models; their results revealed that the PTT and simplified viscoelastic models were the most remarkable candidates for describing the swelling behaviour in capillary dies.

Mohammad Javadi et al.[39] studied the flow balancing of rubber's extrusion in automobile weather strip production. They used a control volume computational approach in the simulation of the flow characteristics in the 3D flow patterns. The constitutive equation parameters were extracted by the least square fitting of the experimental data, which was determined by using the Rubber Process Analyzer (RPA) instrument. The simulation results were compared with experimental results and revealed that the balance in the flow at the die

exit was greatly affected by the die design and that some modifications in the die design would ensure proper balancing of the complex flow. Moreover, they found that the profile section tended to contract in the low velocity regions. The main deficiency in their work can be attributed to using the power law and Arrhenius-law models in describing the shear viscosity of the melted compound. These two models were weak in capturing the upper and lower band of shear viscosity at both a low and high shear rate regime. Moreover, memory and elastic effects are difficult to predict using pure viscous model [40]. In addition, they neglected the effects of the swelling phenomenon by assuming a completely moderated velocity distribution in the flow regions.

G. Zhao et al. [4] investigated the swell phenomenon and flow patterns of low-density polyethylene (LDPE) based on the penalty finite element simulation of a three dimensional viscoelastic flow. The multimode differential PTT constitutive mathematical model was used for this purpose in addition to using discrete elastic-viscous split stress (DEVSS) algorithm to improve the computational stability in the numerical scheme. The design parameters of the hollow profile extrusion die were discussed as well as the flow characteristics and mechanism of the swell generation in this kind of profile based on the proposed model. The normal stress, predicted with a multimode and single mode PTT model, was calculated along the flow path at four different points and compared to each other to specify the region of high stress. Also, the velocity distribution through the flow pattern was presented. The results from this study revealed that there was no significant difference between the flow stress obtained by utilising both the multimode and the single mode. Based on this finding, saving on computational costs and reducing in the computer memory can be achieved by using the application of single mode analysis in the simulation of a polymer melt flow. Moreover, the

swell phenomenon was affected by both velocity redistributions beyond die exit and release of flow stress.

#### **1.2.4 Die design**

Yuankan Dai et al. [41] studied die balancing and die design by utilizing the Computer Aided Engineering (CAE) technique in the extrusion of the automotive rubber seal. The results showed that modification in the die design, which was simulated by CAE technology, provided more uniform velocity distribution at the die exit.

O. S. Carneiro et al.[42] proposed a methodology for the rheological design of profile extrusion by the adoption of different constitutive equations. The constitutive equations needed to couple with field equations to achieve the final solution for the polypropylene polymer flow. There were different operating and post-extrusion parameters by which most relevant phenomena involved were studied such as rheological defects, post-extrusion phenomena and flow balancing. Relating to flow balancing, the methodology was implemented in two case studies using different constitutive equations. Commercial software PolyFlow package based on the finite volume approach, which was used in three dimensional simulations, was briefly described. In those studies, both capillary and rotational rheometers were used for the rheological tests. The shear viscosity fitted by the least squared method to the Bird-Carreau model. The extracted material parameters for the Bird-Carreau model included upper and lower limit viscosities, time constant, and flow index. Relating to the flow balancing, two die designs were used to evaluate the effect of the die design on the flow balancing at the die exit. The correction in the die design was based on the ratio of the predicted velocities from the simulation and required average velocities. The length of the



die at the constant thickness was taken as the optimized length and keeping the other dimension constant. The final results revealed that good balancing of the complex flow at the die exit could be attained by the insertion of the flow separators.

Dai, Y. K. et al.[43] implemented inverse extrusion simulation in the design of the extrusion die for the rubber seal application. A rotational rheometer and capillary rheometer were used for the viscosity measurement of the EPDM mixture in the low shear rate and high shear rate regimes, respectively. In their work, PolyFlow software package was used to perform the analysis. This provided the capabilities to handle complex polymer flow problems as well as a unique feature of inverse die design [44]. The Bird-Carreau rheological model was employed for modelling the shear thinning behaviour in the complex flow, of ethylene propylene diene (EPDM), and in three different configurations of the extrusion die. They neglected the effect of elasticity by considering the purely inelastic model in describing the viscosity. A real extrusion die was designed based on the structure of the predicted profile from the simulation and extrusion experimental test conducted for the validation of the simulation results. The results of the direct extrusion simulation coincided more with the experimental test carried out on the manufactured die by using an adaptive channel with a variable cross section.

### **1.2.5 Non-isothermal modelling**

In the extrusion of the rubber weather stripping, which has a constant profile, the raw material is basically fed into the extruder Huber in a solid state. This raw material gradually melts by the heat generated by the internal friction or the viscous dissipation during the material transport through the extruder. The transportation of the material in the extruder is

driven by the force of the pressure gradient. The production rate measured in the mass per hour (kg/hour) is almost dependent on the extruder speed; on the other hand, the energy dissipation increases dramatically with the increase of the extruder speed. Thereby, the dissipated heat may exceed the critical limit and lead to the degradation or “scorch” of the compound due to the temperature rise. A typical schematic representation of a single extruder in a rubber extrusion is shown in **Figure 1.1**.

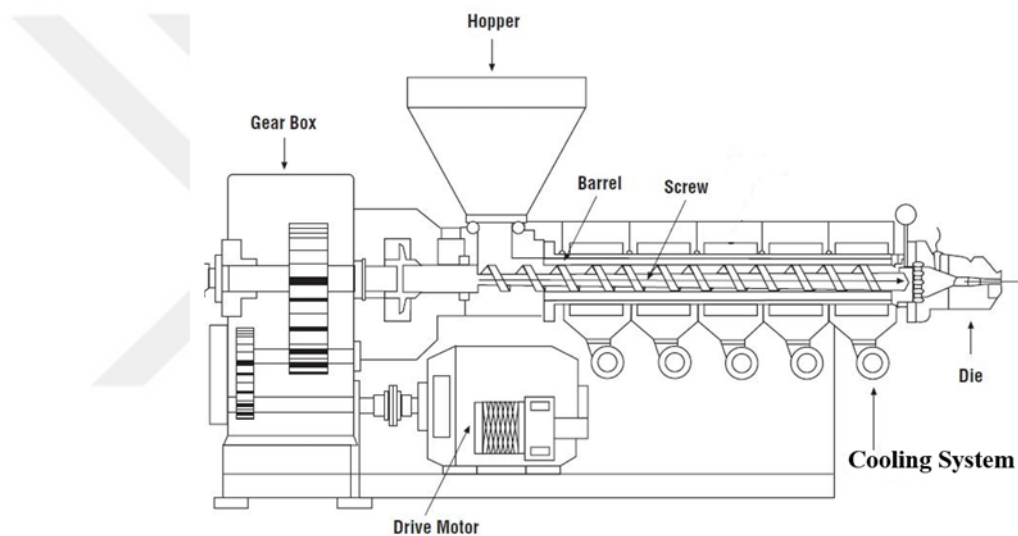


**Figure 1.1:** Typical schematic diagram of single extruder machine [45].

The single screw extruder was commonly used in the polymer extrusion operation due to its many advantages over other kinds of extruder such as low maintenance cost, high reliability, and simplicity of operation. More details about the basic process operation of polymer extrusion can be found elsewhere [45, 46].

Pioneering experimental and theoretical studies investigated viscous dissipation and its effect during the processing of different kinds of polymer [45–49]. A mathematical model was proposed by Campbell et al.[50] to model the effects of the screw and barrel rotation on

the viscous dissipation and mass flow rate of the polypropylene glycol inside a screw pump–extruder. The model was in good agreement with the experimental results, indicating that barrel angular velocity influences the temperature rise by viscous dissipation, and that strong viscous dissipation is generated from the clearance flow inside the extruder.

The EPDM rubber compound used in weather strip industries typically contains a considerable amount of reinforcing fillers, such as carbon black and inorganic additives [51]. In the modelling of shaping flows of EPDM rubbers and elastomers, where the flow occurs through dies or extruders, generalised Newtonian fluids are always used. This assumption relies on the fact that the typical viscoelasticity of the polymer phase is suppressed with considerable amounts of fillers and reinforcements, which are generally used in these products. Thus, such elastomeric formulations with solid particles are generally viscoplastic. This approach is simplified using a simple expression for the shear viscosity (Power law, Carreau–Yasuda, Bingham) and no-slip condition at the wall. Based on this assumption, numerous studies have utilised inelastic models and neglected the elastic effect on the modelling of the flow of the filled polymers, such as the EPDM rubber compound [51–57]. Zheng et al.[51] pointed out that the calculated Weissenberg Number ( $Wi$ ) for the EPDM rubber composite is less than 1, which confirmed that the viscous effect is predominant. Elgeti et al.[56] suggested that elasticity mainly affects the swelling behaviour in the close downstream of the die exit; as such, they assumed the negligible effect of elasticity in modelling the polymer flow for optimising the shape of the extrusion die.

Abeykoon et al.[58] proposed a model of the effects of screw geometry, material, and process setting on the melt temperature profile in a single-screw extruder by using a

thermocouple mesh technique. The experimental results and model predictions revealed that the barrel set temperature, the material, and the screw speed significantly affect the thermal homogeneity of the processed material inside the extruder domain. Borzenko and Shrager [59] numerically studied the effects of viscous dissipation on field temperature, viscosity, and flow parameters during the flow of polymeric material in a flat channel.

Brockhaus and Schöppner [60] conducted an experimental and numerical study to investigate the throughput behaviour of an ethylene propylene diene monomer (EPDM) compound and Styrene-butadiene rubber (SBR) as a function of barrel and screw heating by considering the dissipative heating in the extrusion process. They used two different extruder sizes in their experimental investigation and conducted numerical flow simulation using different temperature combinations of the screw and barrel in the extruder regime. The experimental and numerical results of those studies showed that the throughput increases with the increasing screw and barrel temperatures, but the former had a more significant influence; they also pointed out that the maximum permitted melt temperature of 120 °C in the screw channel should not be exceeded in order to avoid degradation or even vulcanisation.

Kalyon et al.[52] presented numerical simulation based on the Finite Element Method (FEM) for the modelling flow and heat transfer of filled polymer in industrial-scale co-rotating twin screw extrusion. They introduced a new numerical approach to investigate both the wall slip and viscoplastic behaviour through the simulation. The experimental twin-screw extrusion data was compared with the results obtained from the numerical simulation. The results obtained underscored the importance of incorporating the wall slip in the interfacial flow boundary conditions.

Andreas Limper [53] presented a mathematical model to describe the non-isothermal flow of the rubber compound in an extruder screw. The conservation equation was solved in the coupled manner in the combination with the constitutive equation. The Power law model and the Arrhenius equation were used to describe the shear rate and temperature dependency of the EPDM rubber compound. The results of their study reveal that the presented model shows the required flexibility with respect to rubber extrusion simulation. They pointed out the capabilities of simulation to reproduce the experimental data at screw tip for lab scale rubber processing. This indicate the ability to used simulation as an appropriate tool for processing variables optimization purpose.

Coz Díaz et al.[54] investigated the non-isothermal flow in rubber extrusion die by using the finite volume method. The velocity and temperature distribution in the extrusion head were calculated by solving the conservation equations coupled with the constitutive equation represented by the power law model. The results obtained revealed that the temperature distribution of the melt rubber in the extrusion die varied in the range of (65 to 120 °C). The numerical results obtained showed good agreement with the experimental data.

Ha et al.[55] presented 3-D finite element numerical analysis for modelling the melted rubber flow during the extrusion of automobile weather strips. They used the inelastic viscosity model (power law) and Arrhenious-law for describing the shear rate and temperature dependency of the viscosity. The temperature and velocity filed under a steady state condition were approximated based on the finite element in the Eulerian description framework. The results revealed the remarkable effect of the slip condition and mass flow rate on the thermal flow characteristics such as velocity, pressure, and temperature filed.

Elegit et al.[56] used the inelastic viscosity model namely, the Carreau model for modelling the polymer flow for the shape optimizing of the extrusion die. They assumed a negligible effect of the elasticity since the elastic effect was only concerned with the behaviour of the polymer melts behind the extrusion die (i.e. die swell effect). In addition, they considered the homogeneous temperature distribution in the extrusion die when a steady state was reached; consequently, the isothermal process was assumed to save computational time during the costly optimisation step.

### ***1.3 Novelty aspect***

Extrusion is the most relevant process for the production of many polymer-based products with various cross sections for various applications, such as in the automobile weather strip industry. During the extrusion, the quality of the final product significantly depends on the rheological and thermodynamic properties of the rubber compound inside the die. However, in the rubber industry, the extruder speed determines the appropriate operating thermodynamic properties of the rubber compound (melt) during the processing. On the other hand, information about the pressure drop and residence time are important for production engineers to decide on the suitable operating conditions and die design. For highly viscous materials, such as elastomers, viscous dissipation is inevitable; thus, neglecting or underestimating this effect during processing may lead to design mistakes. In an extrusion line, selecting the optimal extruder speed cannot be achieved without the prior numerical investigation of the flow due to the complex behaviour of the rubber compound during the flow inside the die.

The thermal properties of the rubber inside the extrusion die depend on many factors, including the rheological properties, the extruder speed, the design parameters of the die, the entrance temperature from the extruder head, and the amount of viscous dissipation. In addition, the residence time of material can be directly linked to die design parameters and processing condition associated with extruder speed. By increasing the extruder speed or machine output, the viscous dissipation increases in the high-shear region, consequently increasing the risk of die lip build-up, degradation, or even the vulcanisation of the rubber melts inside the die due to excessive heat generation [49]. In this regard, monitoring and controlling the fluid temperature is the key to producing high-quality products, especially those with complex geometries.

Previous works have focused on the effects of the operating condition and screw design on the thermal properties or temperature rise due to the viscous dissipation in the extruder domain. The viscous dissipation effect continuously occurs even in the extrusion die. Many typical problems in rubber extrusion, such as scorching, gelation, and die deposit accumulation, are associated with the poor heat control of the rubber compound in the extrusion process [61]. Therefore, monitoring the thermal properties of the extruded melt in the extrusion die as a function of the extruder screw speed is important in fabricating high-quality extruded products. On the other hand, the results obtained from numerical modelling will be helpful to design engineer to make a decision about the necessary modification in die design if required.

In this regard, the first question to address is how much the extruder speed can be increased, for specific die design, without the evolution of a detrimental effect due to viscous

dissipation or increase in stress field at die exit. To answer this question, an experimental study was performed on a real extrusion line together with numerical simulation to investigate the effect of the extruder speed on the extruded product quality. The result obtained from this work will be helpful to increase the productivity by choosing the maximum allowable extruder speed.

The analysis of polymeric material extrusion has been conventionally regarded as a relatively difficult problem due to the high viscoelastic nature of such materials and the challenge in selecting suitable rheological models. Rubber compounds are characterized by high levels of nonlinear viscoelasticity [62]; consequently, an extrudate swell is obtained when the materials emerging from the die lips. The extrudate shape deviates from the original die profile, and this deviation depends on various parameters, including the memory effect, the shear rate (flow rate), the strain history, the operating temperature, the die geometry, and the rheological properties of the polymer blend [61, 62]. In this regard, the computational analysis of the flow domain is important at the primary stage of the die design for the extrusion of the complex profiles. The modelling of the nonlinear viscoelastic properties of the rubber compounds also remains an intensive research area because of the involvement of many parameters.

Extensive effort has been dedicated to the modelling of highly viscoelastic polymer melts or solution flow using differential, integral, and molecular constitutive equations in profile extrusion [63–66]. Most of these investigations have been focused on the effects of the geometric parameters of the dies and the adopted numerical schemes regardless of the effects of the viscoelastic model parameters on the numerical results. The authors believed



that the parameter values of the widely adopted viscoelastic model exert an influence on computational results. However, only a limited number of studies have considered numerical simulations involving the effects of constitutive equation parameters [37].

Different constitutive models (the integral of differential forms), which can describe rheological data equally well, have been reported. However, these models generate different swell predictions, and this situation leads to an intriguing problem that remains unexplained according to Konaganti et al.[69] . Thus, predicting swelling by using a specific constitutive model for a specific rubber compound is necessary. In this regard, the second question to address is how much the change in the adopted viscoelastic model can influence the swell prediction.

In spite of numerous studies that applied different constitutive models for swell prediction, the application of Giesekus model with different relaxation times and relaxation modes has not yet been studied extensively. Therefore, analysing swelling in capillary die extrusion by applying Giesekus model is important in analysing the model's prediction ability. This technique can also be extended to the analysis of material behavior in other complex domains.

The correct predictions of swelling and circulation help design engineers to take measure for these phenomena in the primary stage of die design, thereby reducing problems related to form deviations in final product geometry and die plating or in some case evolution of surface defect due to increase in tensile stress near the die exit. In this regard, the third question to address as “is there any correction in die design is required to prevent or minimize

these problems in a specific industrial extrusion die and how much the change in the adopted viscoelastic model can influence the swell prediction.

The present work shows the framework for conducting such simulations with necessary accuracy. In addition, given that the basic measurements of the rheological properties of a polymeric material can be obtained by using a capillary rheometer, understanding the flow behavior in capillary die is useful in understanding the physics behind rheological measurements.

#### **1.4 Objective**

The design of a rubber product is considered as a challenging task since any change in the processing variable or die design will have a significant effect on product quality, which can sometimes not be logical [70]. Therefore, understanding the rheological behaviour through modelling the flow will be helpful for giving more insight into the optimum processing variable for product quality improvement. On the other hand, the information about the rheological variable such as the velocity field, the pressure drop, the temperature distribution, and the residence time, will be necessary for die design engineering.

The inclusion of many factors which influence product quality during the extrusion process cause the relationship between the die design and the flow field to not-be intuitive. The current conventional die design is required running-in the experimental trials during which the manufactured die is reworked in several trials to guarantee the required product quality. This classical process of die design is illustrated in **Figure 1.2**. Therefore, the numerical modelling of the complex flow is a powerful tool to replace these costly

experimental trials by using numerical experiments. The results obtained from numerical experiments will be very helpful to design engineers for making the required correction in the die design.

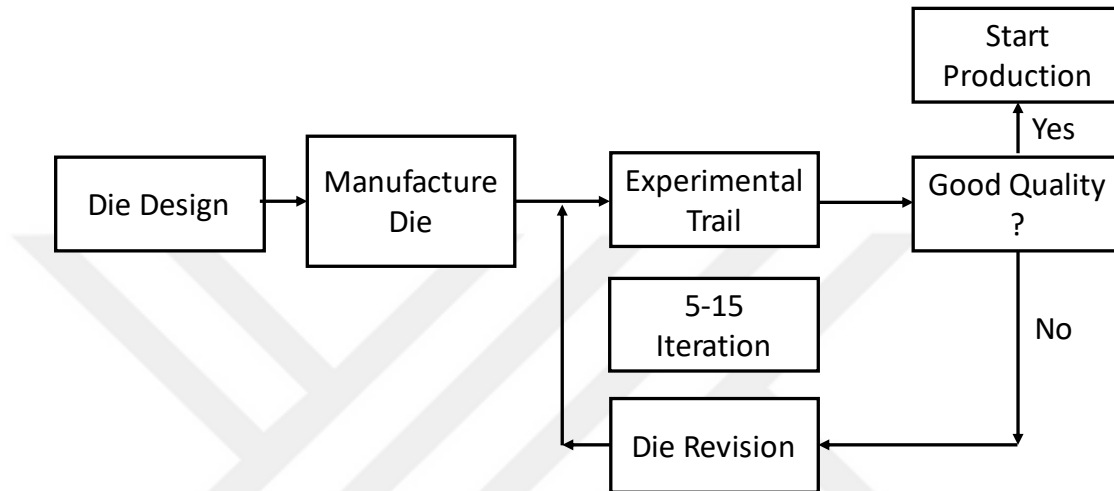


**Figure 1.2:** Conventional design procedure for rubber extrusion dies.

The first objective of this study is to validate a specific industrial scale die design for extrusion of rubber compound profile based on finite element modelling. Temperature rise due to viscous dissipation and a pressure drop in the entire flow domain of the extrusion die, which was especially designed for this purpose, was monitored by conducting extrusion experiments with different extruder speeds in a real extrusion line. Nonisothermal flow simulations based on a finite element method were also conducted. Information about the temperature rise linked to the residence time can be used in rubber machinery to avoid the possible scorch or premature vulcanisation inside the flow domain. Moreover, the analysis of the stream line, stress field and velocity uniformity can provide sufficient information for the final quality of extruded product and required correction in die design. The entire flow domain of the extrusion die was considered by solving the continuity, momentum, and energy

equations. The Power Law Model and Arrhenius Law were used to describe the shear rate and temperature-dependent viscosity. The results obtained from the modelling consider rigorous outcomes since they are taken from an industrial scale die, which was the primary design for this purpose.

The second objective in this study was to establish a numerical model to provide a fundamental basis potentially useful in predicting the swelling during the extrusion of the rubber compounds. Swelling is a phenomenon caused by the viscoelastic fluid flow behaviour of the rubber compounds in the profile extrusion processes. In the continuous extrusion processes, the swelling causes deviations from the shape of a die. Moreover, a flow field that includes circulation regions in the die can create production problems such as plating. Capillary die extrusion is selected as a benchmark case because of its simplicity and the availability of experimental data. The effect of the viscoelastic model parameters on the predicted results was investigated by using the experimental data. In this work, we applied the Giesekus model to predict the swelling in a capillary die and selected the capillary die extrusion as the benchmark problem. The guidelines for the establishment of the relaxation time and relaxation mode variables of the Giesekus model were also suggested. The predicted computational swelling results obtained by using the Giesekus model application were analysed and compared with the published experimental results [37]. In addition to the pressure and the flow field, the effects of the mass flow rate on the flow circulation patterns were further analysed.

## 1.5 Methodology

The conclusion from the previous studies associated with rubber extrusion indicated that the rheological behaviour of the complex flow in the extrusion die together with design parameters of the extrusion die has a significant effect on the product quality of the extruded parts. Some of this work was conducted at a company to solve a real industrial problem accompanied by the manufacturing of the rubber seal in the standard profile company. To do this experimental and numerical study, firstly, a special extrusion die instrumented with special sensor was designed and manufactured utilising a non-traditional manufacturing method. The transducer sensors coupled with the data acquisition systems device which was specially designed to process the output signal from the sensors. The collected data included the pressure and temperature at different locations inside the die. The extrusion experiments were conducted in a real extrusion line to collect the rheological data during the experiments.

The flow chart in **Figure 1.3** below describes the first stage of the experimental work.

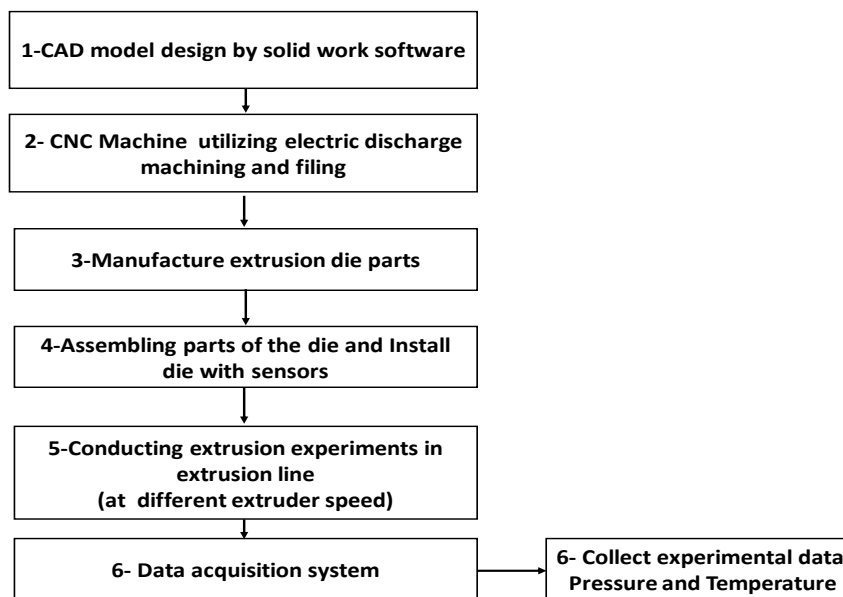


**Figure 1.3:** Flow chart of the first stage experimental methodology

The manufactured die was installed on a single screw extruder for conducting the extrusion experiments and collecting the experimental rheological data, which was used later for the validation of the numerical simulation results.

The numerical simulation based on the mixed finite element method was conducted to analyse the complex flow behaviour in the full domain of the extrusion die. The implementation of this numerical simulation required the choice of a suitable material model to describe the real physics of the material behaviour during processing. Therefore, in the second experimental stage, the rubber compound was characterized by using a different device especially designed for this purpose. Those steps are described in the flowchart depicted in **Figure 1.4**.

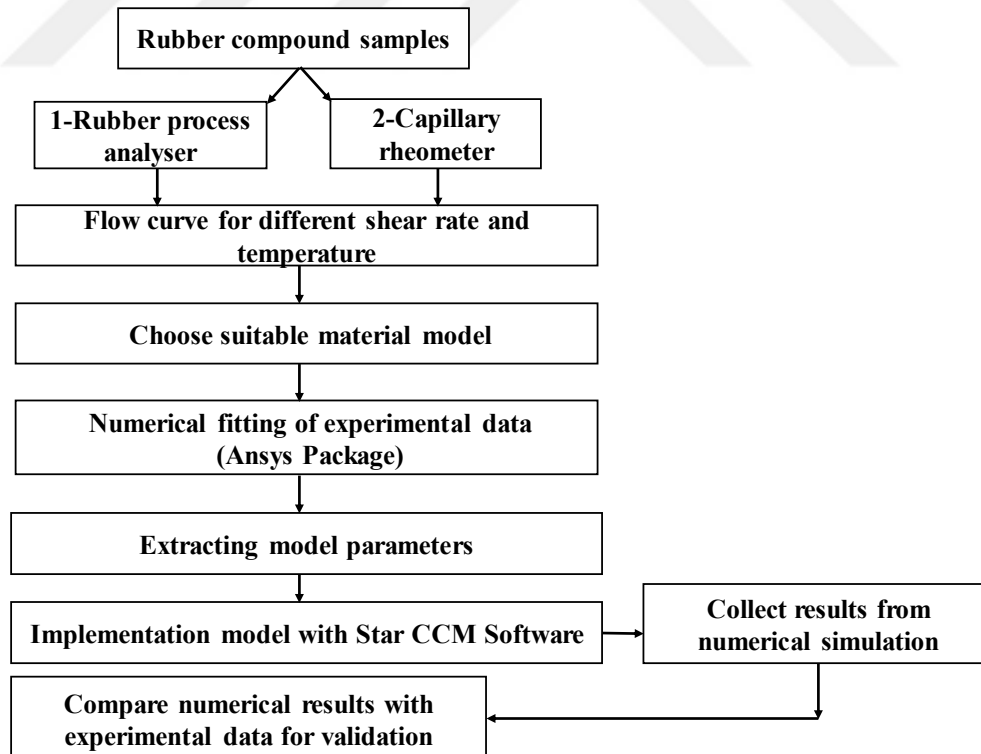


**Figure 1.4:** Flow chart of the second stage of experimental methodology

For characterising the material parameters, up to date measurement methods and equipment (The Rubber Process Analyzer (RPA) and the capillary rheometer) were utilised for this purpose. The data collected from these instruments represented by flow curves were additionally processed by the numerical fitting utilising the Ansys Polymat Package to extract the model parameters.

RPA is also used for testing the isothermal vulcanization behaviour of the rubber compound to construct the curing curve at different temperatures and to find the scorch time. The physical properties of the EPDM rubber compound such as density, thermal capacity, and thermal conductivity were measured utilizing the appropriate device. The measured physical thermodynamical properties were also required for the implement simulation.

The simulation experiments were conducted adopting the Star CCM+ Package, and the results obtained were then compared with the experimental data for validation.

During the modelling complex fluid flow based mixed finite element method, different techniques were employed including the streamline upwind/Petrov–Galerkin (SUPG), Galerkin and Newton linearization finite element procedures. Those techniques are required for numerical stabilisation and for reducing errors during computation. Details of this method will be introduced in chapter II. The solution strategies were based on the Mixed Finite Elements methods (MFEM) described in the following flowchart as shown in **Figure 1.5**.

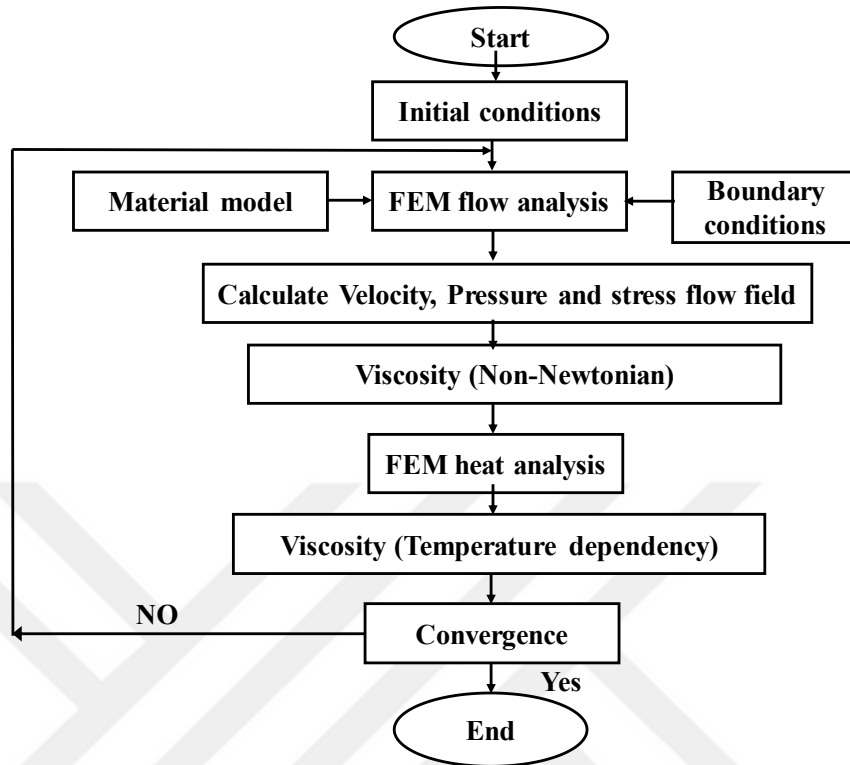


**Figure 1.5:** Flow chart of FEM simulation strategies.

The second task was devoted to modelling the swelling behaviour through adopting the viscoelastic rheological model. The methodology used for the implementation of the proposed model is described by the flow chart in **Figure 1.6**.

After the validation of the proposed model, the same model was used to investigate the swell phenomenon of the EPDM rubber compound in both simple and complex geometry.



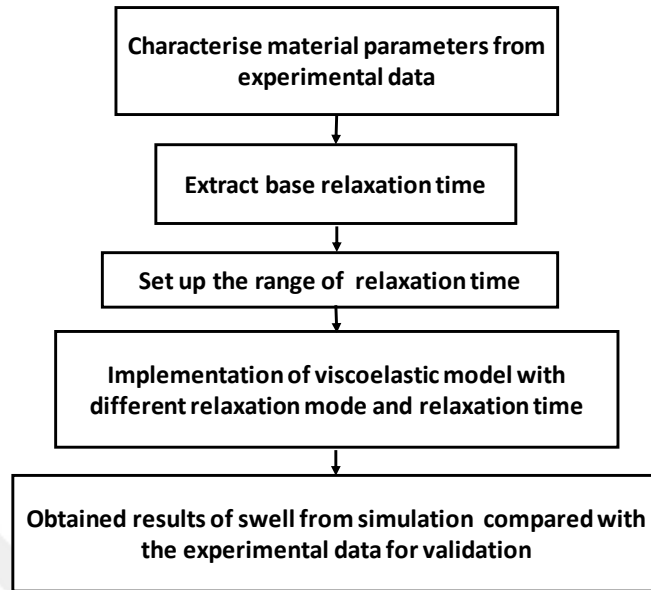


**Figure 1.6:** Flow chart of frame work for viscoelastic modelling.

## ***1.6 Thesis organization***

This thesis is organized as follows:

**Chapter 1** presents the background and reviews of previous studies on rubber extrusion modelling and extrusion die design. Several studies on the modelling complex rheological behaviour of complex flow (melt polymer) have been conducted by many researchers. These studies introduced many models, which can be used to capture the physical behaviour experience by the material during the flow in the extrusion die. A review in terms of the method of characterising the material parameters, the numerical strategies, the die design, and the viscoelastic modelling are presented. In addition, reviews on the influence of the viscous dissipation on the rheological behaviour during the non-isothermal flow are presented. At the end of this chapter, the objectives and methodology of the study are presented.

In **Chapter 2**, different constitutive equations and viscosity models used for describing the polymer flow are presented. The governing equation (field equations), represented by continuity, momentum and the energy equation, which are coupled with the constitutive equations to solve the coupled heat flow problem are presented. Different kinds of differential viscoelastic models are presented and the fundamental physics behind its behaviour are described. The method of formulation based on the mixed finite element was discussed. The numerical strategies by adopting the Elastic Viscous Stress Splitting (EVSS), SUPG, and Galerkin methods are described mathematically through the implementation of this numerical scheme based on the Giesekus model constitutive equation. At the end of the chapter The basic theory for oscillatory shear flow measurement are also presented and described.

In **Chapter 3**, the methods used to characterize the material parameters are introduced and discussed. The advantages and the most important design features of RPA are explained and analysed. Extrusion's die design criteria, manufacturing methods and materials used for the extrusion die are also presented. The testing procedure for the curing characteristic was discussed and the field experiments on the extrusion line are introduced in detail.

In **Chapter 4**, a numerical simulation, test cases, and die geometry are presented. The industrial scale extrusion die is used to investigate the effect of the extrusion speed on the rheological parameters in the entire flow domain, and capillary die is used to study the viscoelastic behaviour by adopting viscoelastic modelling. The detail of the mesh applied to the geometry is introduced in this chapter. The flowchart of the physical model is presented,

including the non-isothermal pure inelastic model and the viscoelastic model. Simulations are applied to two cases, namely, the pure inelastic model and the viscoelastic model. STAR CCM+ is used to test all the simulation models.

In **Chapter 5**, the obtained results associated with the rheological parameters in the entire flow domain are discussed and analysed for different extruder speeds. The outlet parameters include temperature, pressure, velocity field, and residence time. The obtained results were validated with the experimental data. From the final analyses a suggestion can be given about the optimum extruder speed suitable for this application in terms of the maximum productivity. In addition, a decision can be made to put the proposed die design in the extrusion line without any production defects arising, which can occur due to the viscous dissipation or the circulation flow.

In **Chapter 6**, the results of the viscoelastic modelling adopted on the capillary die as a benchmark problem are discussed and analysed. The framework for the implementation of the Giesekus rheological model and the setting up of the relaxation time are proposed and discussed. The effect of mass flow rate on the extrudate swelling and rheological field variable of (SBR) are presented and analysed. The obtained results are validated through comparison with the experimental data available in the literature for the capillary extrusion of (SBR). In the second section, the proposed model is applied to modelling extrusion process in simple and complex geometry of the EPDM rubber to investigate the swelling behaviour of this material.

In **Chapter 7**, the overall conclusions of the investigations and suggestions for future research are provided.

Finally, the Appendix contains the calculations of the local convective heat transfer coefficient by using empirical equations based on the natural convection theory.



## CHAPTER II

### THEORETICAL MODEL

#### 2.1 *Newtonian Fluids*

The first categories of fluid such as water and air are known as Newtonian fluid, whose viscosity does not change with the change of the shear rate. An explicit constitutive relationship can be used to relate the viscous stress tensor  $\tau$  to the velocity field through the constant viscosity for describing the Newtonian fluid behavior. In this case the constitutive relationship can be described by the simple linear relationship between the shear stress and the shear rate, as expressed below [71].

$$\tau = 2\mu D \quad (2.1)$$

where:  $\tau$  and  $\mu$  are viscous stress tensor and Newtonian constant viscosity, respectively.

For a particular fluid the viscous stress tensor  $\tau$  is a variable function of velocity field that typically expressed in the form of rate of deformation tensor ( $D$ ) as given below.

$$D = \frac{1}{2}(\nabla v + (\nabla v)^T) \quad (2.2)$$

The velocity vector field and velocity gradient described in three-dimensional Cartesian components as given by.

$$v = \begin{pmatrix} u(x, y, z) \\ v(x, y, z) \\ z(x, y, z) \end{pmatrix}, \nabla v = \begin{pmatrix} \frac{\partial u}{\partial x} & \frac{\partial u}{\partial y} & \frac{\partial u}{\partial z} \\ \frac{\partial v}{\partial x} & \frac{\partial v}{\partial y} & \frac{\partial v}{\partial z} \\ \frac{\partial w}{\partial x} & \frac{\partial w}{\partial y} & \frac{\partial w}{\partial z} \end{pmatrix} \quad (2.3)$$

## ***2.2 Non-Newtonian Fluids***

The second categories known as Non-Newtonian fluid whose behaviour in completely different manner from Newtonian fluid. This change in behaviour due to the dependent of viscosity on shear rate and shear history in addition to temperature dependency. Therefore, Non-Newtonian fluid do not follow the law of the classical Newtonian fluids. The non-Newtonian fluid model and in some cases viscoelastic model primary applied to polymeric fluid due to the presence of long chain molecules in their structure [72].

Many industrial fluids such polymer melts, paint, blood, syrup, suspensions of corn starch or quick sand characterized as Non-Newtonian fluid due to their complex microstructure. However, the behavior of non-Newtonian under deformation is different for different type of material which lead to farther classification of this categories to Generalized Newtonian and Viscoplastic material. The typical diagram relates the shear stress with shear rate for different types of fluids depicted in **Figure 2.1** [71].

Referring to **Figure 2.1**, a Newtonian fluid was described by a straight line passing through the origin and the constant viscosity was defined by the slope. For the shear thinning fluid, there is a nonlinear relationship between the shear stress and the shear rate indicated by a concave downward curve with an increase in the shear rate corresponding to the decrease in the viscosity; meanwhile, the opposite behaviour was found in the shear thickening fluid, which indicated the increase in the viscosity as the shear rate increased. The viscoplastic fluid was characterised as possessing a critical yield stress, it behaved as a solid until the imposed stress exceeded the critical yield stress value to start the flow as a fluid.

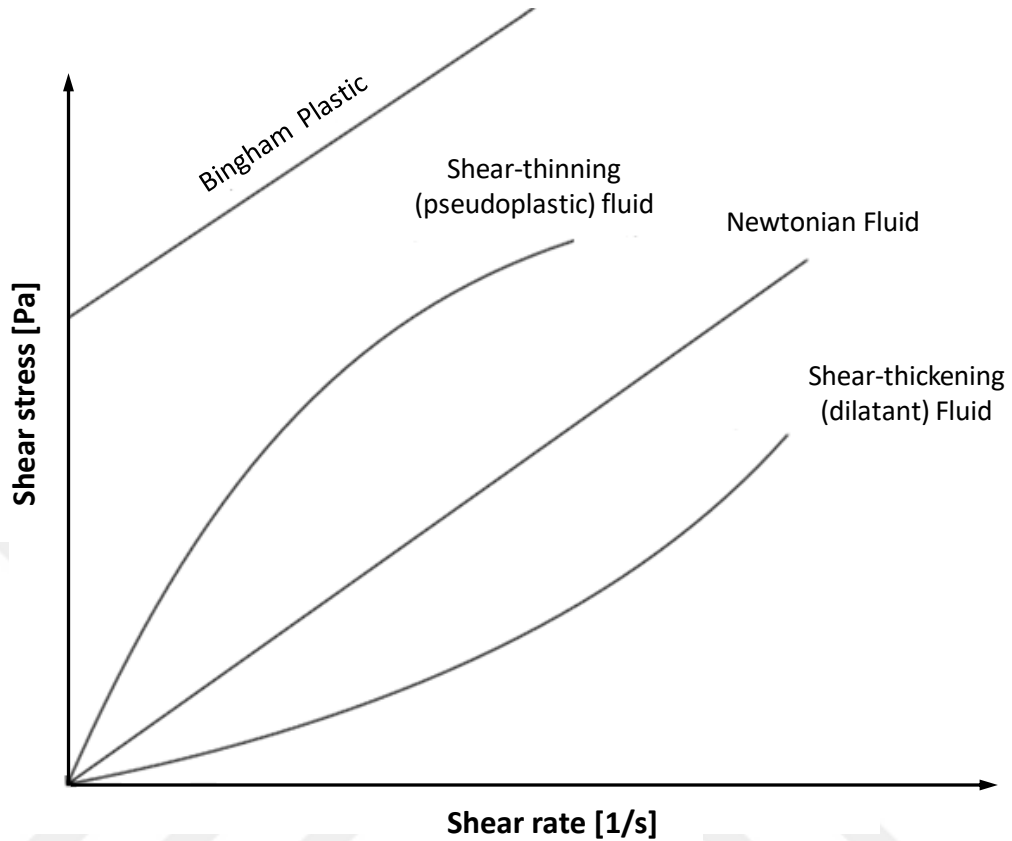


**Figure 2.1:** Shear stress verse shear rate for different class of fluids [71].

Most polymeric materials, such as rubber melt, have shear-thinning behaviour, which greatly influences the rheological properties during processing. For instance, the shear-thinning behaviour introduced remarkable changes in the characteristic velocity profile from a Newtonian fluid due to the decrease in the viscosity in the area of the high shear rate as illustrated in **Figure 2.2** for the pipe flow. In this case, it obviously clear that the maximum center line velocity (velocity peak) for the Newtonian fluid is higher than the shear-thinning fluid [73].

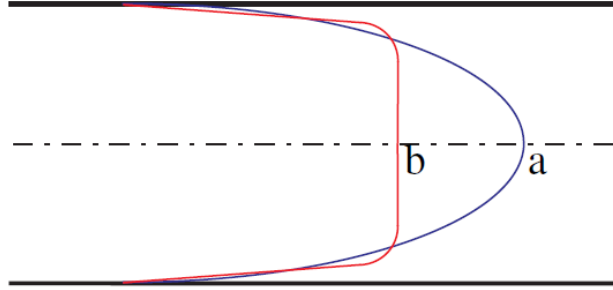


**Figure 2.2:** Characteristic velocity profile in a pipe flow for **a**- Newtonian Fluid, **b**- shear-thinning fluid [73].

The stress tensor for the generalised Newtonian fluid can be described by a simple mathematical relationship by replacing the constant viscosity in the Eq.2.1 by an apparent viscosity  $\eta_a = \eta(\dot{\gamma}, T)$ . In the present case, the viscosity is a function of the shear rate and/or temperature.

$$\tau = 2\eta(\dot{\gamma}, T) D \quad (2.4)$$

The total stress tensor for the generalized Newtonian fluids can then be written as:

$$\sigma = -p\mathbf{I} + 2\eta(\dot{\gamma}, T)D \quad (2.5)$$

Where  $p$ ,  $\eta(\dot{\gamma}, T)$ , and  $\mathbf{I}$  are the hydraulic pressure, Non-Newtonian viscosity, and unit tensor, respectively. The shear rate  $\dot{\gamma}$  is defined by the second invariant of the rate of deformation tensor  $D$  given by:

$$\dot{\gamma} = \sqrt{2D:D} \quad (2.6)$$

### 2.3 Viscosity model

The generalized Newtonian fluid model (GNF) described in the previous section is actually a family of the model. This is because a different function can be used to describe



the viscosity function ( $\eta$ ). Despite the flexibility in the choice of the viscosity function, some constraints should be applied. First, the constitutive equation should be able to translate into any coordinate system. Second, the choice of ( $\eta$ ) must not be exclusive for the particular flow. Third, the final prediction of the constitutive equation should correlate with the real experimental data of the fluid of interest [72].

For the polymer flow, a different function was used in the literature to describe the shear rate dependent of the viscosity such as the power law model, Cross model, and Carreau-Yasuda model [71].

### 2.3.1 Power law model

This model represents the simplest model to describe the shear-rate dependent viscosity first proposed by Ostwald and De Waele [74] expressed as follows.

$$\eta(\dot{\gamma}, T) = a_T K (\dot{\gamma})^{n-1} \quad (2.7)$$

Where: ( $a_T$ ) is the shift factor that introduces to the power law for the nonisothermal flow to overlaid the temperature dependency of viscosity with the shear rate dependency. This value reduces to one in the case of the isothermal condition. The Power law index ( $n$ ), also known as the flow index, is a measure of the deviation of a fluid from the Newtonian or the non-Newtonian-ness. When ( $n$ ) = 1, the power law reduces the fluid into a Newtonian fluid. When  $n$  is in the range between 0 and 1, a fluid is categorized as a shear thinning fluid (pseudo-plastics), such as polymer melts. A fluid is categorized as a shear thickening fluid (dilatant fluids) when  $n$  is greater than 1. The consistency index ( $K$ ) is a measure of the

average viscosity of a fluid, and its value does not exceed the value for the viscosity at a shear rate of  $1 \text{ s}^{-1}$  [71].

The main shortcoming of this model is represented by its prediction ability being limited to a range of the shear rate. However, it is still used to describe the fluid behaviour because of its simplicity and its good prediction ability across the range of the shear rate to which the material parameters were fitted.

### 2.3.2 Cross model

The cross shear dependent model is often used for polymer processing modelling and flow simulation. It can give a good description of the viscosity curve shape at the Newtonian, the transition, and the shear thinning regions with three material parameters [75]. This model is written as follows [71].

$$\eta(\dot{\gamma}, T) = a_T \left[ \eta_\infty + \frac{\eta_o - \eta_\infty}{1 + \left( \frac{a_T \dot{\gamma}}{\dot{\gamma}_c} \right)^m} \right] \quad (2.8)$$

where:  $m$ ,  $\eta_o$ ,  $\eta_\infty$ ,  $\dot{\gamma}_c$  are the cross rate constant, the zero shear viscosity which is responsible for captures the low shear rate viscosity, the infinite-shear viscosity, which is responsible for captures the high shear rate viscosity, and the critical shear strain-rate at which the transient shear-thinning begins, respectively.

### 2.3.3 Carreau-Yassuda model

This model is also used to describe the shear-rate dependent viscosity in some kind of polymeric fluid. The typical variation of the viscosity with the shear rate of this model is presented in **Figure 2.3**.

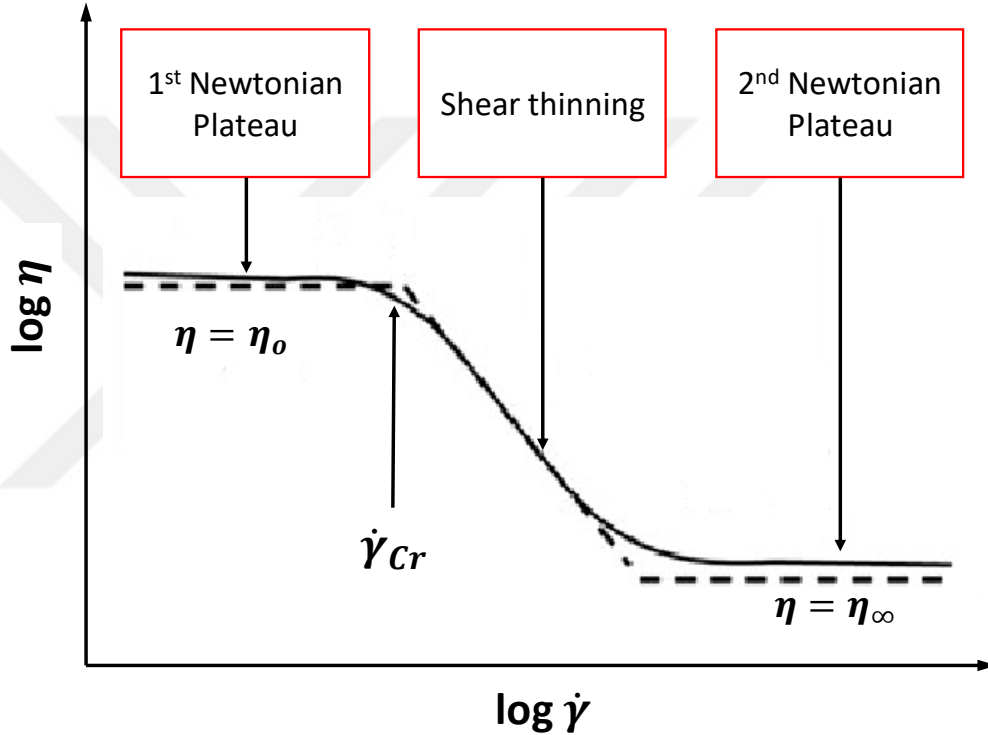


**Figure 2.3:** Typical viscosity curve vs shear rate fitted to Carreau- Yassuda Model (reproduce from style of [71]).

This model has a good ability to capture the viscosity function at both the low and the high shear rate, but with more expensive calculations. On the other hand, this model is unable to predict the elastic effect or normal stress difference as in the case of the other inelastic model [72]. The mathematical discretion of this model expressed by [71]:

$$\eta(\dot{\gamma}, T) = a_T \left[ \eta_{\infty} + (\eta_0 - \eta_{\infty}) \left[ 1 + (\lambda a_T \dot{\gamma})^a \right]^{\frac{n-1}{a}} \right] \quad (2.9)$$

The model includes five parameters, which have some physical meanings expressed by the infinite-shear viscosity; ( $\eta_{\infty}$ ) which capture the high shear rate plateau region, the zero shear rate viscosity; ( $\eta_0$ ) which captures the low shear rate viscosity, relaxation time  $\lambda$  which determine the shear rate at the end of low shear plateau viscosity, the power law index ( $n$ ) determine the slope of the linear portion of the curve and a shape parameter ( $a$ ) which is responsible for the transition portion between the linear and the upper plateau portion of the curve.

## ***2.4 Temperature dependency***

There are two main models described in the literature that represent the temperature dependency of the viscosity. The Arrhenius equation and the Williams-Landel-Ferry (WLF) models are well-known in the field of polymer processing and they are used to correct the viscosity with a temperature change. The Arrhenius model is preferred for the use in the case of temperature range higher than the glass transition temperature ( $T_g + 100$  °C). Meanwhile, the (WLF) model works better when the reference temperature is close to the glass transition temperature [71]. Arrhenius model expressed as:

$$\log(a_T) = \frac{E_a}{R} \left( \frac{1}{T} - \frac{1}{T_0} \right) \quad (2.10)$$

For the Williams-Landel-Ferry (WLF) model the mathematical description given by:

$$\log(a_T) = \frac{C_1(T-T_0)}{C_2-(T-T_0)} \quad (2.11)$$

In Eqs. (2.10 and 2.11),  $E_a$ ,  $T_0$ , and  $R$  are the activation energy, the reference temperature, and the universal gas constant equal to 8.314 [J/mol.K], respectively.  $C_1$  and

$C_2$  are the material parameters at a given reference temperature. The approximate values of  $C_1$  and  $C_2$  for polymer is 15 and 50 , respectively.

## ***2.5 Viscoelastic fluid***

Viscoelastic fluid is defined as the material that shows both the elastic behaviour of a solid and the viscous behaviour of the fluid. A typical example to explain this behaviour is by throwing silly putty (silicon material) onto the ground as it will bound like an elastic solid. In contrast, it will spread out onto a flat surface if one puts it on the ground for a long period of time and it will show a liquid like behavior. These two phenomena occur on a small time scale and a large time scale, respectively. Meanwhile, the silly putty shows mixed elastic-viscous behaviour at a moderate time scale. Such behaviour cannot be described by the generalised Newtonian fluid model, but needs a more complex rheological model. In the present work, the viscoelastic behaviour was investigated through the extrusion of the rubber compound in the capillary extrusion die. The stress response with the time after the step increase in the strain for the different class of materials, including a Newtonian liquid, Hookean solid, and viscoelastic liquid as illustrated in **Figure 2.4** [76].

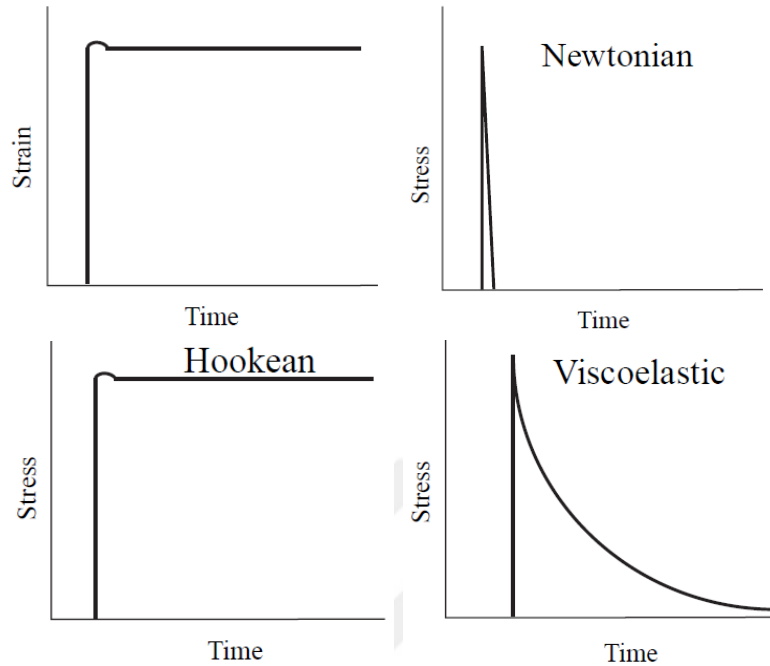


**Figure 2.4:** Response of stress after step strain for different material. ( reproduced from Macosko [76] ).

The interpretation of the stress response in **Figure 2.4** shows that for the Newtonian fluid, the stress response is proportional to the derivative of the strain thereby the stress diminishes as the strain becomes constant. Meanwhile, the stress response of the solid is directly proportional to the strain. In contrast to the Newtonian fluid, the viscoelastic material shows a stress response with time dependency and it needs some time to become fully relaxed.

The viscoelastic fluids show striking phenomena, which is qualitatively different from the Newtonian fluid. These flow phenomena are ubiquitous not only in rubber industries, but also in nature such as the blood flow in the human body and it is attributed to the evolution of normal stress within the viscoelastic fluid flow. Such well-known effects are:

## 1. Weissenberg (rod climbing) effect

This effect can be demonstrated by a rotating rod, where one end is inserted into the Newtonian fluid. The rotating of the rod in the Newtonian fluid such as water, will generate a centrifugal force (inertial forces), which leads to pushing the liquid away from the rod. By contrast, repeating the experiment with viscoelastic liquid such as polymer melts, generates tension forces (referred to as normal stress), which lead to a rise in the fluid on the rod surface. This effect is important in industrial mixing processes such as rubber compound mixing. **Figure 2.5** demonstrate these effects [77].

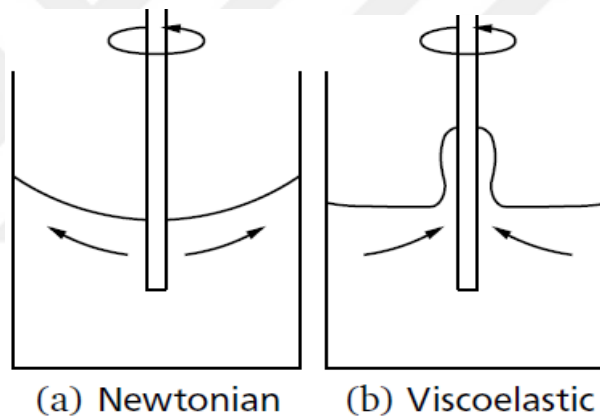


**Figure 2.5:** Weissenberg (rod climbing) effect [77].

## 2. Die swell

Die swell is another significant effect which generate normal stress during the flow of the viscoelastic fluid in the extrusion die. The transvers dimensions of the free jet at the die exit are usually not equal to the real dimension of the die due to this phenomenon. For the Newtonian fluid, the change in the dimension depends on the Reynold number. At a high Reynold number, the inertia effect will increase leading to a decrease in the diameter of the free jet; meanwhile, there is slight change in the diameter at a low Reynold number. When

the elastic effect is predominant, the fluid shows a remarkable increase in diameter at the die exit. See **Figure 2.6**. More interpretation of this behaviour can be explained by considering the evolution of tension forces due to the shear flow inside the pipe. As soon as these forces relax at the die exit, the free jet expands in the normal direction of the flow velocity (transverse direction) and shrinks in a longitudinal direction [78].

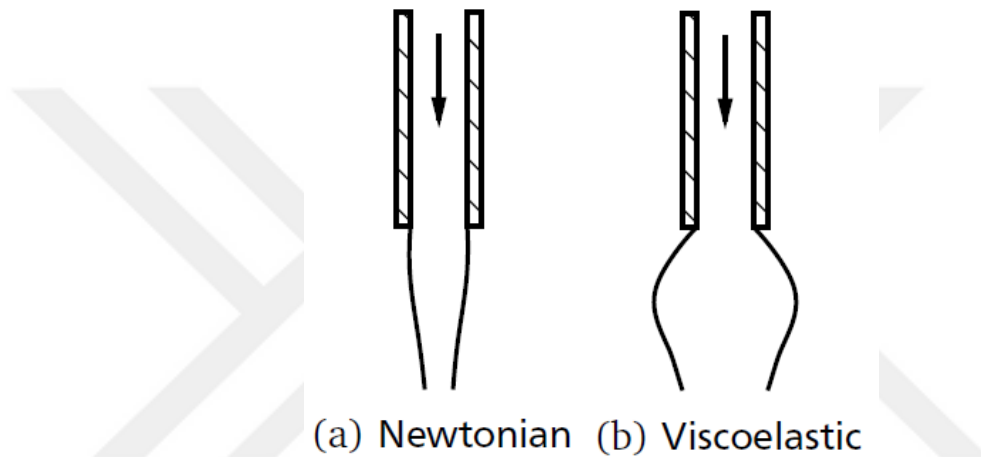


**Figure 2.6:** Die swell a-Newtonian fluid, b- Viscoelastic fluid (from style of Bird [78]).

### 3. Elastic recoil

Elastic recoil phenomenon is a dramatic mechanism occurring when cutting free stream flow down from the vessel containing the viscoelastic material. Consequently, the top part of the liquid recoils back into the container due to the elastic recoil effect.

### 4. Open siphon

When tilting a vessel containing the Newtonian fluid to a small angle, the liquid inside pours down from the vessel and the flow will stop when the level of the liquid surface coincides with the edge of the container as shown in **Figure 2.7 a**. By repeat this experiment



with viscoelastic material the flow will continue to empty the vessel as demonstrated in **Figure 2.7 b**.

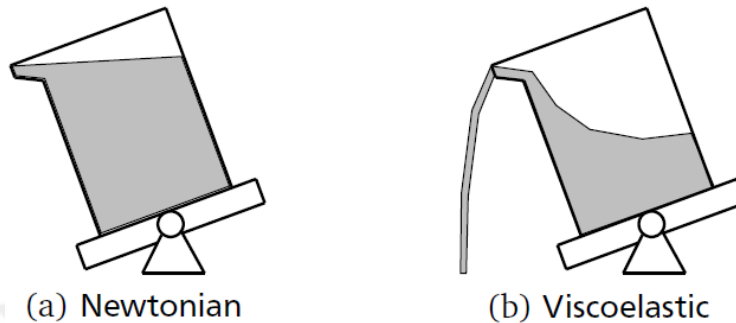


**Figure 2.7:** Open siphon for Newtonian and viscoelastic fluid [74].

When viscoelastic material such as polymer melts forced through extrusion die, it is deformed, both due to shear flow as a result of velocity gradient, and due to compression in convergent parts of the channel. Some of this deformation energy is stored elastically in the material which mean it will reverse when the melts leave the extrusion die. This phenomenon is known as “memory effect” as the melt seem to remember the deformation history. This memory effect characterized by relaxation time of material and the polymer melts retract partially if exhibiting “fading memory”. No memory appears in Newtonian fluid meanwhile elastic solid show perfect memory [79].

## ***2.6 Constitutive equations for viscoelastic fluid***

In the field of numerical computation, the balance between accurate results and computational cost always stands as primary target. From a physical point of view, sometime, the most appropriate model may not be suited well for numerical computations.

In general, the viscoelastic models for the polymer processing are classified into two categories namely, integral and differential models. Integral models offer the advantage of considering the past state of stress, but at the same time, this advantage also has difficulties associated with the increasing computation cost with keeping track of the past stresses history in the entire flow domain.

The most important integral model is the K-BKZ model, which was first introduced in 1963 by Bernstein et al.[80]. This model involves a finger strain tensor, a damping function and a time memory function. Numerous refinements were introduced to this model as presented by the work of Wagner [81, 82].

Differential models provide more advantages over integral models in terms of computation costs. This reduction in cost relies on the fact that computation only keeps the value of the variables at the current time step. This makes them easier to handle than the integral ones in the computing polymer flow problem; especially in complex geometry. The earliest model, known as the Maxwell model, was first proposed by James Maxwell in 1867. In this model, the viscoelastic elements are represented by the spring and damper connected in series. This model has some drawbacks such as a lack of fitting typical data, the predicted normal stresses independent on the shear rate. In addition, it does not represent the shear thinning behaviour well [83]. In 1950, the Maxwell model was extended by Oldroyd who presents the constitutive law through the concept of Oldroyd-B model, and added another damper connected in parallel to the Maxwell element [84]. This improvement allowed for the representation of creep and relaxation with reasonable accuracy in addition to improvements in numerical stability [85].

Phan-Thien and Tanner developed a new differential model in 1977 based on the network theory [86]. This model shows very good results in computing die swell in capillary die extrusion [37]. A more advanced model introduced later by Giesekus in 1982 was based on the Oldroyd-B model in which another material parameter known as ( $\alpha$ ) was introduced to account for the anisotropic movement of the molecules [87]. The model is excellent in describing shear flow behavior, but some deficiencies appear in the extensional flow [83].

### 2.6.1 Maxwell Model

A typical experimental method to quantify the viscoelastic phenomenon of the material is by measuring the stress relaxation after a step strain. Purely viscous fluid stress relaxes instantly, in contrast, no relaxation occurs for a purely elastic solid. Meanwhile, viscoelastic material shows a decrease in stress in an exponential fashion. The ratio between the stress and strain are defined by the relaxation modulus  $G(t, \varepsilon)$  expressed as [83].

$$G(t, \varepsilon) = \frac{T(t, \varepsilon)}{\varepsilon} \quad (2.12)$$

Since the Maxwell model is derived from linear viscoelasticity, the assumption implies that the relaxation modulus depends on the elapsed time and is independent of strain. The Maxwell equation is derived by representing the viscoelastic fluid via the series connection of a purely elastic spring and a purely viscous dashpot as shown in **Figure 2.8**.

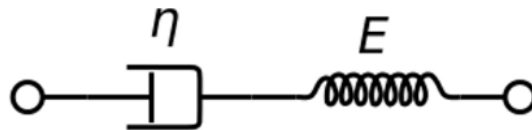


**Figure 2.8:** Maxwell element (reproduce from style of Pauli [88]).

The Maxwell model is constructed from a series of combinations of the Maxwell element. The stress in each element is equal and equal to the total stress; meanwhile, the total strain is obtained by the sum of the individual strain for each element.

$$T_S = T_D = T_{total} \quad (2.13)$$

$$\varepsilon_S + \varepsilon_D = \varepsilon_{total} \quad (2.14)$$

where the subscript S and D denoted the stress-strain in the spring and damper, respectively. Then, the Maxwell equation can be obtained by taking the time derivative and applying the basic relationship of the stress and strain.

$$T + \lambda \dot{T} = \eta \varepsilon \quad (2.15)$$

Equation (2.15) can extend to represent the nonlinear viscoelasticity by replacing the material time derivative with the upper-convected time derivative  $T^\nabla$  which is expressed as:

$$T^\nabla = \frac{\partial T}{\partial t} + v \cdot \nabla T - \nabla v \cdot T - T \cdot (\nabla v)^T \quad (2.16)$$

Then equation (2.15) can be written in the full tensor version to add the nonlinear effect to the Maxwell equation as:

$$T + \lambda T^\nabla = 2\eta D \quad (2.17)$$

Equation (2.16) is known as the upper-convected Maxwell equation, which implies that the stresses are generated by the deformed particle only, and that rotation is not sufficient to produce stress [83].

## 2.6.2 Oldroyd-B Model

The Oldroyd-B Model is represented by adding the second dashpot connected in parallel with the Maxwell element; therefore, it is regarded as an extension of the Maxwell model as shown in **Figure 2.9** [88].

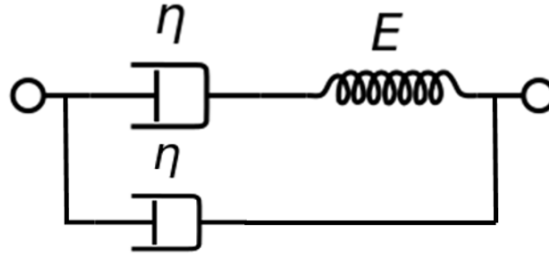


**Figure 2.9:** Configuration of Oldroyd-B model (reproduce from style of Pauli [88])

This model was basically developed for the macromolecules dispersed in the viscous solvent. However, it is possible to apply this model successfully to describe the single phase flow such as the polymer melts [79]. The model shows a good description of the viscoelastic fluid in the shear flow, but unphysical singularities appear in the extensional flow. In addition, the model is capable of describing the normal stresses under the constant shear, but shows a deficiency in modelling the shear- thinning behaviour [89]. This model is mostly applied to polymer melts of low concentration under the moderate shear rate. The addition of the solvent component of the stress improves the numerical stability [8].

Oldroyd derived his equation by splitting the extra stress tensor  $T_f$  into two components represented by the Newtonian or viscous part denoted by  $(T_2)$  and the viscoelastic (polymeric) part denoted by  $(\tau_1)$  as follows:

$$T_f = T_2 + \tau_1 \quad (2.18)$$

Where the viscous stress is given by:

$$T_2 = 2\eta_2 D \quad (2.19)$$

where  $\eta_2$  is the solvent viscosity, also known as zero shear rate dynamic viscosity, which can be constant or dependent on the shear rate and  $D$  is the rate of deformation tensor. The addition of the solvent component of stress improves the numerical stability [8]. The viscoelastic stress tensor is then obtained from the following equation.

$$\tau_1 + \lambda \tau_1^\nabla = 2\eta_1 D \quad (2.20)$$

where  $\eta_1$  and  $\lambda$  are the polymeric viscosity and relaxation time, respectively. The operator  $\nabla$  over  $\tau_1$  represents the upper convective time derivative. Then, the total stress experienced by the fluid particle through the deformation histories is calculated by the following equation.

$$\sigma = -p\mathbf{I} + T_f \quad (2.21)$$

The implementation of all viscoelastic constitutive models can be done by utilising the single mode or multi-mode; therefore, for the latter case (spectrum of  $N$  relaxation mode), the total viscoelastic stress is obtained as the sum of the contribution from each individual mode.

$$\tau_1 = \sum_{i=1}^N \tau_{1i} \quad (2.22)$$

### 2.6.3 Phan-Thien Tanner model

Phan-Thien Tanner model (PTT) model first proposed by Thien and Tanner [86] has been used extensively by many researchers to describe complex flow behavior of polymer melt and it show its excellent ability in practical application [90 – 92].

The first version of the PTT model presented in linear form is written as:

$$\left[ 1 + \frac{\epsilon_i \lambda_i}{\eta_{1i}} \text{tr}(\tau_{1i}) \right] \tau_{1i} + \lambda_i [\tau_{1i}^\nabla + \xi_i (\tau_{1i} \cdot D + D \cdot \tau_{1i})] = 2\eta_{1i} D \quad (2.23)$$

The second version (exponential PTT model) is found by placing the exponential factor on the first term as given by the following equation.

$$\exp \left[ \frac{\epsilon_i \lambda_i}{\eta_{1i}} \text{tr}(\tau_{1i}) \right] \tau_{1i} + \lambda_i [\tau_{1i}^\nabla + \xi_i (\tau_{1i} \cdot D + D \cdot \tau_{1i})] = 2\eta_{1i} D \quad (2.24)$$

where:  $(\epsilon_i)$  is the non-dimensional model parameter responsible for the elongation or extensional properties. This parameter also has a major impact on the circulation flow and vortex growth mechanism [37]. The model is reduced to the Johnson-Segalman model when  $\epsilon_i$  is zero.  $(\xi_i)$  is the non-dimensional model parameter responsible for the shear properties, and it also gives the combination of the lower-convected and upper-convected derivatives of the stress tensor and takes a value between 0 and 2 [71].

### 2.6.4 Giesekus Model

There was improvement in the Oldroyd-B model by adding a quadratic stress term in equation (2.20), and the new material parameter  $(\alpha)$  lead to a new model namely, the Giesekus model, which was first developed by Giesekus [87]. The new material parameter  $(\alpha)$  is introduced to trace the interaction between the individual molecule inside the fluid.

Consequently, it will enhance the anisotropic movement properties induced by the flow characteristics. Thus, it is also known as the mobility factor, that lie in the range between zero and one. Moreover, it is responsible for the nonlinearity in the Giesekus equation; this parameter also describes the shear thinning character of the viscosity [93]. The Giesekus model can describe the normal stresses in all directions extremely well, but it shows its prediction deficiency in the extensional flow. Further details about the properties of the Giesekus model are described in the original publication by Giesekus [94] and the book by Larson [95]. The Giesekus model in its tensor notation is expressed by the following equation:

$$\tau_{1i} + \lambda_i \tau_{1i}^{\nabla} + \frac{\alpha_i \lambda_i}{\eta_{1i}} \tau_{1i} \cdot \tau_{1i} = 2\eta_{1i} D \quad (2.25)$$

Where  $\lambda_i$  and  $\eta_i$  are material parameters representing the relaxation spectrum in the viscoelastic linear regime and denote the relaxation times and viscosity coefficients, respectively. The parameter ( $\alpha$ ) is the mobility factor which takes a value between 0 and 1. When  $\alpha$  take a value of 0, equation (2.25) reduces to the upper convective Maxwell model. It is important to mention that this single material constant is responsible for non-linearity of Giesekus constitutive model. The Symbols  $\nabla$  over the stress tensor is representing the upper convective time derivatives.

Equation (2.25) represent the multi- mode Giesekus model in its general form. It is worthy to mention that this Giesekus equation contains a quadratic stress term represented by,  $(\tau_1 \cdot \tau_1)$ , which apparently increase its ability to predict the viscoelastic material function of polymer melt. This non-linear term also seems to give more realistic experiments prediction of Giesekus model as compared with Oldroyd model.



The Single mode Giesekus model consider as a special case of the multimode Giesekus model in its general case. However, the multi-mode version is expected to predict the experimental data better than single-mode version as pointed out by the work of Bird et al.[78].

The expression of material functions steady-state shear flow, associated with shear viscosity  $\eta(\dot{\gamma})$  and normal stress difference  $N_1$  &  $N_2$ , were derived from Giesekus model as in the following [63].

$$\eta(\dot{\gamma}) = \frac{\eta_0(1-g)^2}{1+(1-2\alpha)g}, N_1 = \frac{(2\eta_0/\lambda)g(1-\alpha g)}{\alpha(1-g)}, N_2 = -(\eta_0/\lambda)g \quad (2.26)$$

$$\text{Where: } g = \frac{1-j}{1+(1-2\alpha)j}, j^2 = \frac{\sqrt{1+16\alpha(1-\alpha)\lambda^2 \dot{\gamma}^2}-1}{8\alpha(1-\alpha)\lambda^2 \dot{\gamma}^2}$$

Note that the material functions obtained from Giesekus model given by Eq. 2.26 do not show explicitly how  $\eta(\dot{\gamma})$ ,  $N_1$  and  $N_2$ , respectively, vary with shear rate ( $\dot{\gamma}$ ).

The Giesekus model is different from the other constitutive equations in that it can be considered as having molecular origin [63]. This property may be attribute to improve its ability in prediction flow behavior of polymer melt which directly linked to stretching and orientation of polymer chain. In addition, it shows excellent ability to describe normal stress coefficients, the growth of elongational viscosity, shear-thinning behaviour of viscosities and non-linear effects of the relaxation phenomena associated to transient flow. Therefore, this rheological model is considered a promising candidate to be able to predict the flow behaviour of polymeric material [93].

### 2.6.5 Pom-Pom model

The Pom-Pom molecular constitutive equation has been successfully applied for the modelling of entangled polymer melts such as low density polyethylene (LDPE). This kind of branched polymer shows very extreme strain hardening in the extensional rheology, while it has very shear thinning behaviour under shear rheology. Therefore, the Pom-Pom rheological model was first proposed by McLeish and Larson to work with the tube model for the entangled polymer melts [96]. This mathematical model represents the molecule of the polymer by a single backbone tube with internal dangling arms that pass through it with multiple branches emerging from each end. The structure describing the molecular structure of pom-pom family is depicted in **Figure 2.10**.

The structure of pom-pom molecule consists of 2 dangling arms and three branch emerged from each end of backbone. The stretch of backbone depends on variable  $\lambda(t)$  and the length of breached arm withdraw inside the backbone tube is defined by the variable  $S_c$ . Indeed, this complex structure computationally and rheologically can be exhibit improved formulation to deal with special nonlinear rheology of branched polymer melts [97].

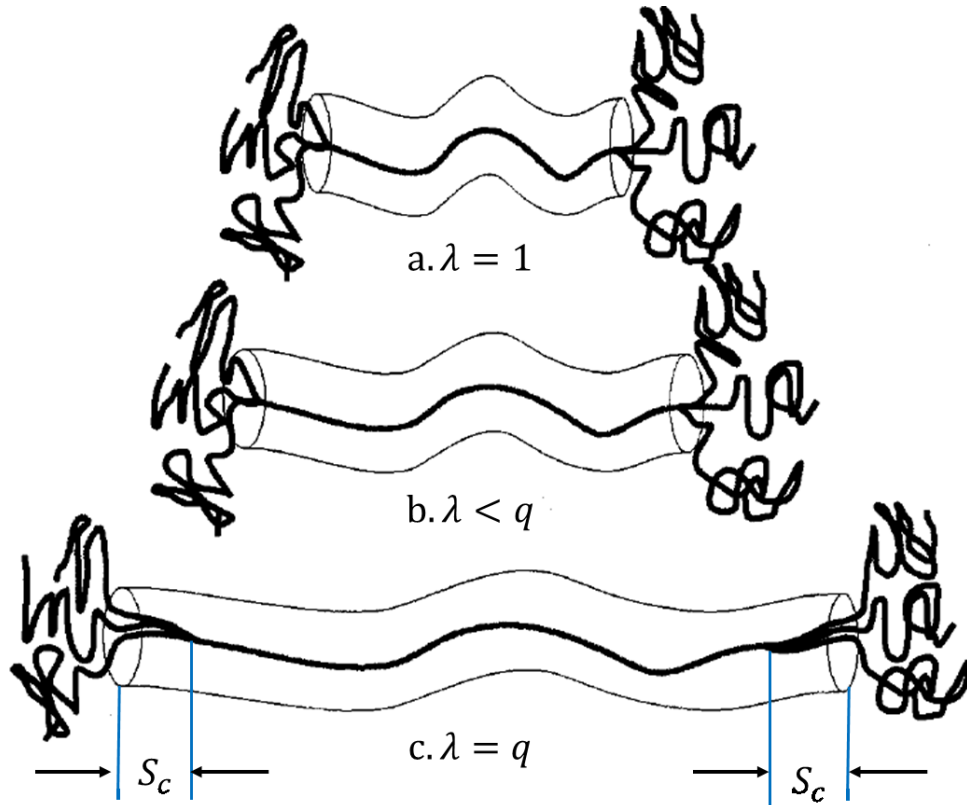


**Figure 2.10:** The structure of the idealised pom-pom molecule under various degrees of stretch. (From style of McLeish and Larson [96])

The single-mode version of the extended Pom-Pom model (XPP) expressed by the following equations.

$$f(\Lambda, \tau_1)\tau_1 + \lambda_b \tau_1^\nabla + G(f(\Lambda, \tau_p) - 1)I + \frac{\alpha_p}{G}(\tau_1 \cdot \tau_1) = 2\eta_0 D \quad (2.27)$$

The function  $f(\Lambda, \tau_1)$  is defined by the following equation.

$$f(\Lambda, \tau_1) = \frac{2}{\epsilon} e^{\frac{2}{q}(\Lambda-1)} \left(1 - \frac{1}{\Lambda^2}\right) + \frac{1}{\Lambda^2} \left(1 - \frac{\alpha_p \text{tr}(\tau_1 \cdot \tau_1)}{3G^2}\right) \quad (2.28)$$

where:  $\Lambda$  is the stretch factor of material and  $\epsilon$  is defined as the ratio of the relaxation time of the backbone stretch ( $\lambda_s$ ) to the relaxation time of the backbone tube orientation of the polymer ( $\lambda_b$ ) as express by the following equation:

$$\Lambda = \sqrt{1 - \frac{tr(\tau_1)}{3G}}, \quad \epsilon = \frac{\lambda_s}{\lambda_b} \quad (2.29)$$

where:  $G$ ,  $\alpha_p$ ,  $q$  are defined as the shear modulus, anisotropy parameter and number of arms on the polymer molecule, respectively.

## 2.7 Oscillatory Shear Flow

Oscillatory shear properties also known as dynamic viscoelastic properties have been widely used to describe the viscoelastic properties of polymer melts [98]. This measurement required an instrument that can imposed sinusoidal strain on the tested sample and record the stress output results from the deformed sample. For such purposes, RPA can be used especially for rubber compound testing (as will described in the next chapter). Under linear viscoelastic behaviour condition, the input sinusoidal strain signal will also generate a stress signal that vary in sinusoidal manner, but with out-of- phase angle as presented in **Figure**

### 2.11

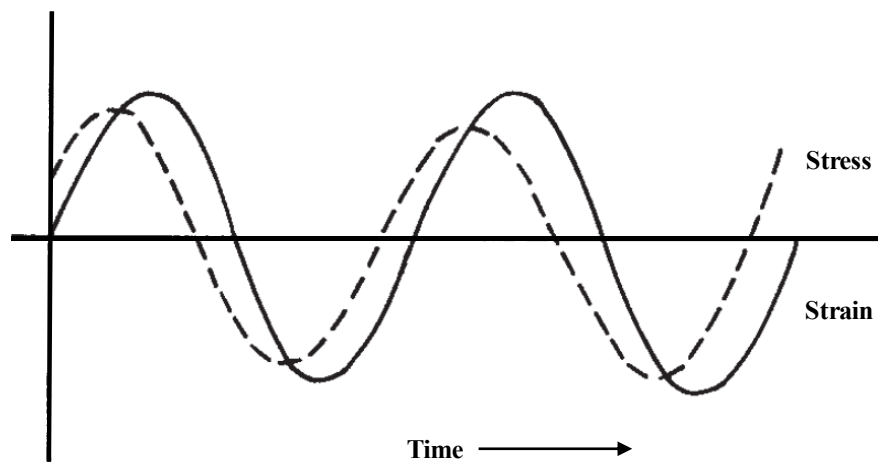


**Figure 2.11:** The sinusoidal imposed strain and the out-of-phase output stress response for linear viscoelastic fluid [63].

The representation of sinusoidal motion in complex domain can be used to defined the following quantities.

$$\gamma^*(i\omega) = \gamma_o e^{i\omega t} = \gamma'(\omega) + i \gamma''(\omega), \quad (2.30)$$

$$\sigma^*(i\omega) = \sigma_o e^{i(\omega t + \varphi)} = \sigma'(\omega) + i \sigma''(\omega), \quad (2.31)$$

Herein,  $\gamma_o$ ,  $\sigma_o$  and  $\varphi$  are the strain amplitude, stress amplitude and phase angle between strain and stress, respectively. The superscript prime represents the real part of this complex quantities and the double prime represent imaginary parts of associated complex quantities. In the above equations (2.30 and 2.31), the output response of complex stress  $\sigma^*(i\omega)$  is assumed to have similar angular frequency ( $\omega$ ) to the input strain variable  $\gamma^*(i\omega)$ . This assumption is true only when the fluid under test is a linear body. Complex fluid such as polymer melt would normally behave in a nonlinear manner, but it can display linear response in the range of small angular frequency ( $\omega$ ) [63].

The stress-strain relationship for purely elastic material (Hookean material, spring) and purely viscous Newtonian fluid (dashpot) can expressed as follows.

$$\sigma = G \gamma, \quad \sigma = \eta_o \dot{\gamma} \quad (2.32)$$

Where:  $\sigma$  is the stress,  $\gamma$ ,  $\dot{\gamma}$  are the strain and strain rate, respectively.  $G$  is the proportionality constant, called “elastic modulus”.

Under an oscillatory motion, by applying Eq. 2.30 and Eq. 2.31 in Eq. 2.32, one can derive the following expression for the complex viscosity and complex modulus.

$$G^*(i\omega) = \frac{\sigma^*(i\omega)}{\gamma^*(i\omega)} = G'(\omega) - i G''(\omega), \quad (2.33)$$

$$\eta^*(i\omega) = \frac{\sigma^*(i\omega)}{\dot{\gamma}^*(i\omega)} = \frac{\sigma^*(i\omega)}{i\omega \dot{\gamma}^*(i\omega)} = \eta'(\omega) - i \eta''(\omega), \quad (2.34)$$

$\eta^*(i\omega)$  in Eq. 2.34 can be expressed in term of  $G^*(i\omega)$  as follows.

$$\eta^*(i\omega) = \frac{G^*(i\omega)}{i\omega} = \frac{G''(\omega)}{\omega} - i \frac{G'(\omega)}{\omega}, \quad (2.35)$$

From Eq.2.35 and Eq. 2.34 we can find another expression for complex viscosity components as follows.

$$\eta'(\omega) = G''(\omega)/\omega, \eta''(\omega) = G'(\omega)/\omega, \quad (2.36)$$

Herein,  $G'(\omega)$  is associated with energy stored in the system and defined as dynamic storage modulus and normally have in-phase response.  $G''(\omega)$  is associated with the energy dissipated in the system as heat and defined as dynamic loss modulus. The real component (i.e., in-phase) of the complex viscosity is called the “dynamic viscosity” and  $(\omega)$  denotes the applied angular frequency.

The amplitude of oscillation  $\gamma_o$  and output stress amplitude  $\sigma_o$ , and phase angle ( $\varphi$ ) are normally measure by the device used in the test. Therefore, from oscillatory shear flow test at defined frequency the independent quantities associated with phase angle and amplitude ratio can be provided as in Eq.2.37.

$$|G^*(i\omega)| = \frac{\sigma_o}{\gamma_o} = \left[ (G'(\omega))^2 + (G''(\omega))^2 \right]^{1/2}, \quad \tan \varphi = G''(\omega)/G'(\omega) \quad (2.37)$$

Then, by using inverse relations, the two component of complex modulus can be written as:

$$G'(\omega) = \left( \frac{\sigma_o}{\gamma_o} \right) \cos \varphi, \quad G''(\omega) = \left( \frac{\sigma_o}{\gamma_o} \right) \sin \varphi, \quad (2.38)$$

Then, Eq.36 can be combined with Eq.38 to give the component of complex viscosity  $\eta^*(i\omega)$  as follows.

$$\eta'(\omega) = \left(\frac{\sigma_o}{\gamma_o}\right) [(\sin \varphi)/\omega] , \quad \eta''(\omega) = \left(\frac{\sigma_o}{\gamma_o}\right) [(\cos \varphi)/\omega] \quad (2.39)$$

The measurements of oscillatory shear flow properties of polymeric fluid give us sufficient information about both viscous  $\eta'(\omega)$  and elastic properties  $G'(\omega)$  of a complex fluid.

Small-amplitude oscillatory analysis can readily be applied to any nonlinear constitutive equation. For instance, applying the preceding analysis to Giesekus model yield the following equations [17].

$$G' = \sum_{i=1}^n \frac{\eta_i \lambda_i \omega^2}{1 + \lambda_i^2 \omega^2} , \quad G'' = \eta_o \omega + \sum_{i=1}^n \frac{\eta_i \omega}{1 + \lambda_i^2 \omega^2} \quad (2.40)$$

Herein,  $\eta_o$  is the solvent or Newtonian viscosity. The relaxation spectrum represented by the pairs of  $(\eta_i, \lambda_i)$  can be determined using the results of oscillatory shear measurement.

The formula in Eq.2.40 allow to decomposition of  $G'$  and  $G''$  into n contribution, each of them characterized by viscosity factor ( $\eta_i$ ) and relaxation time ( $\lambda_i$ ). The number n of individual modes is chosen to provide a good fit for the experimental data. Increase n will increase number of mode and lead to computational complexity. Therefore, the value of n should be chosen carefully. In this work, the Ansys Package was used to perform numerical fitting of oscillatory data and extracting viscoelastic model parameters. The third parameter of Giesekus model represented by mobility factor ( $\alpha$ ) is also extracted during fitting of shear viscosity expressed by Eq.2.26 with experimental data of steady shear viscosity.

## 2.8 Characteristic values

The viscoelastic behaviour can be quantified by utilizing two dimensionless characteristic numbers namely, Deborah number and Weissenberg number. The Deborah number  $D_e$  gives an indication of the expected degree of elasticity in the material and is defined by the ratio of the characteristic relaxation time  $\lambda$  and the characteristic time of observation  $\tilde{t}$  as follows [92].

$$D_e = \frac{\lambda}{\tilde{t}} \quad (2.41)$$

Very low Deborah numbers occur with a long observation time which promote fluid like properties (viscous fluid), whereas a short observation time leads to very high Deborah numbers consequently, solid properties are dominate [90].

The Weissenberg number indicates the strength of the viscoelastic material or Non-Newtonian behaviour and is defined by the relationship between the elastic forces to the viscous forces [73].

$$W_i = \lambda \dot{\gamma} \quad (2.42)$$

An increase in the Weissenberg numbers leads to an increase in the nonlinearity in the material behaviour; consequently, numerical difficulties also arise and in such situations one needs to be satisfied with the ability of the constitutive equation to describe the flow behaviour.



## 2.9 Conservation equations

For modelling fluid flow in the framework of continuum mechanics, the constitutive equation described in the previous section is coupled with the governing equations (field equations), which are represented by three basic conservation laws, conservation of mass, momentum, and energy. The balance of the mass is expressed by the following.

$$\frac{\partial \rho}{\partial t} + \nabla \cdot (\rho v) = 0, \quad (2.43)$$

where:  $\rho$  and  $v$  is the density (mass per unit volume) and continuum velocity vector, respectively. The change in linear momentum with respect to time written as:

$$\frac{\partial(\rho v)}{\partial t} + \nabla \cdot (\rho v \cdot v) = \nabla \cdot \sigma + f_b, \quad (2.44)$$

where:  $f_b$  is the body forces per unit volume acting on the continuum.  $\sigma$  is the total stress tensor, which can express for the fluid in terms of the normal stresses (pressure contribution to stress) and shear stresses as given in equation below.

$$\sigma = -pI + T_f \quad (2.45)$$

where:  $p$ ,  $I$  and  $T_f$  are the pressure, identity tensor, and extra stress tensor, respectively [72].

Then the combined Eq. 2.44 and Eq.2.45 gives.

$$\frac{\partial(\rho v)}{\partial t} + \nabla \cdot (\rho v \cdot v) = -\nabla \cdot (pI) + \nabla \cdot T_f + f_b \quad (2.46)$$

The symmetric properties of the stress tensor are valid for the conservation of the angular momentum therefore, in the present case  $\sigma = \sigma^T$  [71].

The energy equation applied for the modelling non-isothermal fluid flow is to account for the temperature change in the flow domain due to viscous dissipation. The standard form of energy equation is derived when applying the first law of thermodynamics to the control volume, which is written as:

$$\rho C_p \left( \frac{\partial \hat{T}}{\partial t} + (v \cdot \nabla) \hat{T} \right) = \nabla \cdot \kappa \nabla \hat{T} + \psi, \quad (2.47)$$

where:  $\rho$ ,  $C_p$ , and  $\kappa$  are the material density, heat capacity, and thermal conductivity, respectively, and  $\nabla$  represents the Hamilton differential operator.  $\hat{T}$  is the temperature, and  $\psi$  is the viscous dissipation term, which can be expressed in terms of the stress tensor and the rate of deformation tensor based on a previous study [91].

$$\psi = \tau : D \quad (2.48)$$

The first term on the right-hand side of Eq.2.47 represents the thermal diffusivity, and the second term is the viscous dissipation term that generates the heat along with the fluid flow. This frictional heat will change the temperature and velocity field of the flow.

## ***2.10 Finite element formulation***

The finite element method FEM provides a powerful tool to predict the complex flow behaviour for both the Non-Newtonian and the viscoelastic fluid. This approach is applied to predict the velocity, pressure, and polymeric stress by solving the conservation laws of the flow field coupled with a specified constitutive equation, which is adopted to describe the physics of the flow. In this section, the strategies of applying the mixed FE approach on the Giesekus rheological model as a typical example will be described to provide full insight into this procedure and the effect of the elasticity on flow field. Through this approach different

techniques were employed such as the Stream-Upwinding-Petrov-Galerkin (SUPG), the Galerkin and Newton linearisation finite element procedure to capture the real behaviour of the flow domain [99].

For the Newtonian fluid it is easy task to incorporate the stress field into momentum equation to yield satisfactory seen form of the Navier-Stokes equations. However, this is not the case when dealing with viscoelastic fluid which need to special separation treatment of the rate-of-strain tensor and extra stress tensor.

The main difficulty in solving the viscoelastic constitutive equation arises from its high convective character of stress evolution. However, some reductions in these difficulties can be achieved with the addition of the Newtonian solvent in the EVSS formulation. In addition to the non-linear feature of the viscoelastic equation, other difficulties are introduced with the arising advection term when performing discretisation. These properties make a strong argument for solving the stress and velocity in a coupled manner with a computational approach. The above feature of the viscoelastic fluid flow makes computation of this kind of flow extremely difficult to handle without special stabilisation strategies as described in the following sections.

### **2.10.1 Elastic-Viscous-Split-Stress (EVSS) Formulation**

The EVSS formulation of the Giesekus model is derived based on the change of variables as follows. The elastic stress for Giesekus model is defined as:

Recall the definition of Newtonian fluid constitutive equation as:

$$\tau_f = \eta(\nabla v + (\nabla v)^T) \quad (2.49)$$

where  $(\tau_f)$  is the total extra stress,  $D = (\nabla v + (\nabla v)^T)$  is the rate of the strain tensor.  $(\eta)$  is the viscosity. Eq.2.25 associated with constitutive equation of Giesekus model can be expanded by substituting the upper convective time derivative as given by the following equation.

$$\tau_1 + \lambda_1 \left( \frac{\partial \tau_1}{\partial t} - \nabla v^T \cdot \tau_1 - \tau_1 \cdot \nabla v \right) + \alpha \frac{\lambda_1}{\eta_1} \{ \tau_1 \tau_1 \} = \eta_1 (\nabla v + \nabla v^T) \quad (2.50)$$

For the viscoelastic model, the total extra stress tensor  $(T_f)$  decomposed to polymeric stress tensor  $\tau_1$  and solvent viscous stress tensor  $T_2$ . Then the EVSS formulation gives:

$$\tau_f = T_1 + \eta_1 D \quad (2.51)$$

$$\left. \begin{aligned} T_1 + \lambda_1 (T_{1(1)} - (1 - \beta)\eta D_{(1)}) + \alpha \frac{\lambda_1}{(1 - \kappa)\eta_1} \{ T_1 \cdot T_1 \} - \alpha \lambda_1 (T_1 \cdot D + D \cdot T_1) + \\ \alpha \lambda_1 (1 - k)\eta D \cdot D = 0 \end{aligned} \right\} \quad (2.52)$$

where:  $\beta = \lambda_2/\lambda_1$  is the ratio of the retardation time to the relaxation time;  $k = \eta_2/\eta$ ,  $\eta_1$  is the polymeric viscosity,  $\eta_2$  is the solvent viscosity and  $\eta = \eta_1 + \eta_2$  is the total viscosity.

## 2.10.2 Computational formulations

The weight residual method is utilised to drive the weak forms of the mass, the momentum and the constitutive equations. The Streamline-Upwinding-Petrov-Galerkin (SUPG) [100] approach was used as a weighting function for the constitutive equations to account for the stabilization of the polymeric stress and the presence of the convective term. Meanwhile, the rate of strain, the momentum and the continuity equations are weighted by

the Galerkin weighting function. The details of these methods are presented next. The weight residual method was applied to solve the finite element equation through the following steps.

1. All the flow variables were replaced by a new approximate finite element variable and then the residuals of the equations were obtained.
2. The value of the residuals multiplied by the appropriate weighting function and then integrated over the element domain.
3. The divergence theorem was applied to the total stress term in the momentum equations to find the weak form by reducing the order of the integration.
4. Impose the boundary conditions.
5. Use Newton method to linearize the system.
6. Obtain the stiffness matrix of the total elements and right hand vector.
7. Assemble the final stiffness matrices of the system.

Apply step 1 and 2 to average momentum equations, we found the equation below:

$$\int_{\Omega} \left[ \nabla P - \nabla T_1 - \eta \nabla^2 v - \eta \nabla \cdot \nabla^T v + \rho_f \frac{\partial v}{\partial t} \right] w_m d\Omega = 0 \quad (2.53)$$

Let  $\sigma$  represent the total stress tensor where  $\sigma = P\delta - T_1 - \eta(\nabla v + \nabla^T v)$ ,  $\delta$ ,  $w_m$  are the unit tensor and the weighting functions. Then, the implementation of the 3<sup>rd</sup> step on the total stress field gives:

$$\int_{\Omega} \nabla \cdot (\sigma w) d\Omega = \int_{\Omega} (\nabla \cdot \sigma) w d\Omega + \int_{\Omega} \sigma \nabla w d\Omega \quad (2.54)$$

$$\int_{\Omega} \nabla \cdot (\sigma w) d\Omega = \int_{\Omega} (n \cdot \sigma) w d\Gamma \quad (2.55)$$

Now, applying the divergence theorem or the Green theorem gives:

$$\int_{\Omega} \nabla \cdot \sigma w d\Omega = - \int_{\Omega} \sigma \cdot \nabla w d\Omega + \int_{\Gamma} (n \cdot \sigma) \cdot w d\Gamma \quad (2.56)$$

Finally, the desired result of the weak form is produced by using the homogeneous boundary condition as given by:

$$\int_{\Omega} (\nabla \cdot \sigma) w d\Omega = - \int_{\Omega} \sigma \cdot \nabla w d\Omega \quad (2.57)$$

Now, imposition step 1 and 2 on the rate-of-strain tensor and continuity equations give the following equations.

$$\int_{\Omega} \left[ D - \frac{1}{2} (\nabla v + \nabla^T v) \right] \cdot w_d d\Omega = 0 \quad (2.58)$$

$$\int_{\Omega} \left( \frac{\partial u}{\partial x} + \frac{\partial v}{\partial y} \right) w_p d\Omega = 0 \quad (2.59)$$

where:  $w_d$  and  $w_p$  are the weighting functions corresponding to the rate-of-strain tensor and pressure field, respectively. Then for the constitutive equation we get;

$$\int_{\Omega} \left[ T_1 + \lambda_1 \left( \frac{\partial T_1}{\partial t} + 2\eta(1 - \beta) \frac{\partial D}{\partial T_1} \right) + \alpha \frac{\lambda_1}{\eta_1} \{ (T_1 + 2\eta(1 - \beta)D)(T_1 + 2\eta(1 - \beta)D) \} \lambda_1 [(v \cdot \nabla)(T_1 + 2\eta(1 - \beta)D) - (T_1 + 2\eta(1 - \beta)D) \cdot \nabla v - \nabla v (\nabla v)^T (T_1 + 2\eta(1 - \beta)D) \cdot \nabla v - (\nabla v)^T (T_1 + 2\eta(1 - \beta)D)] \right] \cdot w_s d\Omega = 0 \quad (2.60)$$

### 2.10.3 Newton's Linearization Method

The final set of Partial Differential Equations(PDF's) represent the mathematical model of a physical process. Theses set of equation given in its general form as follows.

$$\frac{\partial u}{\partial t} = F(u(x, t)) \quad (2.61)$$

where:  $u(x, t)$  ,  $x$  ,  $t$  ,  $F$  are the vectors of field variables, the position vector and the time and nonlinear differential operator, respectively. The initial condition at  $t = 0$  and the boundary conditions are imposed to define the above equation on the domain  $\Omega$  . for the unsteady state of the solution required for the full simulation in space and time. While , for the steady state, the time derivative is zero; therefore, only spatial simulation for  $F(u(x)) = 0$  is required. The finite element/Newton algorithm was used successfully to obtain the solution of the complicated rheological model including the viscoelastic fluid flows [101].

After the discretisation of partial differential equation and imposing boundary conditions with finite elements, the results obtained represent nonlinear system of algebraic equations are written as follows.

$$F(u(x)) = 0 \quad (2.62)$$

The Newton's method is used to solve this non-linear set of algebraic equations through iteration and applying the equations as follows.

$$F_u^k \delta u^k = -F^k, \text{ and } u_u^k = u^k + \delta u^k \quad (2.63)$$

where:  $F_u^k$  is the Jacobian matrix at step  $k$  with entries  $\{F_u^k\}_{ij} = (\partial F_i / \partial u_j)^k$ , and  $\delta u^k$  is the correction vector to the solution at step  $k$ .



## **CHAPTER III**

### **EXPERIMENTAL SET UP**

#### ***3.1 Introduction***

In this chapter, the die design and experimental work on an extrusion line together with the instruments used for the characterizing rheological behaviour are presented and described. The data collected from the experiments will be used to validate the numerical results obtained from the simulation. Some measured data from the experiments are further analysed using the Ansys Software Package to extract the model parameters required for the simulation. The underlying physics behind the rheological testing are also explained.

#### ***3.2 Die design***

The experimental rubber extrusion die was initially designed to include six separate disk parts, which were stacked on top of each other to construct the assembled die. This approach in die manufacturing is purely used to simplify the manufacturing process for the complex geometry. This die is especially designed to analyse and to be able to understand the pressure drop and temperature gradient along the flow channels. Thus, the die is manufactured to facilitate reading and to minimize the shape effects of the die on the reading. However, in the present case, the extrusion die can be subdivided into three sections: the inflow straight channel, the bended section, and the distribution section. The inflow channel serves as the connection to the extruder head and the grantee for the pre-distribution of the compound. The bend part is used to analyse and understand the effect of bending on the pressure and temperature field. The distribution part is responsible for directing the flow in

a smooth contraction to form the final shape at the die exit without the layer separation or circulation flow. Therefore, the extrusion die plays a major role in product quality. The proposed design does not include the parallel zone at the die exit as is used in the traditional extrusion die design.

The general rules which should be consider in die design for rubber extrusion industries includes the following.

1. Minimize the sharp edge to eliminate dead spots in corners and maintaining steady shear history and heat flow distribution.
2. Minimize the tensile stress at die exit which can lead to some defect such as melt fracture or sharkskin at extrudate surface. This is important to minimize the distortion of streamline in flow domain.
3. Increase the die length to extend the process time which assists to eliminate memory effect of earlier deformation history in extruder screw.
4. The total processing time at specific temperature should not exceed the curing time of material to prevent premature vulcanization or gelation inside the die. This processing time is depending on both die design and extrusion speed.
5. Easy assembly and disassembly
6. Maintain steady increase in velocity along the flow channel.

Based on the above rule the basic parts of the die were designed utilizing Solid work software. The extrusion die is installed with three transducer sensors (for pressure and

temperature measurements), which are placed through the screwed holes in the die body as shown in **Figure 3.1**.

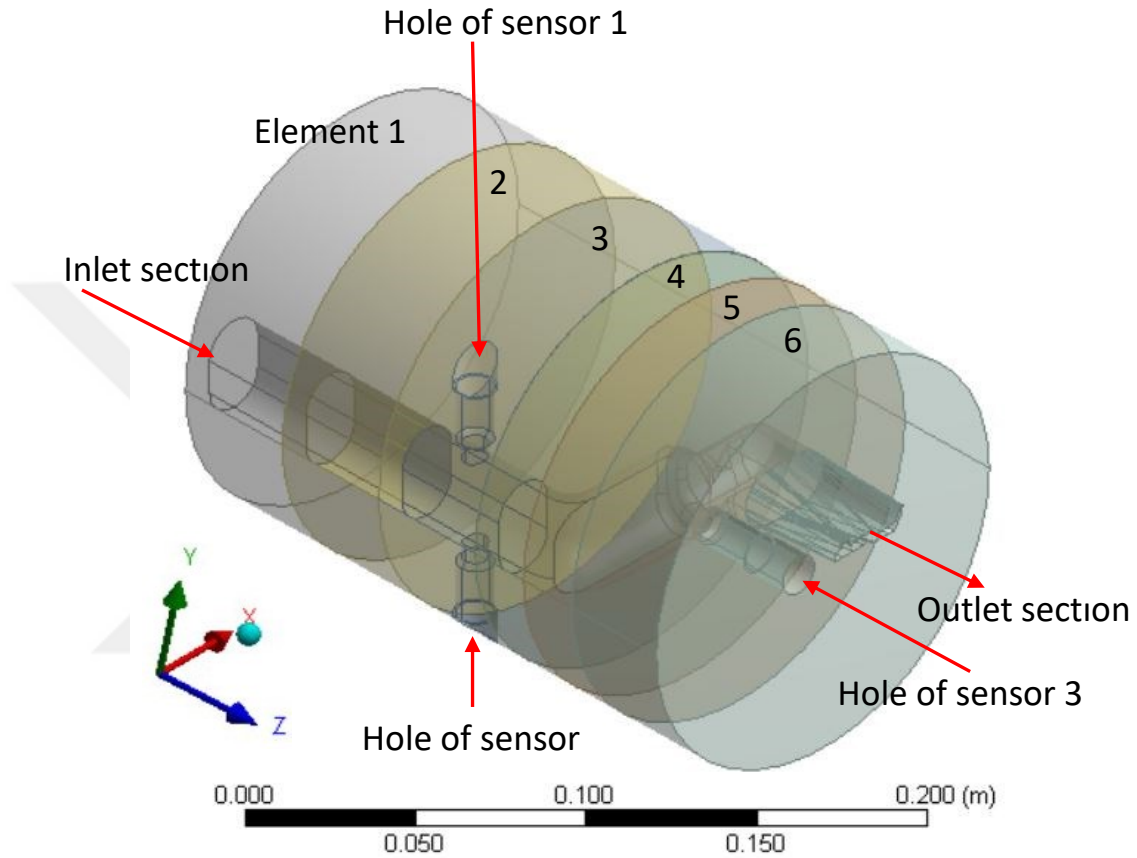


**Figure 3.1:** Schematic isometric view of the assembled extrusion die (with permission and courtesy of Standard Profil A.S./Düzce).

The special transducers sensors received from (Gefran SPA company/Italy) were used to measure the pressure and temperature simultaneously at the same location inside the die. These sensors were specifically designed to be used in high temperature environment and large-scale stationary industrial tool, for instance, extruder head or polymer extrusion die. In addition, these kind of sensors characterised by the ability to read temperature up to 400 °C and supported by fluid-filled system to assures the temperature stability. The physical

quantities of pressure and temperature are transformed to electrical signal based on hydraulic transmission and strain-gauge technology. Therefore, these series of sensors are specially used for research and development purpose according to the European Directive 2011/65/EU.

The first and second transducers are located opposite to each other for cross-checking of the validity of the reading. The third transducer is located on the right face of the channel after the 90° elbow to determine the effects of the elbow on pressure drop. The actual die parts were fabricated from **Nimax Steel**, which was provided by Uddeholm (Turkey). Computer-controlled non-traditional and traditional machining methods were applied to fabricate the die parts.

EDM (electric discharge machining) is a nonconventional manufacturing process, which is specifically used for the machining of high-hardness materials, such as extrusion moulds. In this process, the desired shape of the product is obtained using an electric spark (electrical discharges) as the cutting tool. Filing is a material removal process used mostly in the finishing operation on a wide range of materials, such as extrusion moulds. This operation helps achieve the final product with the required surface finish by removing excess materials. Detailed information about this manufacturing process can be found in the reference book of Stephen et al.[102].

### ***3.3 Extrusion experiments***

The extruder head supplies the die with a melt flow at sufficiently high temperatures, and is homogeneous, and pulsation free. The melt flow is then reshaped into the required profile dimensions with the extrusion die. In the final step of the weather strip industries, the

output profile from the extrusion die is directed by a puller system to pass through a long vulcanisation unit at which additional heat is applied to complete the curing of the product and give it its final functional properties. Additional details about the basic polymer extrusion process can be found in previous studies [45,46]. The manufactured extrusion die was mounted onto a single-screw extruder head as shown in **Figure 3.2** to conduct the extrusion experiments in a real extrusion line.

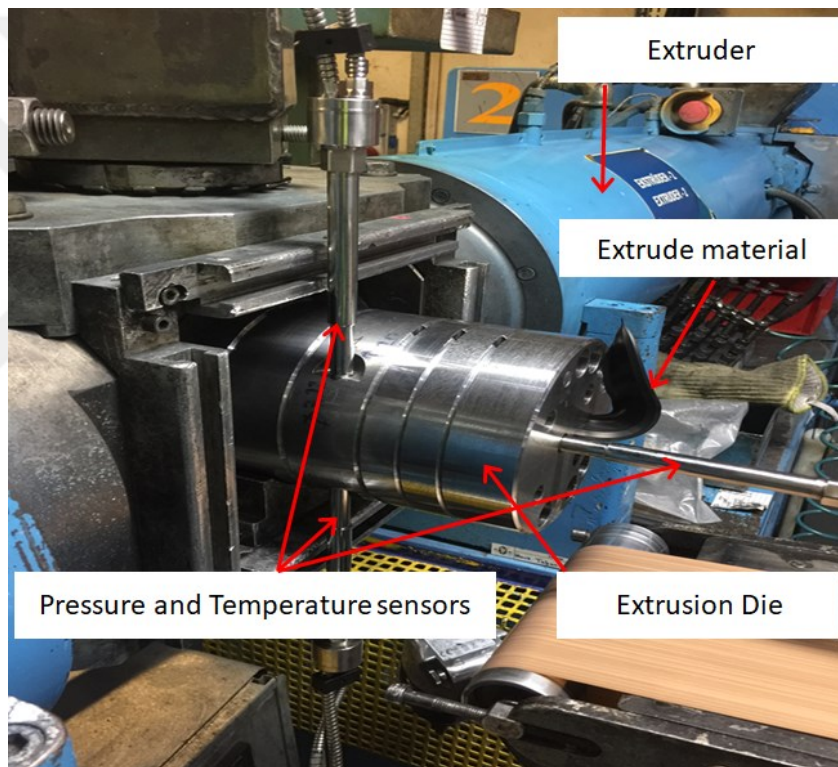


**Figure 3.2:** Extrusion die mounted on a single-screw extruder in an industrial extrusion line.

To investigate the effect of the extruder's speed on the rheological behaviour of the rubber compound, the extrusion experiments were conducted at three extrusion speed. The temperatures and pressure from the sensors were recorded at three extruder speeds: 10, 15, and 20 rpm. For each speed, the corresponding mass flow rate was measured by marking a

sample of the extrudate for the specific time and weighing of that sample. The signal from the sensors additionally process with the data acquisition device which records the output signal of the pressure and temperature as shown in **Figure 3.3**. The measured signal contains some peak values at the start of each speed. This indicates that some time is required to reach a stable response. The mean value is then taken from the most reasonable stable range as shown in **Figure 3.3**.

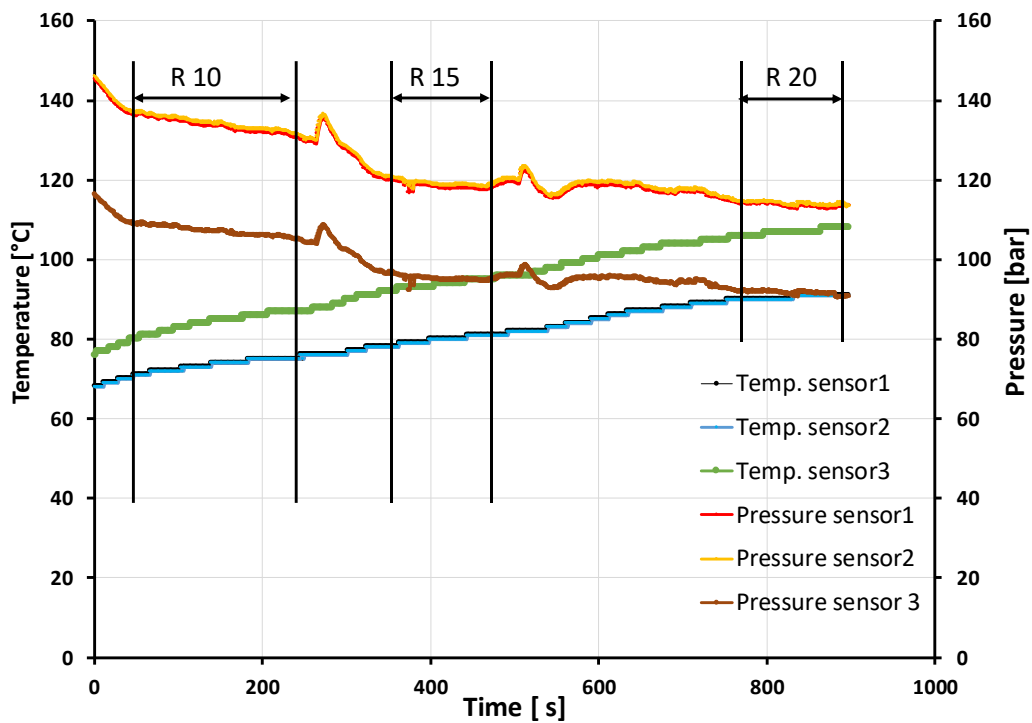


**Figure 3.3:** Measured signal of temperature and pressure from sensors (R10-extruder speed10, R15-extruder speed15,R20-extruder speed=20 rev/min).

The temperature on the surface of the steel die was measured using a Testo 925 ( from Testo Inc. Germany) temperature measuring instrument depicted in **Figure 3.4**. This digital portable device was specially designed to measure surface temperatures in a wide range up to 1000 °C with an accuracy of ( $\pm 0.5^{\circ}\text{C} + 0.3\%$  of a reading) [103]. The temperature on the

surface of the die was measured at three points and the average value ( $T_{average}$ ) was taken. The average temperature value thereby was used to evaluate the local convective heat transfer coefficient, which is required for calculating the total heat flux across the thermal boundary (as will be described in detail in the following chapter).



**Figure 3.4:** Portable surface temperature measurement instrument.

### ***3.4 Material and rheological testing***

The EPDM rubber blend used in this study was provided by the Standard Profile Company (Turkey). Some ingredients are normally added to the compound to improve its processing behaviour and curing characteristic. The detailed formulation is stated in **Table 3-1**.

**Table 3-1:** Formulation of the EPD Rubber/Carbon Black Compounds.

<b>Ingredient</b>	<b>Amount (Phr)</b>
EPDM Rubber	100
Carbon Black(CB)N230	30
Natural Silica	4.57
Whiting	8.57
Paraffinic Processing Oil	11.71
Zinc oxide	3.07
Stearic acid	5
S (sulphur)	3

The rheological characterisation of the unvulcanised EPDM rubber compound was performed with a Rosand RH7 capillary rheometer (Malvern Instruments, UK). The standard bore diameter and length were 15 and 290 mm, respectively. The capillaries of a 1 mm diameter and different lengths were used for the Bagley correction [104]. The shear rate at the wall of the capillary for the non-Newtonian fluid was corrected based on the Rabinowitsch correction [105,106].

The capillary tests were conducted at temperatures of 60°C, 80°C, and 100°C within the shear rate ranges of 10 – 284.39 and 10 – 1000 s<sup>-1</sup> to investigate the effect of temperature dependence. The experimental data was fitted with the power law model and the Arrhenius relationship with the ANSYS Polymat Package as shown in **Figure 3.5**. The thermal capacity was measured at 100°C by differential scanning calorimetry [107], and the thermal conductivity was determined with the Hot Disk TPS-2500 at 100°C [108]. The physical and rheological properties of the rubber compound used in this study are presented in **Table 3-2**.



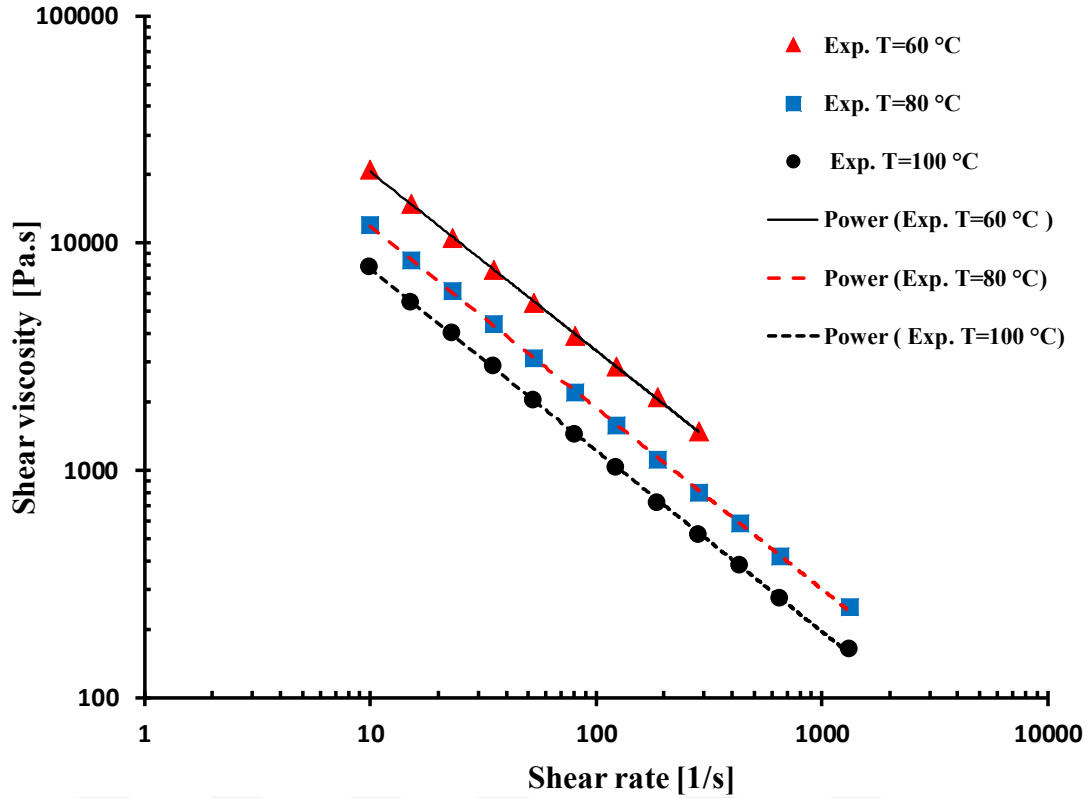


**Figure 3.5:** Viscosity against the shear rate of the rubber compound at 60°C, 80°C and 100 °C

**Table 3-2:** Physical and rheological properties of the EPDM rubber compound.

Rheological and Physical properties		Unites	
Consistency index,	$K$	[Pa.s <sup>n</sup> ]	110750
Power law exponent,	$n$	-	0.29
Reference temperature,	$T_o$	[K]	351
Activation energy,	$E_a$	[J.kmol <sup>-1</sup> ]	979
Universal gas constant,	$R$	[J.mol <sup>-1</sup> .K <sup>-1</sup> ]	8.314
Melt density ,	$\rho$	[kg.m <sup>-3</sup> ]	1297
Thermal conductivity,	$\kappa$	[W.m <sup>-1</sup> .K <sup>-1</sup> ]	0.38
Specific heat,	$C_p$	[J.kg <sup>-1</sup> .K <sup>-1</sup> ]	1290

### 3.5 Rubber process analyser tests

The rubber process analyser (RPA 2000, from Alpha Technologies Co., UK) is a dynamic mechanical analyser used in major topic applications to characterise dynamic

properties, rheological properties, curing properties and the network structure of raw elastomers and un-vulcanized rubber. In addition, it has been used to characterise the blending of different elastomers, dispersion and molecular weight distribution [109].

The rubber process analyser was designed to solve many problems associated with the testing of uncured rubber samples by using other conventional rheometric devices such as the effect of the slip. To reduce the slip effect, this device was equipped with a grooved surface's cavity of two biconical dies as shown in **Figure 3.6**.

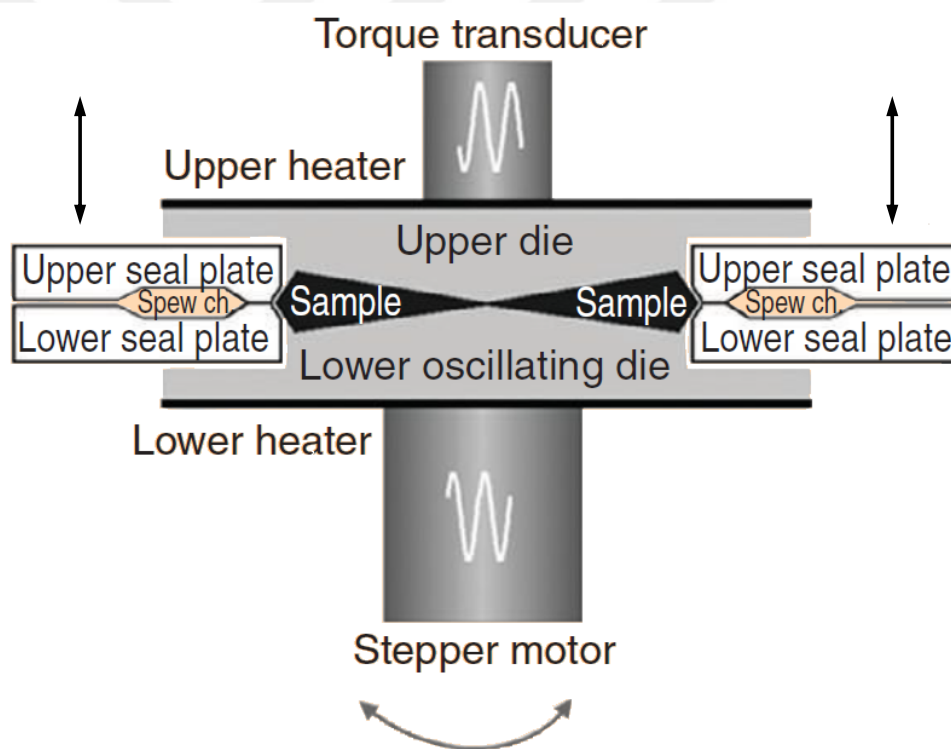


**Figure 3.6:** Biconical die configuration for RPA 2000 [110].

The closed cavity in **Figure 3.6** was designed to form a sample with a thin cross section and large surface area to minimize the thermal gradient and maximize the heat transfer from the die surface to the test sample. This special design cavity has the advantage

of producing uniform, rapid, and accurate heating of the sample during testing [110]. The lower die of the cavity mould is connected on the same axis with the direct drive motor's system. The motor's system uses position control with a high resolution (0.0005 degree of arc) integral position encoder. The position control can test the high range of the oscillation angle (from 0.02 to 90 degrees) and has a high frequency range of about 2 to 2000 cycles per minute.

The combination of high frequency and large angle give the maximum limit of shear rate of about 30 [1/s] [110]. The heating in the device supported with a digital temperature control algorithm to increase the accuracy of the measurements.

The outer edge of the closed cavity contains two seals, which function to completely seal the sample under high pressure. The sample is prepared by weighting or cutting a specific volume, which should exceed the cavity volume (between 5 and 6 cm<sup>3</sup>) to be sufficient for the test. After a sample is placed on the lower die (see **Figure 3.7**), a constant pressure is imposed by the movement of the upper die down to form the sample geometry inside the cavity mould. The high pressure imposed on the sample, which reaches 3.5 MPa helps to prevent slippage during the test. The controlled frequency and strain is imposed on the lower die by imposing the oscillatory sinusoidal signal, which is generated from the driving motor system. This torque signal will transmit to the upper die through the rubber specimen enclosed in the cavity. Then, the output signal is measured by a torque transducer attached to the upper die [110]. The above feature of the RPA, which can work in both a dynamic and relaxation mode, gives it specific characteristics, which are different from other conventional rheometers.

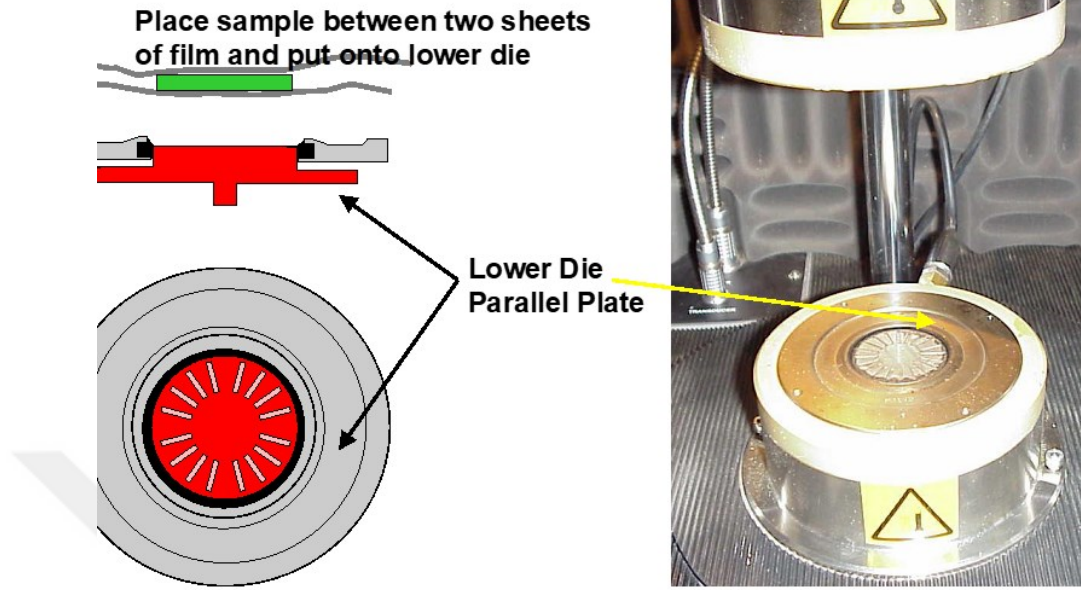


**Figure 3.7:** Preparation test specimen using rubber process analyser [110].

### 3.5.1 Viscoelastic properties

Advance calculations based on the Fourier transformation were used with built-in software of RPA 2000 to separate the measured output signal of the torque from the RPA into the elastic and viscous components as shown in **Figure 3.8**. The elastic torque  $S'$  represents the torque signal which is in a phase with an imposed strain. While, the viscous torque  $S''$  represents the torque signal that is  $90^\circ$  out of the phase with an imposed strain,  $\varphi$  is the phase angle shift [110].

The imposed strain and cavity dimensions are used to convert the output complex torque  $S^*$  to the complex modulus  $G^*$  by using the flowing rheological equations.

$$S^* = \frac{2\pi r^3 G^* \phi}{3\theta} \quad , \quad \text{The strain for biconical specimen } \gamma = \phi/\theta, \quad (3.1)$$

where:  $\phi$  is the oscillation angle,  $\theta$  is the biconical angle=0.1251 rad, and  $r$  is the die radius equal to 20.63 mm [110]. The analysis of oscillatory shear measurements described in preceding chapter (chapter II) was used to determine the other viscoelastic material variables.

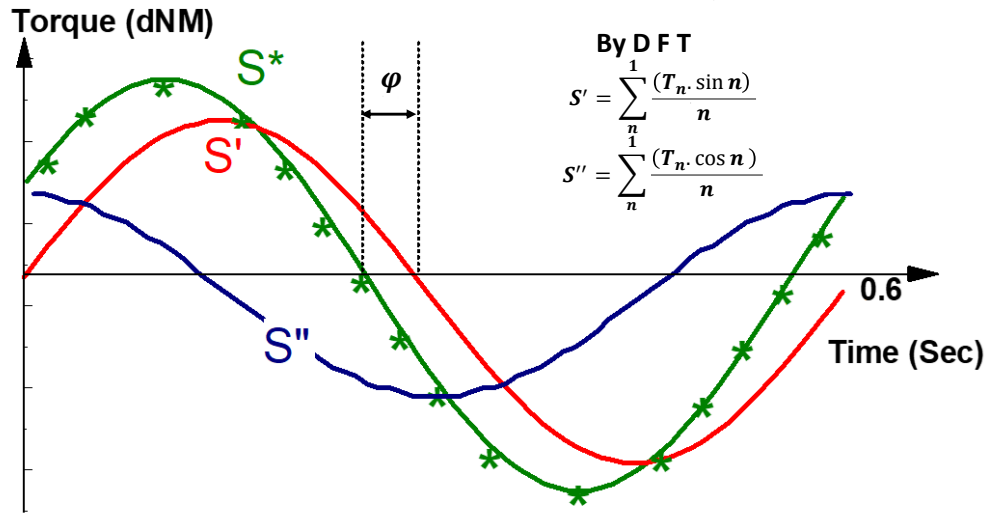


**Figure 3.8:** Discrete Fourier Transformation to access the real elastic and imaginary viscous phase[110].

To measure the viscoelastic properties of the rubber compound firstly, the RPA was used in shear-strain-controlled modes to identify the domain of the linear viscoelastic regime [11]. The measured material functions in terms of storage  $G'$  and loss modulus  $G''$  as a function of a strain as illustrated in **Figure 3.9**. The strain sweep was conducted at a constant frequency and temperature of  $f = 0.3 \text{ Hz}$  and  $100 \text{ }^\circ\text{C}$ , respectively.

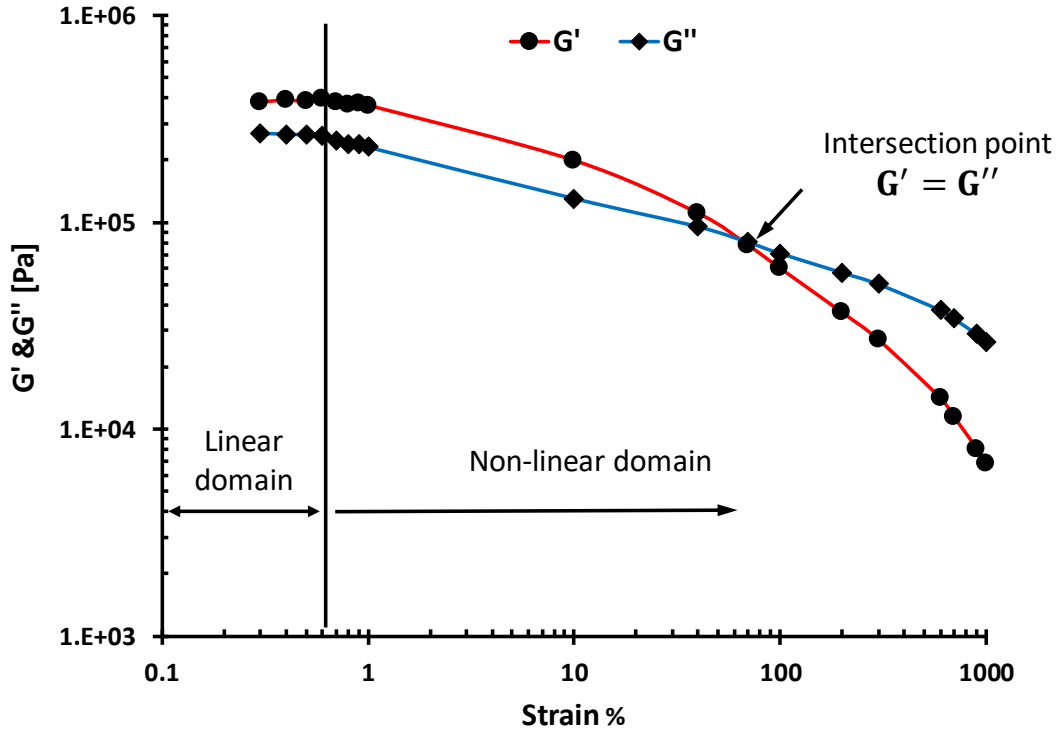


**Figure 3.9:** Shear modulus in strain sweep at 100 °C to find linear and No-linear domain.

Since the material used in this study was carbon black filled elastomers, the transition region from the linear to non-linear regime was greatly affected by the filler volume fraction [11]. However, in the present case the transition region appeared with an approximate 0.5 % strain as shown in **Figure 3.9**.

According to the ASTM D6204 standard [111], the frequency sweep tests were conducted over a range of frequencies (2.049-225.45) rad/s at constant strain ( $\gamma^o = 0.3\%$ ) with a temperature of (100) °C. The results obtained in terms of the material functions' shear modulus and viscosity are depicted in **Figure 3.10**.

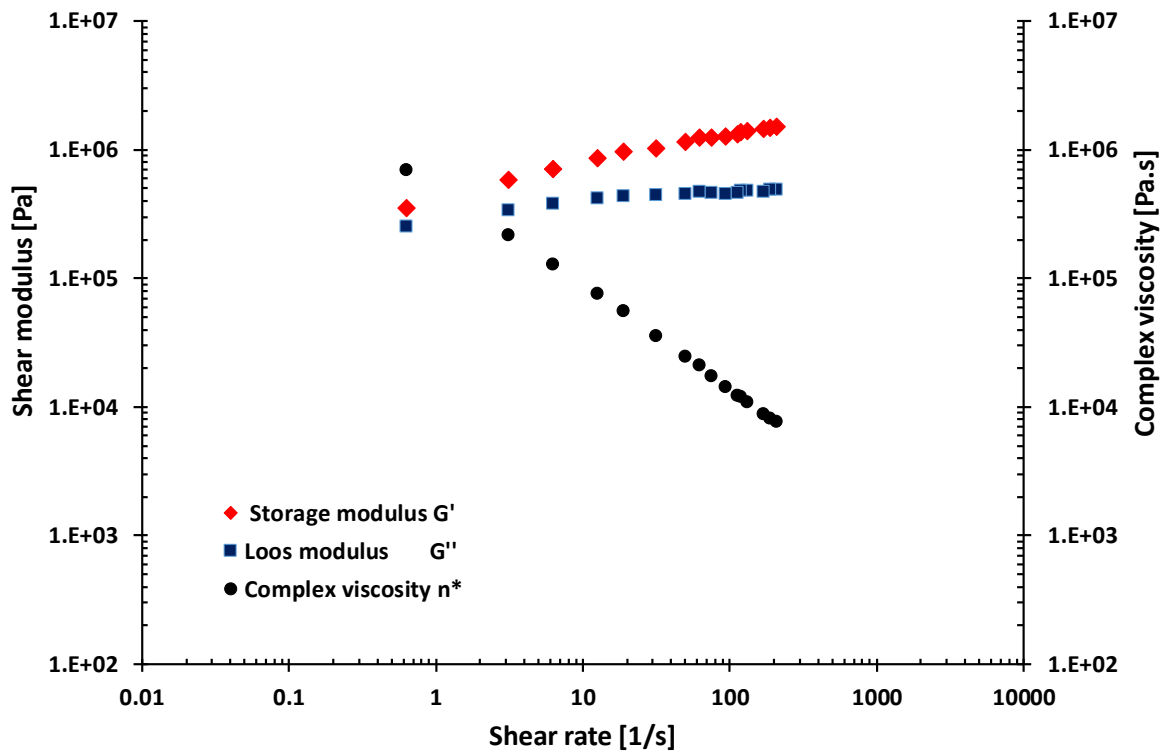


**Figure 3.10:** Frequency sweep at constant temperature (100°C) and strain amplitude.

The numerical fitting of the experimental data with the Giesekus model was performed as depicted in **Figure 3.11** utilizing the Ansys Package to extract the viscoelastic model parameters. The Giesekus model parameters extracted from the fitting are presented in the Table 3-3.

**Table 3-3:** Giesekus model parameters for EPDM rubber extracted from numerical fitting.

Mode number	Relaxation time $\lambda$ [s]	Giesekus, Mode1	Giesekus, Mode2	Giesekus, Mode3
		Parameter: $\eta, \alpha$	Parameter: $\eta, \alpha$	Parameter: $\eta, \alpha$
3- Mode	Min $\lambda = 0.0036$ Mid $\lambda = 0.018$ Max $\lambda = 0.09$	$\eta = 8.341617$ $\alpha = 0.7259203$	$\eta = 10.85195$ $\alpha = 0.745459$	$\eta = 1015.515$ $\alpha = 0.4288714$

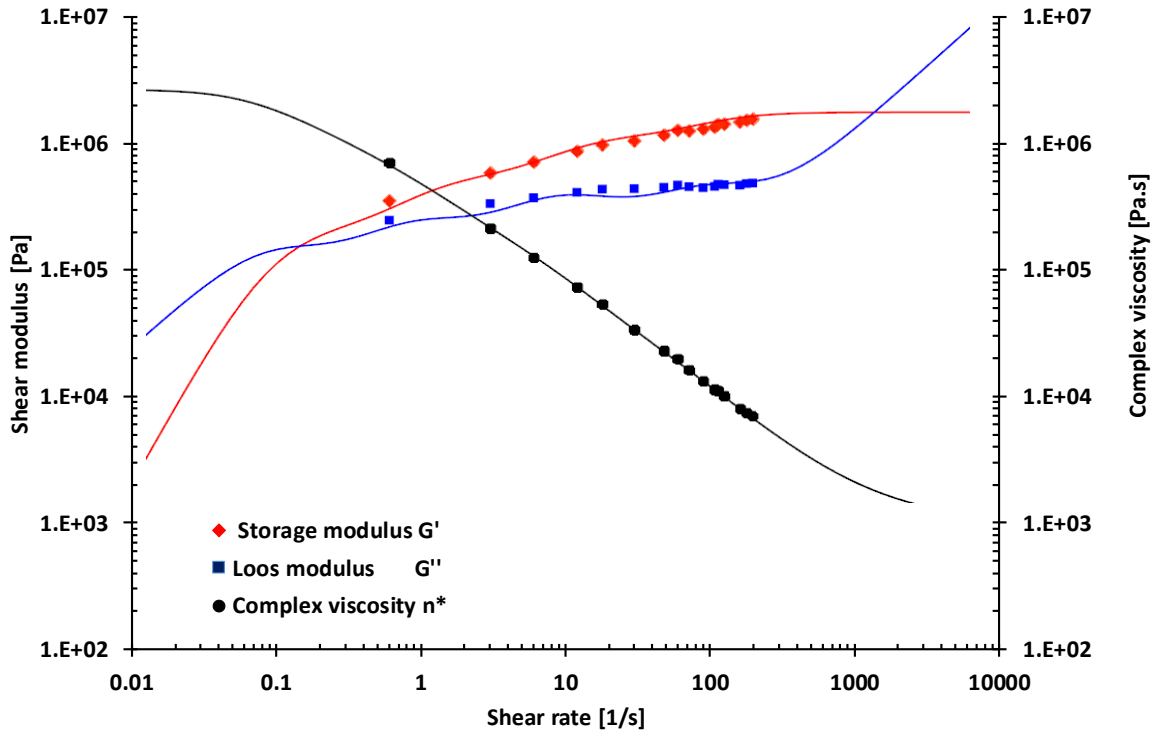


**Figure 3.11:** Fitting experimental data of EPDM rubber to Giesekus rheological model.

### 3.5.2 Curing test

During the production of the highly reactive materials, such as EPDM rubber, finding the less reactive condition in the extrusion to avoid the risk of degradation or curing inside the die due to the rise in temperature is important. The curing characteristics were investigated using a rubber process analyser (RPA 2000). The constructed rheometric curve at a temperature range of 120 °C–150 °C (with 10 °C step increment) as depicted with the semi-log scale is presented in **Figure 3.12**.

The vulcanisation curves represent the fingerprint of the curing and processing behaviour of the compound. RPA is a rotorless oscillatory shear rheometer, which is especially designed for testing raw elastomer and their compounds to reduce the effect of slip



and difficulties associated with high viscosity [112]. All tests were conducted at a specific range of temperature by using a frequency of 1.6667 Hz and a decimal fraction of strain of 0.14 (equivalent to 100 cpm and  $0.5^\circ$  arc, respectively).

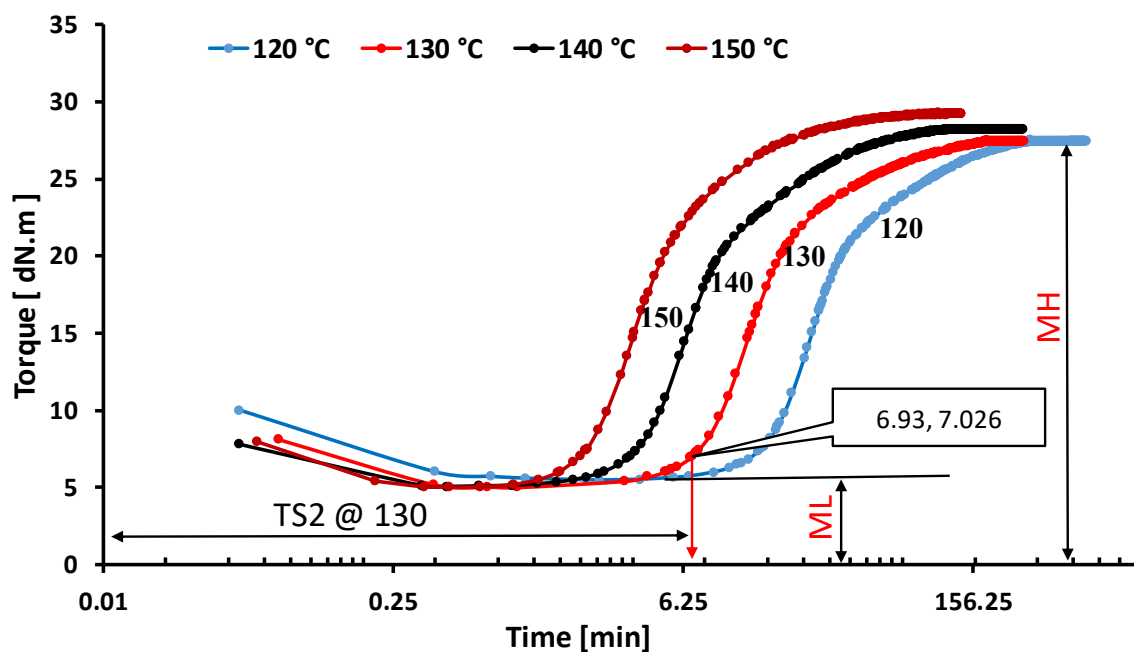


**Figure 3.12:** Cure curves obtained from the RPA2000 for the rubber compound at 120 °C, 130 °C, 140 °C, and 150 °C.

According to the testing standard, the scorch time value associated with TS2 is defined as the time to achieve a 2-unit increase in torque from the minimum torque (ML). For instance the scorch time at temperature of 130 (TS2@130) is equal to 6.93 min as shown in **Figure 3.12**. Meanwhile, the optimum curing time (T90) is defined as the time required to reach 90% of the maximum torque (MH) [110]. For the test at minimum temperature, the total experiment takes a time of 9 hours. The test time was decreased with increase in test temperature as shown in **Figure 3.12**. Detailed information about the vulcanisation characteristics and testing method can be found in the reference book of [113].

# CHAPTER IV

## NUMERICAL SIMULATION SET UP

### ***4.1 Introduction***

Computational fluid dynamics is a powerful tool used in modelling the complex flow in the extrusion die. Through this analysis, the rheological field variable which includes, velocity, pressure, temperature, and residence time, can be monitored and analysed. Those rheological parameters have a great impact on the finished product quality and at the same time, this data is important in die design engineering. Due to the high nonlinearity of the rubber compound which arises from the shear thinning behaviour of the viscosity or temperature dependency, numerical simulation is considered to be a difficult task. Numerical simulations are widely used for complex processes, such as polymer processing, instead of analytical calculations.

The numerical simulations of the complex fluid flow problems are based on the solution of the main governing equations which are coupled with a suitable constitutive equation to describe the flow of the melt rubber. In addition, a suitable initial and boundary condition should be imposed.

In this study, the STAR-CCM + Package was utilised to solve these equations. This chapter focuses on the numerical simulations applied to the models using STAR-CCM+. In addition, the mesh and all the essential physical processes, which included the solving of both pure viscous model and viscoelastic model being introduced. The description of the geometry, the mesh construction and boundary condition are presented in this chapter.

The entire volume of the flow domain was extracted from the previously designed CAD model of the die. Extensive work utilizing the SpaceClaim and Star CCM+ package was performed to repair some faults in the extracted volume, which is primarily required for a successful mesh operation. The industrial-scale geometry and boundary condition illustrated in 4.1, the total length of the industrial scale extrusion die was 195.2 mm and the total height was 95 mm. The other irregular dimension is described in **Figure 4.1**.

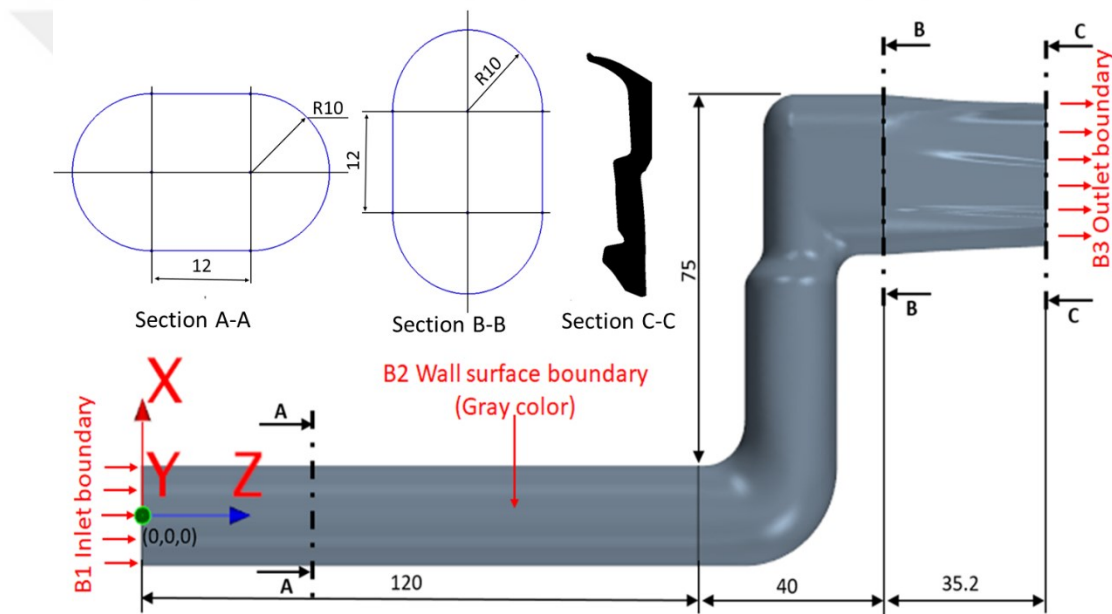


**Figure 4.1:** Geometry and boundary conditions of the flow domain. (all dimension in mm).

The field equations coupled with the constitutive equation of the inelastic viscosity model should be solved under a suitable flow and thermal boundary conditions. The atmospheric pressure of 1 bar is imposed as the initial condition on the inlet and outlet boundary denoted by B1 and B3, respectively. The mass flow rate and inlet temperature imposed at the inlet boundary B1 for the various extruder speeds described in **Figure 4.2**.

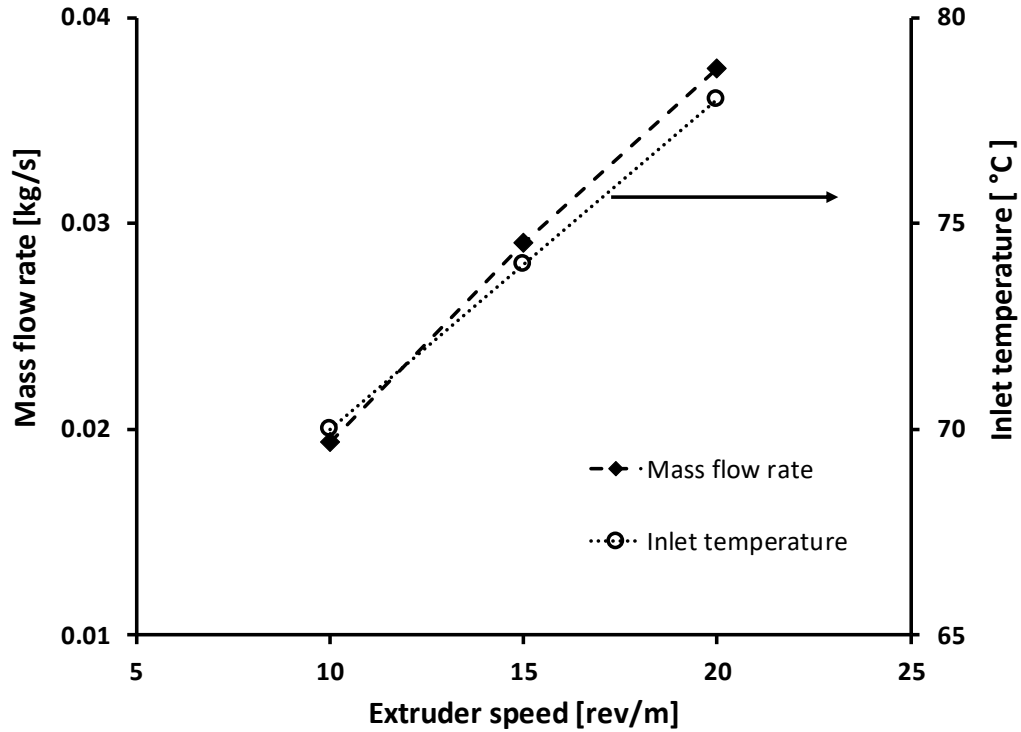


**Figure 4.2:** Mass flow rate and temperature at extruder head versus extruder speed.

A no-slip boundary condition with a constant heat flux was imposed on the outer surface of the die wall as denoted by B2. For the inlet and the outlet boundaries (represented by B1 and B3 in **Figure 4.1**), a fully developed flow and pressure outlet were imposed, respectively as used in a previous study [57]. This assumption implies that all the derivatives normal to these boundaries are zero, except the pressure gradient which took a constant value. The velocity profile at the inlet boundary will be calculated from the mass flow rate which was imposed on the inlet boundary [114]. The adiabatic thermal conditions were imposed on the outlet boundary denoted by B3. The flow and thermal boundary conditions of the flow domain are presented in **Table 4-1**.

**Table 4-1:** Flow and thermal boundary conditions.

Surface boundary	Imposed conditions
Inlet section B1	Fully developed Constant temperature
Outer surface B2	No-slip Constant heat flux
Outlet section B3	Pressure outlet Adiabatic $DT/dz = 0$

For a suitable choice of the thermal boundary conditions on the outer boundary B2, we conducted a numerical experiment by imposing adiabatic thermal boundary conditions. The numerical experiment overestimated the experimental temperature data. In this regard, a suitable heat flux should be imposed on boundary B2. Accordingly, the heat transfers from the external surface boundaries (BS2 and BS3) were calculated using the natural convection theory for the cylindrical shape of the steel die as shown in **Figure 4.3**

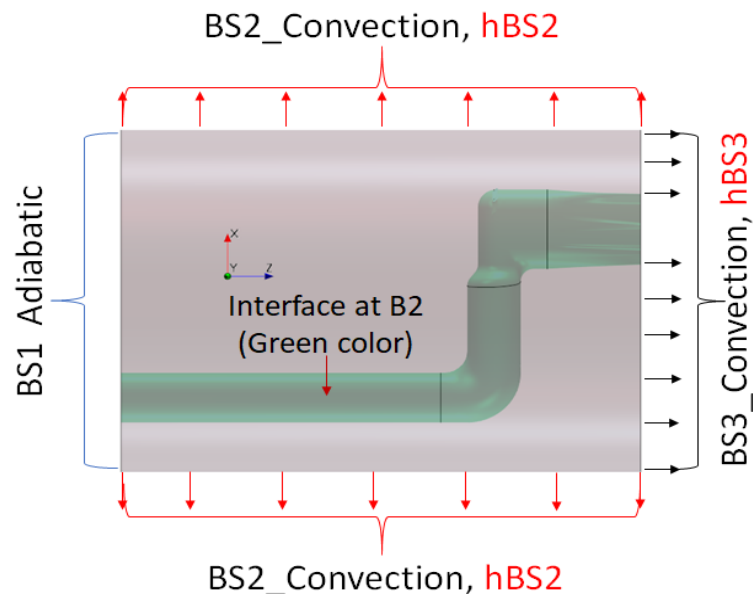


**Figure 4.3:** External thermal boundaries of the steel die and interface boundary.

For the external boundary BS2, the value of the local convective heat transfer coefficient was calculated by simplifying the geometry to the horizontal pipe flow. By using this assumption, the local heat transfer coefficient  $h_{BS2}$  was calculated by applying the natural convection theory for the horizontal aligned hot pipe flow, while for the other external surface boundary BS3, the shape was simplified to a vertical plate. According to the heat balance equations, the amount of the heat flux across the interface (the surface boundary B2 in **Figure 4.3** was equal to the heat flux across external boundaries (BS2 and BS3) of the steel die. The total heat on the outer surface was calculated assuming a constant temperature on the die surface and the convection mechanism was predominant (i.e. radiation is neglected). The surface temperatures were taken as an average value from the three measurements of the surface temperatures on the outer surface boundary BS2 as shown in **Figure 4.4**. This assumption relies on the condition of the high thermal conductivity of the steel. The detail of the applied empirical equations for the manual calculation of the local convective heat transfer across the external boundary BS2 and BS3 are presented in the Appendix.

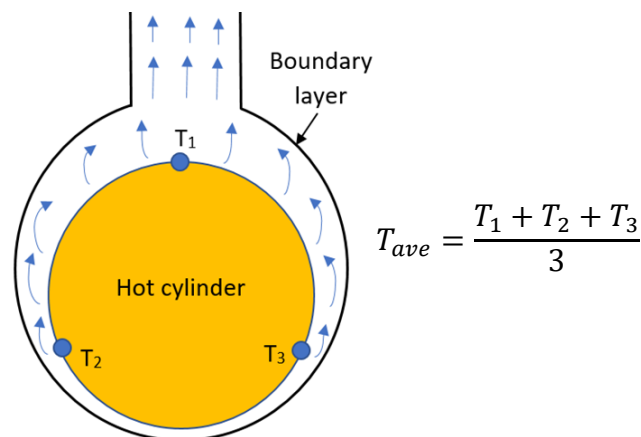


**Figure 4.4:** Side view of hot cylinder with boundary layer flow due to natural convection.

The following equation was used to calculate the total heat loss out of external boundaries (BS2 and BS3) [115]:

$$\dot{Q} = h A_s (T_s - T_\infty) \quad (4.1)$$

where  $h$ ,  $A_s$ ,  $T_s$ , and  $T_\infty$  are the heat convection coefficient, the surface area, the surface temperature, and the air surrounding temperature, respectively.

The calculated convective heat transfer coefficients on the external boundaries and the total heat flux at the interface boundary B2 are presented in **Figure 4.5**.

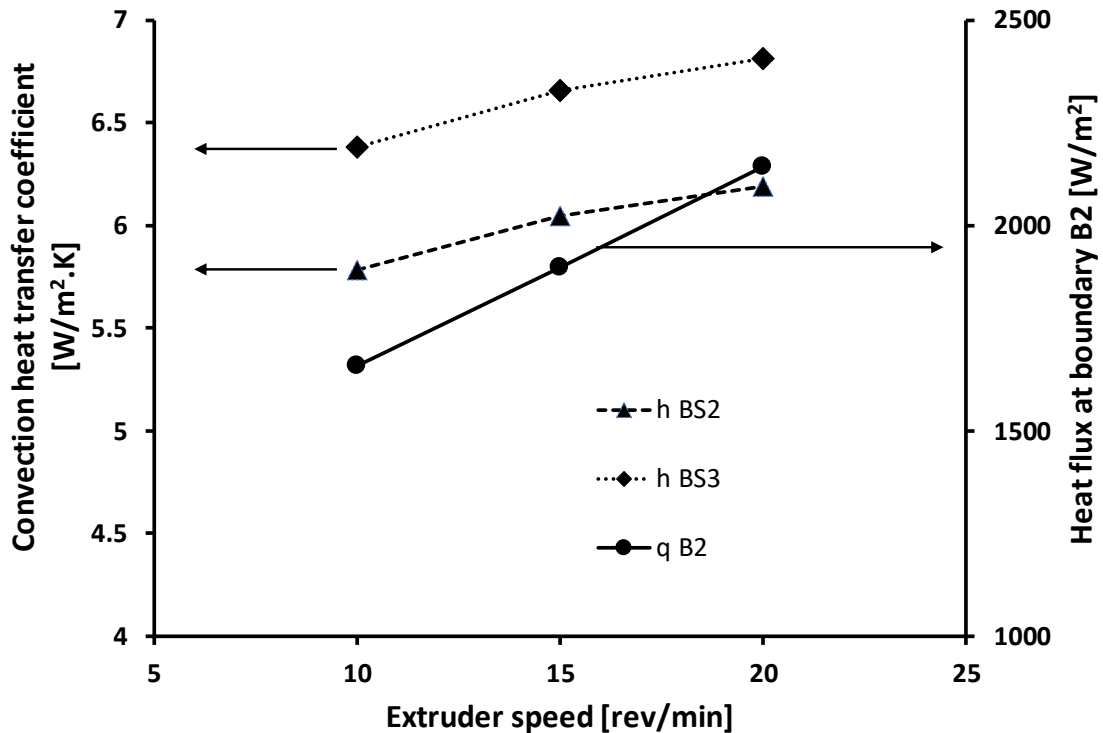


**Figure 4.5:** Variation of convective heat transfer coefficient at boundaries BS2 and BS4 and heat flux across the interface boundary (B2).

The calculation of the heat flow at the thermal boundaries described above includes many assumptions which cannot be avoidable for the solution of any heat flow problem.

However, to confirm the results of this calculation, additional simulation with conjugate heat transfer based finite volume method was conducted to calculate the heat flow across the thermal boundaries.

## 4.2 Finite volume simulation

The finite volume method F.V.M was implemented to solve the coupled fluid and solid phase problem with a conjugate heat transfer. This method has advantages in terms of time cost, and memory usage (computation cost). Therefore, it can be used efficiently for modelling of large scale heat flow problems. In this method, the field equations in terms of energy, momentum, and continuity equations are recast in a conservative form and then solved over a discrete control volume. Since the inlet flux to a given volume is equal to that migrating to the adjacent volume, this discretization ensures the conservation of the fluxes through control volume. The tree of the physical simulation chart for the control volume including two physics for the solid and the liquid phase is presented in **Figure 4.6**.

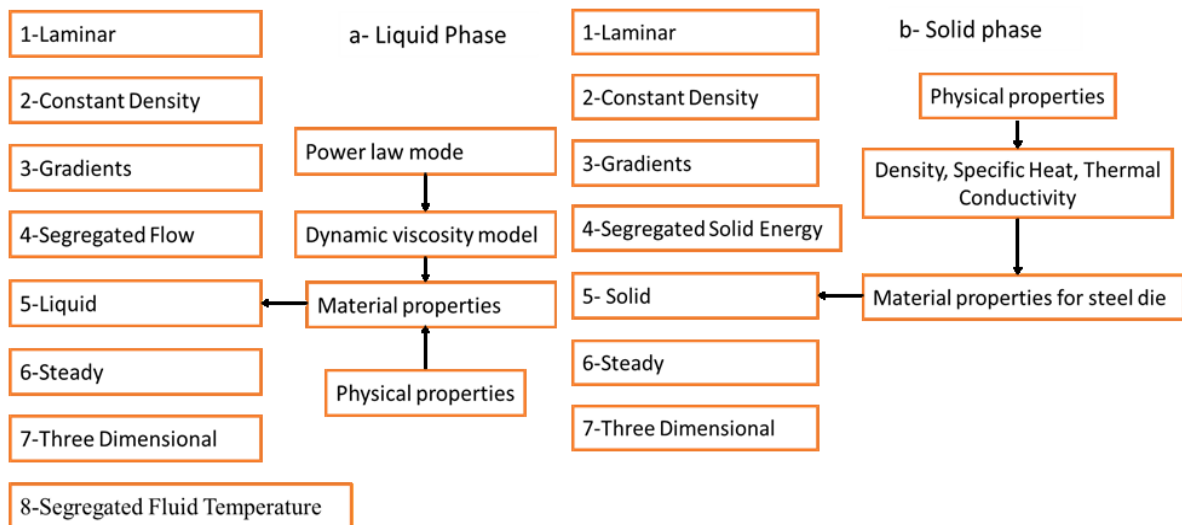


**Figure 4.6:** Chart of physical model adopted by STAR CCM++ for control volume method a-Liquid phase b-solid phase.



In the finite volume method, both solid and liquid phase in the computational domain were discretised using the automated mesh that generates a tetrahedral linear element with four nodes. The mesh size distribution in terms of the cell diameter is presented in **Figure 4.7**.

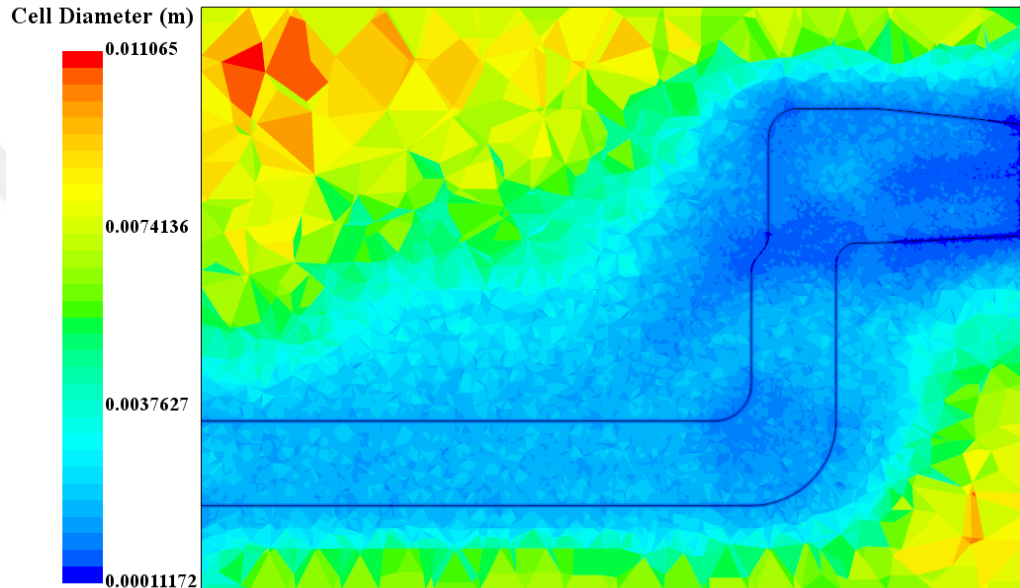


**Figure 4.7:** Generated finite volume mesh elements for both liquid and solid phase at section plane.

The finite volume solution was verified using three meshes with a number of elements increasing from 286278 elements to 1614391 elements as presented in

**Table 4-2.** The predicted results showed a stable condition at a mesh size M2, which was then used to conduct all other simulation. The imposed flow boundary conditions in this case were similar to F.E.M. The thermal boundary conditions for adopting the F.V.M simulation are previously described in **Figure 4.3**.

**Table 4-2:** Properties of FVM mesh.

Mesh	Cell	Face	Vertices	Min. cell volume[m <sup>3</sup> ]	Min. cell diameter[m]	Base size [m]
M1	286278	581000	74765	1.009E-12	1.26377E-4	0.007
M2	805683	1689595	221509	7.3028E-13	1.11717E-4	0.005
M3	1614391	3352313	418973	6.206198E-14	4.911723E-5	0.002

The results of the heat flow across the external boundaries BS2 and BS4 together with interface boundary B2 adopting F.V.M are shown in **Figures (4.8,4.9,4.10)** for the extruder speed of 10,15 and 20 rev/ m, respectively.

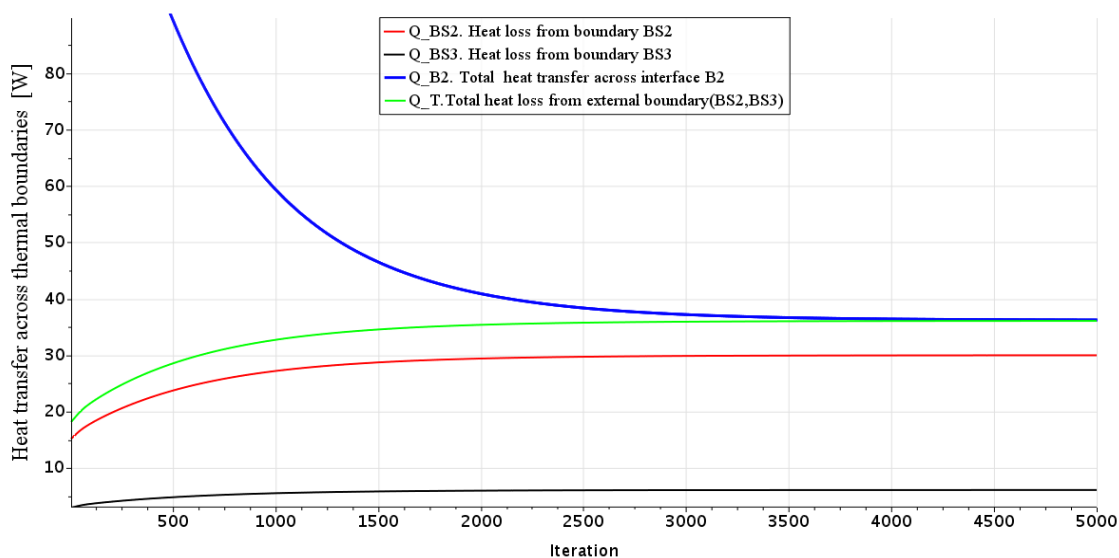


**Figure 4.8:** Predicted heat flow over boundary adopting F.V. simulation for extruder speed 10 rev/min.

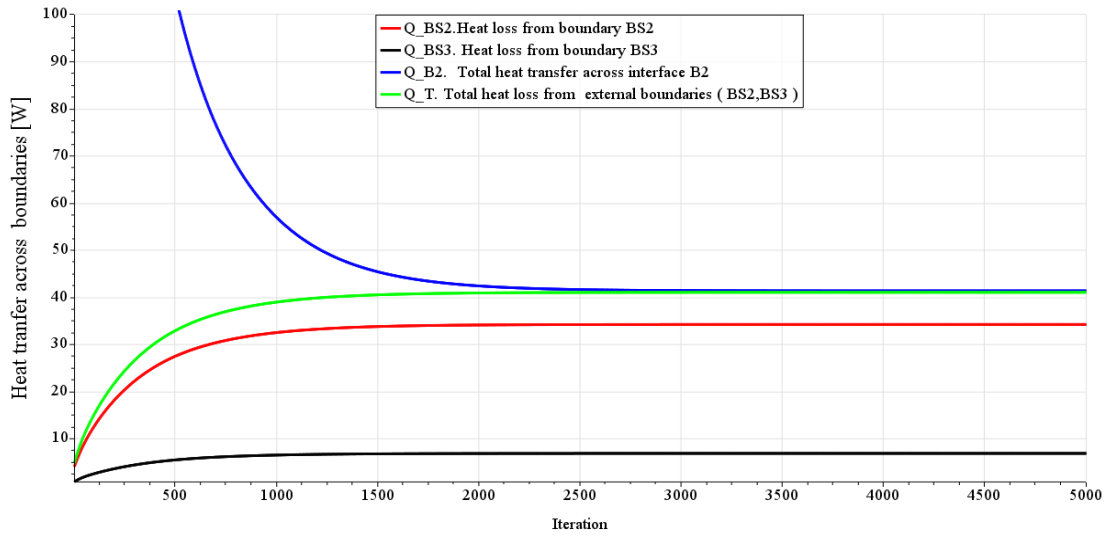


**Figure 4.9:** Predicted heat flow across thermal boundaries adopting F.V. simulation for extruder speed 15 rev/min.

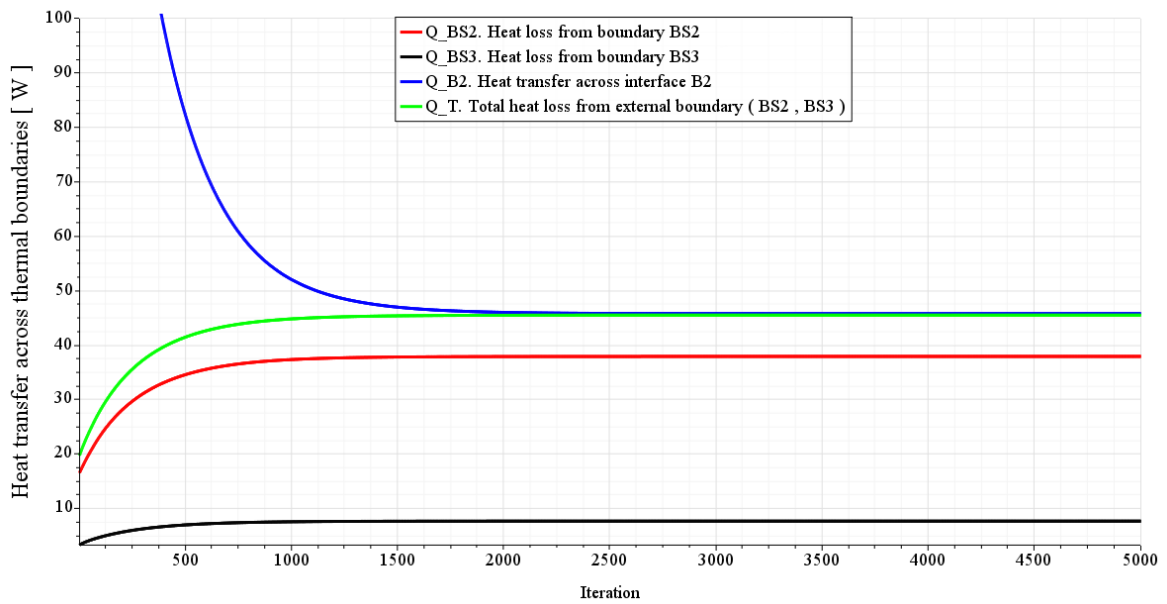


**Figure 4.10:** Predicted heat flow over boundary adopting F.V. simulation for extruder speed 20 rev/min.

A comparison between the calculated total heat loss by applying empirical equations and the calculated total heat loss predicted from F.V.M is depicted in **Figure 4.11**.

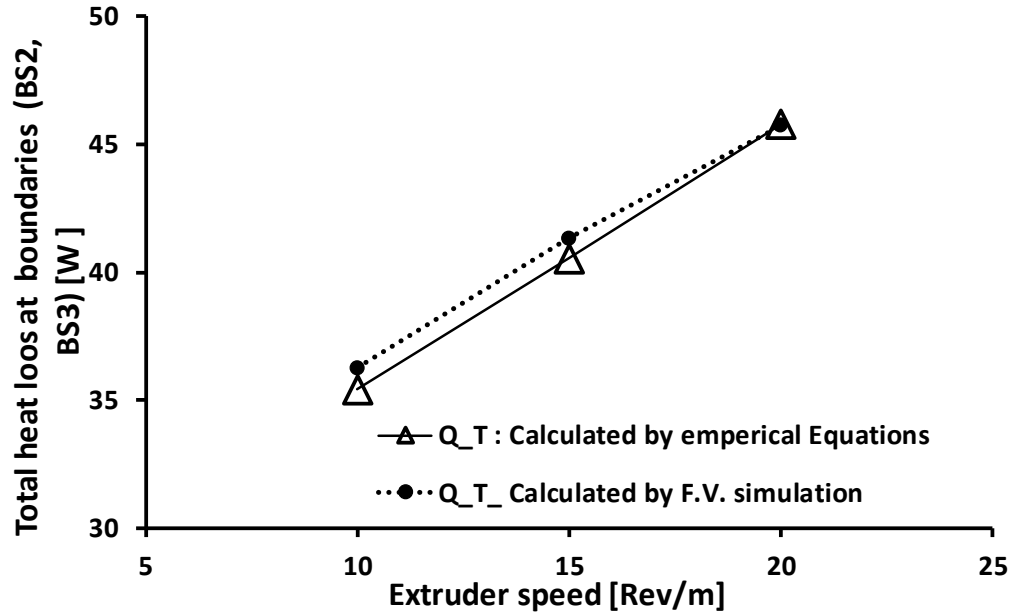


**Figure 4.11:** Comparison of total heat calculated by Empirical Equations and predicted by F.V.M at different extruder speed.

The contour of temperature distribution on the longitudinal section plane adopting control volume simulation for the first extruder speed is depicted in **Figure 4.12**.

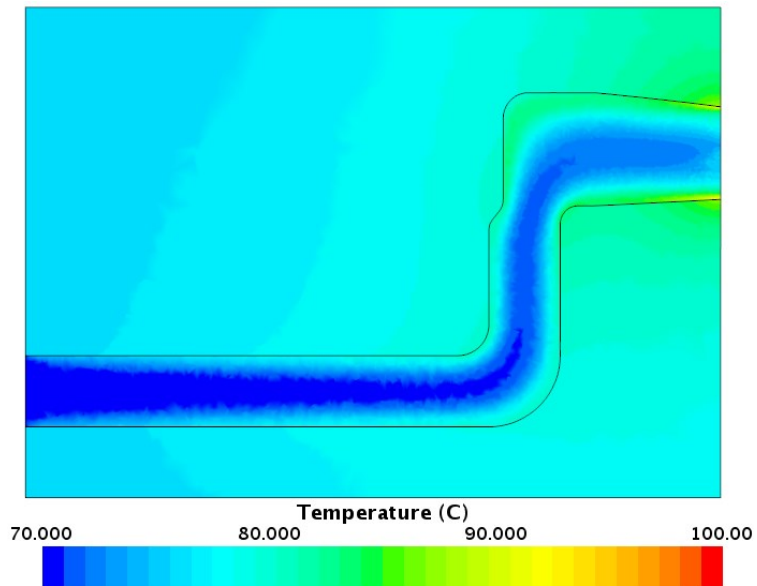


**Figure 4.12:** Contour of temperature distribution adopting F.V.M simulation for extruder speed 10 rev/min.

The estimated maximum error did not exceed 2.5%, which confirms the reliability of the proposed method for calculating the local heat flow across each boundary.

For the solution of the heat flow problem during extrusion, the characteristic of the rubber compound was considered when the steady state was achieved. The following assumptions were applied:

1. The Reynolds number is very low due to the high viscosity of the compound; therefore, an incompressible laminar flow will prevail.
2. The inlet temperature from the extruder head is constant and uniformly distributed.
3. The thermal conductivity  $\kappa$ , and heat capacity  $C_p$  are independent on temperature.
4. The mass density of the rubber compound is constant.

The validity of continuum hypothesis is implicitly assumed. This, in turn, allows the average properties to be defined and assigned values which are not influenced by the dimensions of flow passages. Therefore, as long as the size of micro-structures is much smaller than the characteristic linear scales of the apparatus, one can safely invoke the continuum hypothesis [116].

### ***4.3 Finite element mesh of extrusion die***

For finite element simulation, the flow domain was discretised using the automated mesh that generates a tetrahedral linear element with four nodes as shown with zoom on some surface location in **Figure 4.13**.

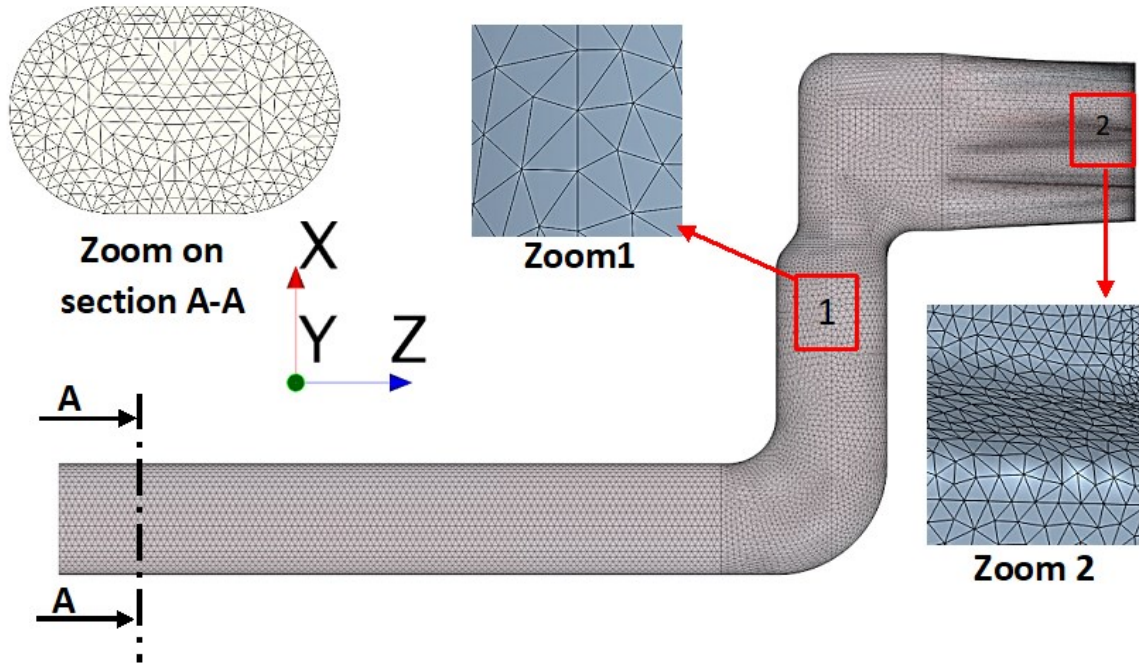


**Figure 4.13:** Generated finite element mesh of the flow domain with zoom picture in the local surface area to demonstrate mesh elements.

The accuracy of predicted results was improved by utilising local mesh refinement based on finite element approximation on the surface of the flow domain. In addition, the mesh density was increased progressively in the direction of the flow exit, especially in the convergence region before the die exit. To verify mesh independency, we performed simulations using three meshes, namely, M1, M2, and M3, with the number of elements increasing from 286278 to 1166190. The total number of cells and the other properties for each mesh size are given in **Table 4-3**.

**Table 4-3:** Properties of FEM mesh for extrusion die.

Mesh	Cell	Face	Vertices	Min. cell volume[m <sup>3</sup> ]	Min. cell diameter[m]	Base size [m]
M1	286278	581000	74765	4.1293E-13	6.27827E-7	0.004
M2	523630	1059916	126152	3.292432E-14	1.77278E-7	0.002
M3	1166190	2366868	264968	1.804042E-14	1.312265E-7	0.0015

Figure 4.14 shows the predicted temperature at three sensors via the number of the mesh elements for the first extruder speed.

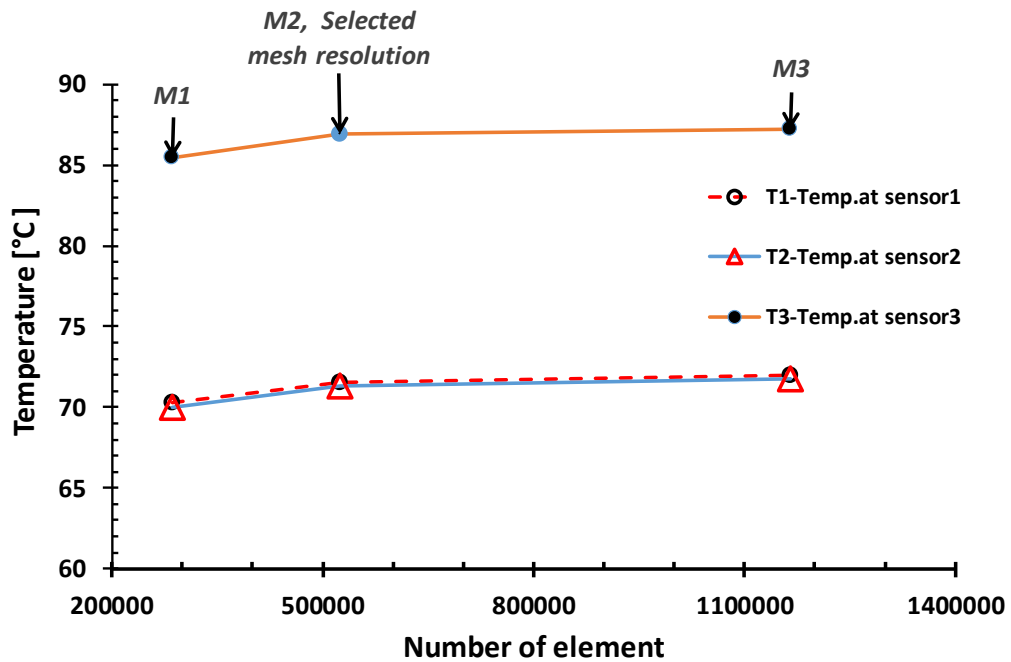
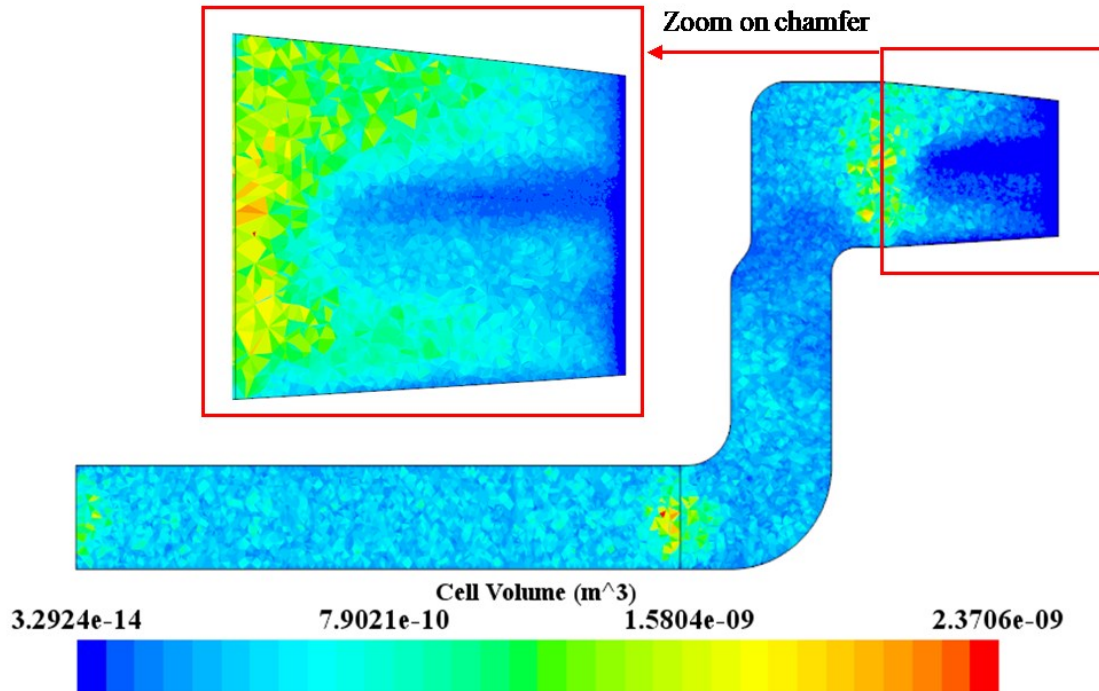


Figure 4.14: Predicted temperature versus the number of elements for an extruder speed of 10 rev/min.

For a low mesh density in M1, a small deviation is detected in the predicted temperature from those of other mesh resolutions. Then, the predicted results reach a stable condition, which satisfy the mesh independency conditions. Therefore, the mesh size M2 is used to conduct all the other simulation experiments. Figure 4.15 shows the calculated mesh volume distribution on the longitudinal section plane.



**Figure 4.15:** Cell volume distribution on section plane of extrusion die (for M2).

In addition to satisfying the mesh independent results, the numerical stability condition is greatly dependent on the mesh quality. Therefore, we should ensure that the mesh is of high quality before proceeding to the physical process. The mesh structure should be fine enough to avoid the singularity due to high stress in the region of the high shear rate. This requirement is essential to reach a stable numerical solution, especially for the complex flow such as polymer. In this sense, the local mesh refinement technique is employed to reduce the expensive computation costs; especially when adopting the viscoelastic model. Since the maximum deformation in the mesh elements was expected to occur in the conversion region before the die exit, the mesh density was increased progressively in the direction of the flow exit; especially in the convergence region.



The linear tetrahedral mesh elements were selected to build the core mesh of the total flow domain. This kind of mesh is essentially required to be used with the finite element discretisation method since it is supported by the Star CCM viscous flow Solver [71]. The shape of the tetrahedral element shown in **Figure 4.16**, which contains 4 corner nodes, 6 edges, and 4 faces.

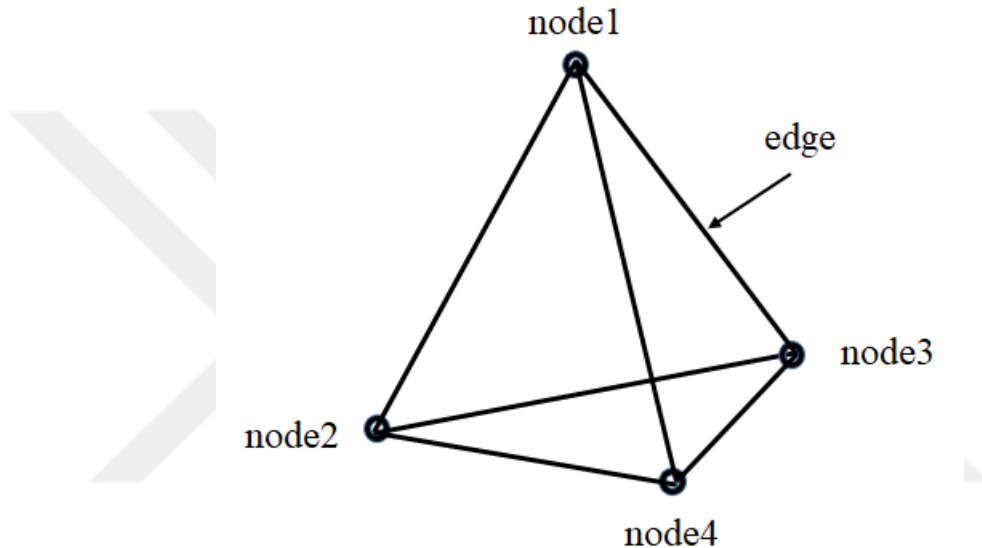


**Figure 4.16:** Tetrahedral mesh element (reproduce from style of [71]).

All the numerical and physical simulations were applied to the extrusion die after completing the mesh. The tree of the simulation chart is presented in **Figure 4.17**.

The viscous energy model is introduced to include the energy equation in the calculation of the field variables, which is required in the case of non-isothermal simulation. In addition, the amount of viscous energy or friction energy, which is generated due to the friction between moving layer as well as the friction between polymer particle and die wall, are also calculated. The residence time is used to calculate the time of fluid particles in the computational domain, which is necessary to evaluate the curing characteristic of high

reactive material such as rubber compound. The viscous dissipation will influence or modify the flow field variable in the entire flow domain.

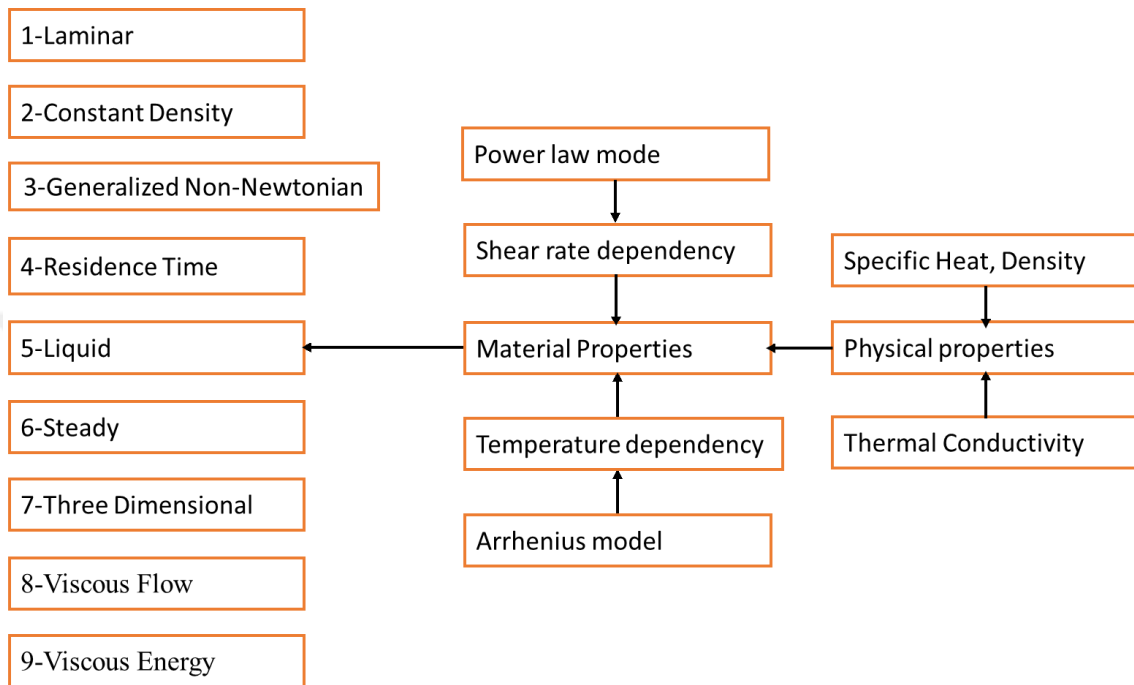


**Figure 4.17:** Chart of physical model adopted by STAR CCM++ software.

#### 4.4 *Viscoelastic simulation*

The second task was devoted to the analyses the swelling phenomenon which normally accompanied the process of extrusion for production of rubber product. In this work numerical modeling was used to provide a fundamental basis that is potentially useful in predicting swelling during the extrusion of rubber compounds. Swelling is a phenomenon caused by the viscoelastic fluid flow behaviour of rubber compounds in die extrusion processes. In continuous extrusion processes, swelling causes deviations from the shape of a die. Moreover, a flow field that includes circulation regions in the die can create production problems, such as plating. Capillary die extrusion is selected as a benchmark case because of

its simplicity and the availability of experimental data. The effect of viscoelastic model parameters on predicted results is investigated by using experimental data.

Giesekus rheological model was selected to predict swelling in a capillary die since this model have approved its good ability in predicting the viscoelastic behaviour and swelling by many studies [117,118].

The engineering values of this study are as follows:

1. The present results revealed that the multi-mode version of the Giesekus differential viscoelastic model can predict swelling, which is a result of complex viscoelastic behaviour of a rubber compound. These results indicate that the Giesekus model can be used as an additional candidate for predicting swelling in addition to the PTT model, the use of which was already validated by Choi and Lyu [37].
2. The established framework adopted to obtain these results can be extended for a complex geometry. Investigation on the effect of model parameters, such as relaxation time and relaxation mode, on flow behaviour helps elucidate the influence of those parameters on flow physics. The effect of these parameters reveals that the number of relaxation mode and relaxation time exert a remarkable effect on elasticity and memory effect, which in turn, influence swelling, circulating flow at die corner and other field variables.
3. The correct predictions of swelling and circulation help design engineers to take measure for these phenomena in the primary stage of die design, thereby reducing problems related to form deviations and die plating. The present work shows the framework for conducting such simulations with necessary accuracy.

4. Given that the basic measurements of the rheological properties of a polymeric material can be obtained by using a capillary rheometer, understanding the flow behaviour in capillary die is useful in understanding the physics behind rheological measurements.

#### 4.5 Geometry and boundary conditions.

The typical geometry of the capillary extrusion die is described in **Figure 4.18**, which consists of the main reservoir with square dimensions of 25 mm  $\times$  25 mm; the die is represented by the length  $L_2=2.5$  and the extrude is represented by  $L_3=25$  mm. The diameter of the die =2.5mm.

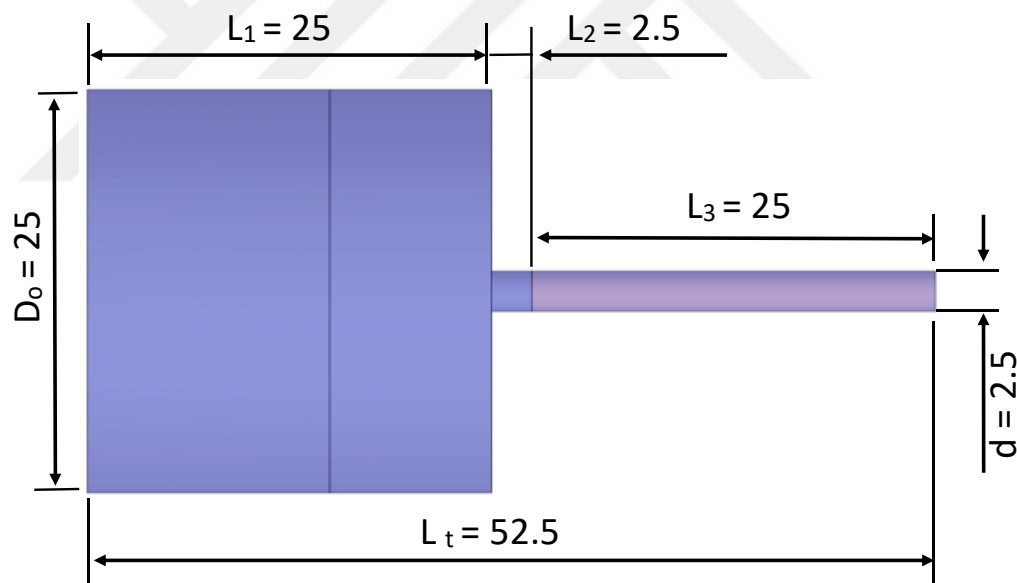


**Figure 4.18:** Geometry of typical capillary die.

To solve the complex flow by implementation viscoelastic model with the presence of free surface at the extrudate, appropriate flow boundary condition should be imposed on the flow domain. In the present case, the simulation was conducted by applying the boundary conditions such as described by Konaganti [69]. The suitable boundary conditions described

with a half section plane are shown in **Figure 4.19**. A mass flow rate was imposed on the inlet section of the reservoir denoted by B1. This inlet condition imposed a fully developed velocity profile at inlet as used in a previous study [57]. The velocity profile at B1 will be calculated from mass flow which is defined in the simulation[114]. Wall boundary conditions imposed on both reservoir's wall and die wall denoted by B2. This implies that no-slip will occur at wall boundary and the tangential velocity of fluid particle equal zero. Free stream boundary imposed with internal morpher displacement on the extrudate surfaces denoted by B3. On the outlet boundary denoted by B4, zero surface tractions (Aligned Exit) and zero transverse velocity were imposed with boundary plane constrain specification. Free stream boundary imposed on the extrudate surfaces denoted by B3. This implies that no flow normal to the surface ( $V \cdot n = 0$ ) and zero surface tractions. Finally, symmetry boundary imposed on symmetry plane denoted by B5. This implies that the shear stresses component and the radial velocity component are zero along the symmetry axis.

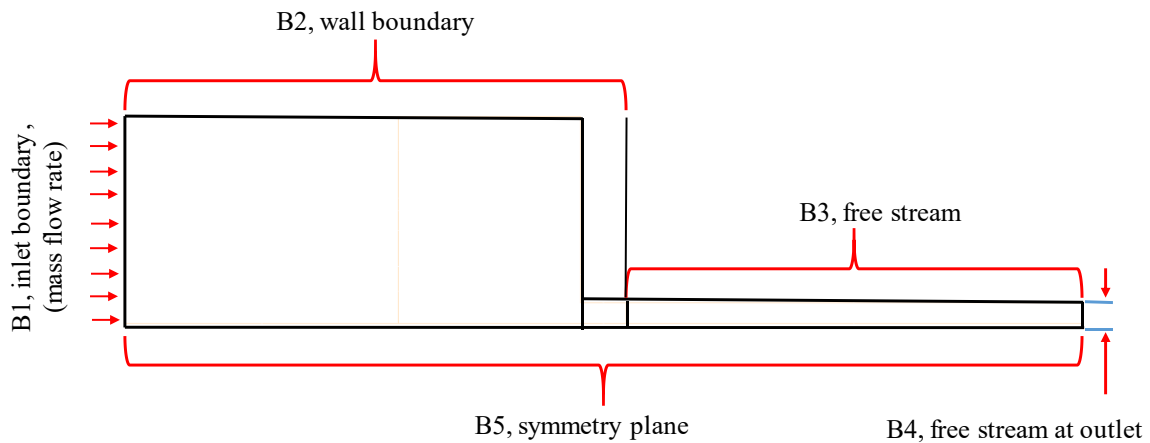


**Figure 4.19:** Boundary conditions imposed on capillary die.

## 4.6 Finite element mesh of capillary die

According to the flow characteristics, the finite element model of capillary die extrusion was divided into the reservoir and die as one region and the extrudate free surface as another region. The first region was discretized using tetrahedral meshes which generate tetrahedral linear elements. Directed meshes that generate linear wedge elements are used on the free surface region as shown in **Figure 4.20** [71].

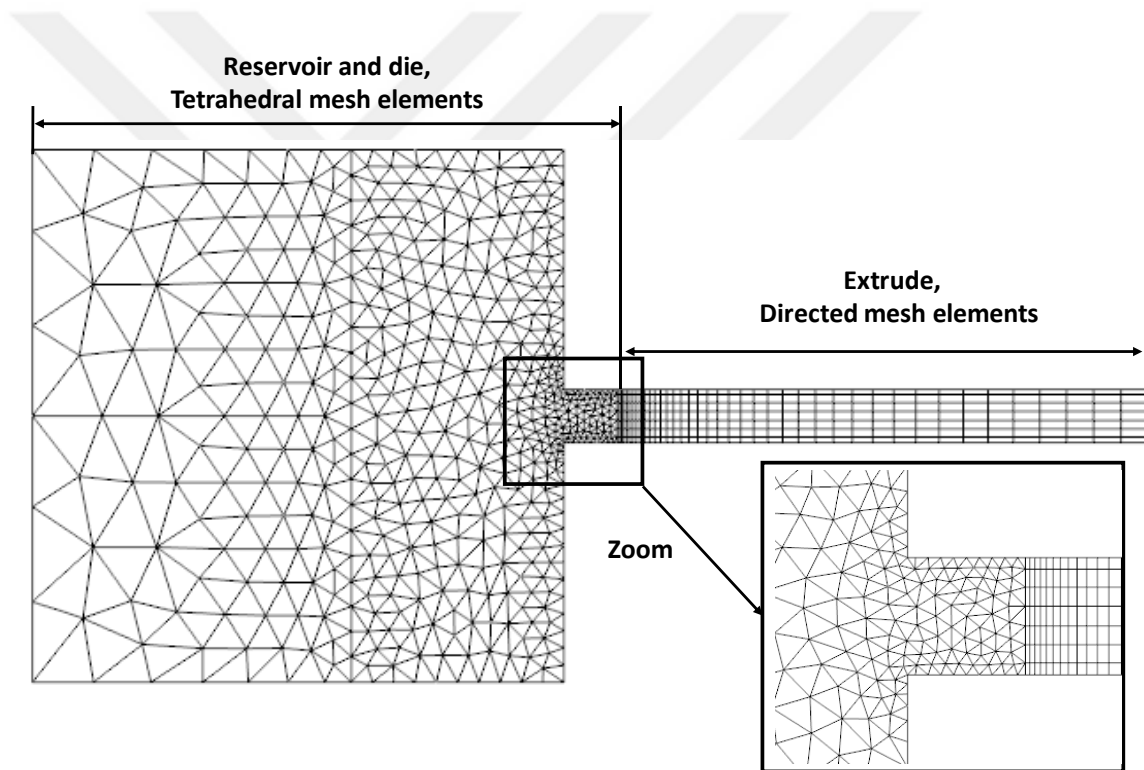


**Figure 4.20:** Section plane show finite element mesh of capillary die (M2).

For the line kinematic condition, the volume mesh of the free surface must be directed in the direction of the extrusion by using a directed mesh. The mesh in the region of the free surface is normally generated in its initial undeformed state. Therefore, the final mesh position of the free surface is calculated as part of the solution. The One-sided Hyperbolic

Function is used to stretch the layer in the direction of the outlet and divides the extrudate into 40 layers. This mesh strategy is important to increase the mesh resolution near to the die exit and assist in reaching the convergence solution for the free surface domain [71].

Half geometry was used in the simulation due to the symmetrical condition to reduce the computational costs. Reasonable assumptions of the incompressible, isothermal, steady and laminar flow were also considered. In addition, the gravity force was neglected due to the high viscosity of the rubber compound. One internal interface was generated in the contact surfaces of the capillary die and the extrudate.

The local mesh refinement approach was used to reduce the computation costs and make a sufficient mesh density in the region of the high stress; especially in the die and near to the die exit regions. The length of the extrude was chosen to be 10 times the length of the die to ensure numerical stability [71]. **Figure 4.21** shows the predicted swelling ratio in the capillary die via the number of mesh elements, which increase from 42648 to 190988 .

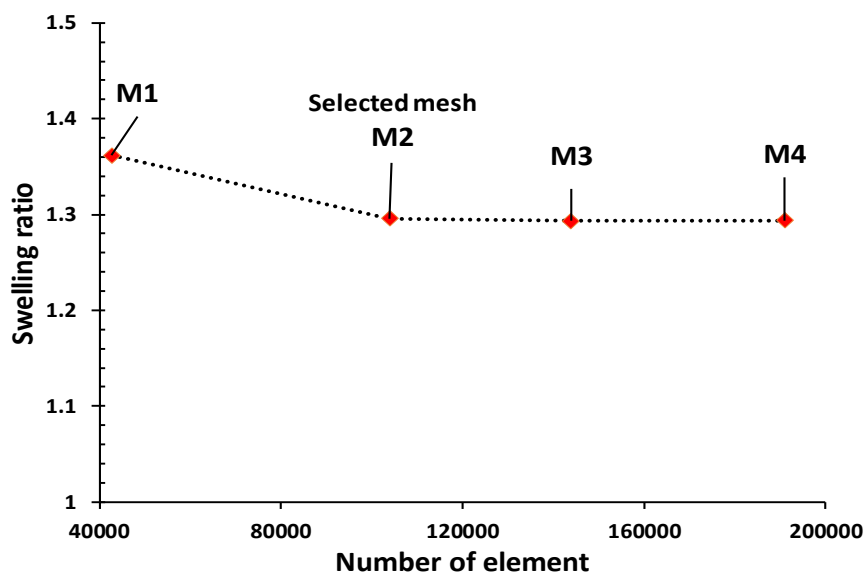


**Figure 4.21:** Predicted swelling ratio vs number of element adopting 3 relaxation mode of Giesekus model.

The mesh independency was determined by increasing the grid density in four steps, during which the number of elements was doubled. For a low mesh density in the M1, a high deviation was detected in the predicted swelling ratio from those of other mesh resolutions. Then, the predicted results reached a stable condition, which satisfies the mesh independency conditions. Therefore, the mesh size M2 was used to conduct all the other simulation experiments. The properties of mesh refinement presented in **Table 4-4** ; the cell diameter was calculated with the assumption that the grid assumed possess a spherical shape.

**Table 4-4:** Mesh refinement properties for capillary die.

Mesh	Cell	Face	Vertices	Min. cell size[m <sup>3</sup> ]	Min. cell diameter[m]	Base size [m]
M1	42648	82795	10596	6.266E-13	1.06E-4	0.0015
M2	103961	203584	22922	2.323E-13	1.0289 E-4	0.0011
M3	143909	282339	30634	1.61978E-13	6.7623E-5	0.00095
M4	190988	374882	39697	8.8054E-14	5.51898E-5	0.000832

The cell diameter distribution shown in **Figure 4.22** which calculated under the assumption that the cell has a spherical shape.

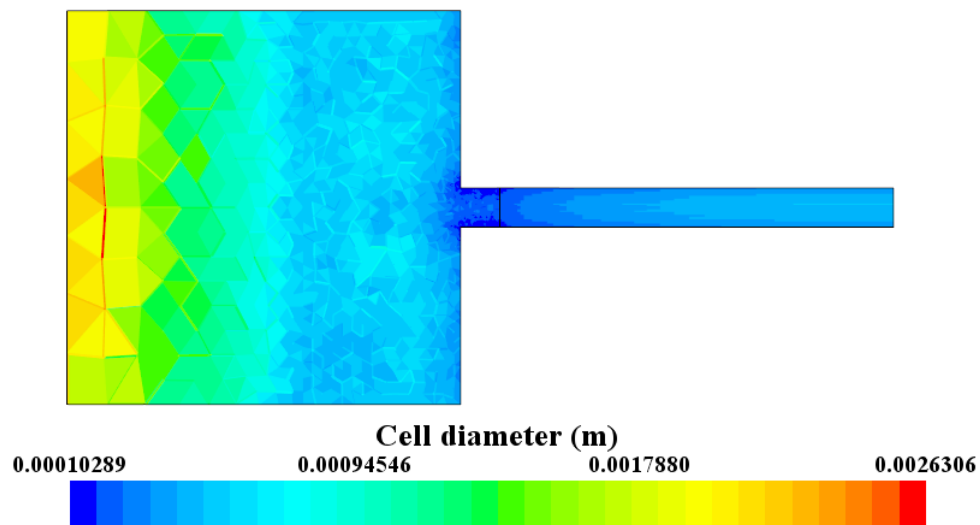


**Figure 4.22:** Calculated cell diameter distribution for M2 in capillary die section plane.



All the numerical and physical simulations were applied to the capillary model after completing the mesh. The tree of the physical simulation chart is presented in **Figure 4.23**.

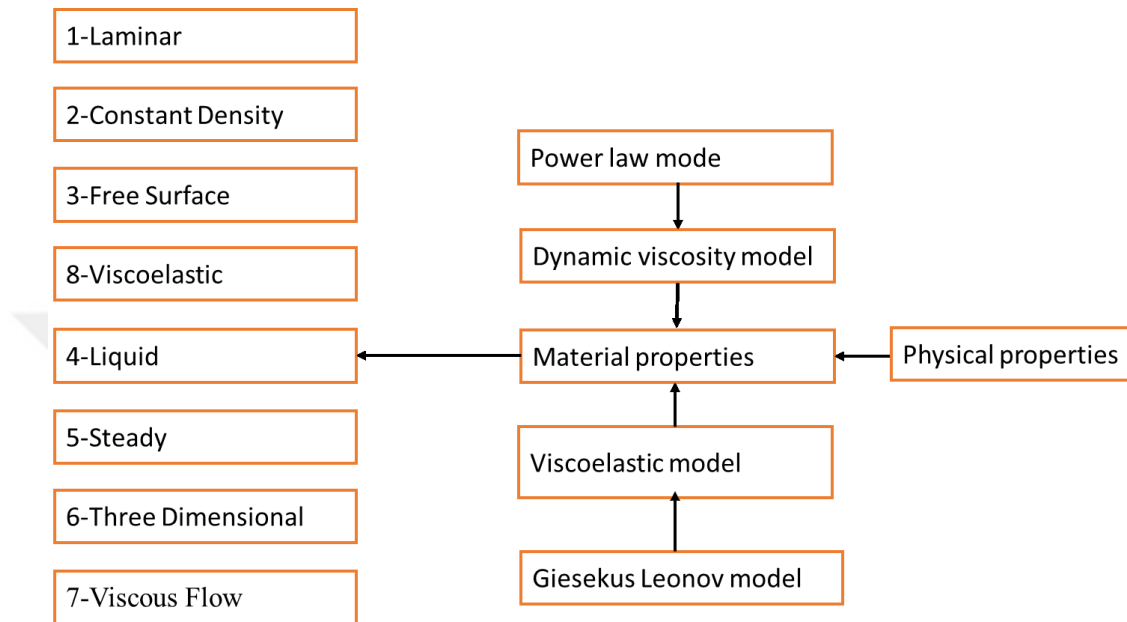


**Figure 4.23:** Physical model for viscoelastic flow in capillary die.

#### **4.7 Modelling mesh motion**

The Arbitrary Lagrangian-Eulerian (ALE) approach was employed by using the STAR-CCM+ to calculate the displacement of free surface at the extrudate region. In this method, the mesh boundary was deformed depending on the position and the shape of the free surface through the mesh morpher [71]. Therefore, appropriate constraints and boundary conditions for the mesh motion must be imposed as described previously.

The use of the Lagrangian framework in the modelling extrudate swell has the advantage of the evolution of the free surface naturally with the material flow. However, there are some problems associated with the requirement of frequent remeshing and mesh distortion. Therefore, the ALE formulation first proposed by Jocelyn et al. [119] successfully

addressed these problems since it has the ability to combine the advantages of both the Eulerian and Lagrangian frameworks. The numerical accuracy of the ALE method was verified by many researchers such as the one presented by Ganvir et al. [120].

#### **4.8 Method of numerical solution**

For the solution of the non-Newtonian incompressible flow problem, such as that for polymer melts, two different finite element formulations, namely, penalty method and mixed method, have been proposed in the literature [121,122]. In the first method, computational cost is reduced by eliminating the pressure variable from the momentum equation by using penalty parameter  $\psi$  in the order of  $10^8$ – $10^{12}$ , as expressed by the following equation.

$$p = -\psi(\nabla \cdot \mathbf{v}) \quad (4.2)$$

In this method, velocity field is approximated using bilinear shape functions. However, a complex technique is necessary to satisfy the stability condition in the absence of pressure variable in the continuity equation.

In the mixed method, pressure and velocity are considered unknown in discretized equations. The numerical difficulty associated with this method is the satisfaction of Ladyzhenskaya–Babuska–Brezzi (or inf-sup) stability condition due to the absence of pressure in the continuity equation [121–123]. In addition, the differentiation of pressure in the momentum equation is one order less than the velocity component in the continuity equation. Thus, oscillatory results can be obtained using equal interpolations for pressure and velocity. With regard to the stability and convergence of the algebraic system of equations for unknown pressure and velocity in the Galerkin formulation this obstacle can be eliminated

by employing pressure-stabilized Petrov–Galerkin (PSPG) method, which was first proposed by Hughes et al. [124], and by using biquadratic and bilinear shape functions for velocity and pressure field approximation, respectively. This approach provides unequal interpolations for pressure and velocity. The detailed procedure of this stabilizing technique can be found in previous studies [124–127].

Another difficulty arises when using a numerical technique for solving non-Newtonian viscous fluid flow, that is, nonlinear convective terms exist in the energy and momentum equations. Convective terms that are associated with energy equation are considered high in polymeric flows because of minimal thermal conductivity. Therefore, polymer melts have a high Peclet number, which is the ratio of the rate of advection of a physical quantity by the flow to the rate of diffusion of the same quantity driven by an appropriate gradient; heat transfer is dominated by viscous dissipation and the convective term. Using standard Galerkin method to solve an energy equation can yield oscillatory results. To overcome this problem, Brooks and Hughes [100] proposed streamline upwind/Petrov–Galerkin scheme (SUPG), which can be successfully applied to obtain stabilized solutions for convection-dominated equations.

For modelling viscoelastic material flow in extrusion under isothermal condition taking into account elastic effect the set of field equations coupled with the constitutive equation yielded a double saddle point problem because the pressure and velocity do not appear explicitly in the field equations. To solve this problem, we performed a viscoelastic flow simulation based on the mixed finite element method using the discrete elastic–viscous stress splitting method (DEVSS) first proposed by Guénette and Fortin [128]. The two

previous technique of stabilization utilizing (SUPG) [100] and (PSPG) [124–127] are also used in viscoelastic simulation.

#### ***4.9 Determination of relaxation time***

The relationship between relaxation time and viscosity of polymer melts is shown in equation below. [74,129]:

$$\eta = \lambda \cdot G, \quad (4.3)$$

Herein,  $\lambda$  and  $\eta$  are the relaxation time and viscosity, respectively.  $G$  is the characteristic modulus which can be defined as the modulus  $G' = G''$  at cross over. For the shear thinning fluid-like polymer, the viscosity decreases with the increase in shear rate; in such a case, relaxation time is commonly expressed as a function of shear rate for the shear flow problem. The time scale relaxation mechanism occurs in the order of  $1/(\text{shear rate})$  [130].

Two methods were adopted in the literature to determine the relaxation time. The first method involves finding the crossover point between elastic modulus ( $G'$ ) and viscous modulus ( $G''$ ) from experimental data and then taking the reciprocal shear rate corresponding to this point. The value of the crossover point is obtained when  $G' = G''$ , and the transition from elastic dominant flow to viscous dominant flow or vice versa occurs beyond this point [114]. However, this crossover point is unavailable in the experimental data. The second method, which was adopted by Choi and Lyu [37], was used in the present work.

In the second method, relaxation time is calculated theoretically by simulating the extrusion process under a non-Newtonian isothermal condition [37]. Subsequently, the average shear rate is predicted in the mid-section of capillary die. Finally, the relaxation time

is the reciprocal number of the average shear rate. This approach is quite important as it enables the setting up of a model that is suitable for typical time scales involved in simulations [131]. Selecting relaxation time from average shear rate in the capillary region implies that Deborah number is 1 for single-mode relaxation and covers a range lower and higher than unity for multi-mode relaxation. In the present work, second method was adopted as follows.

The experimental data of shear viscosity in **Figure 4.24** was used from literature work presented by Choi and Lyu [37] and fitted to the power law by Ostwald and De Waele [74].

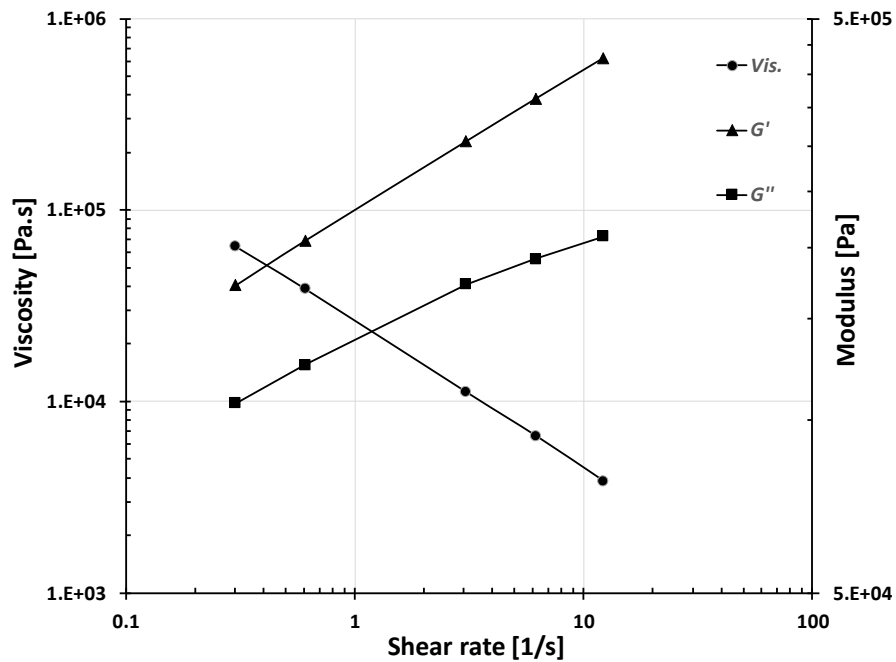


**Figure 4.24:** Shear viscosity, storage and loss moduli of rubber compound. Reproduced from reference [37] under permission from publisher ©Carl Hanser Verlag GmbH & Co.KG.

$$\eta = K(\dot{\gamma})^{n-1}, \quad (4.4)$$

where:  $K$  is the consistency factor equal to  $267637.50 \text{ [Pa}\cdot\text{s}^n]$ , and  $n$  is the power law exponent equal to  $0.23$ . The relaxation time was calculated ( $\lambda_b = 0.0185$ ) by taking the reciprocal of the average shear rate which was predicted using the second approach.

The calculated shear rate distribution in the capillary die was predicted in **Figure 4.25** by conducting isothermal simulation and applying a power law-based non-Newtonian viscosity model.

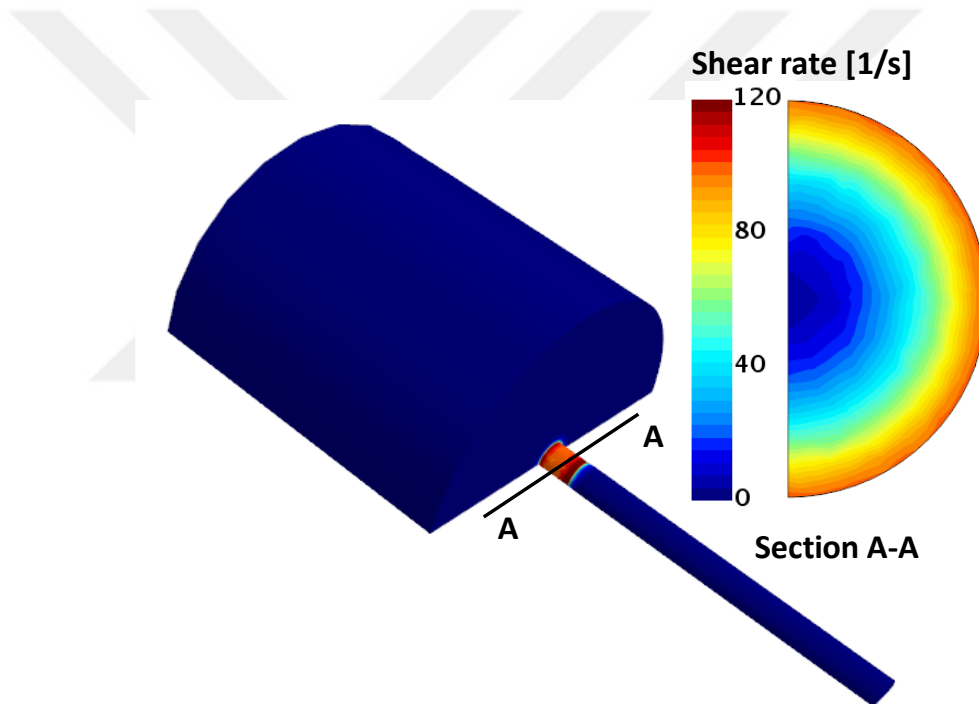


**Figure 4.25:** Contour of shear rate distribution in the middle die section for Non-Newtonian simulation.

The above approach for approximation of base relaxation time is based on the fact that the selected viscoelastic model should reproduce the experimental behaviour for shear rate in the vicinity of the characteristic shear rate of the flow to be simulated. Moreover, during the cessation of steady shear flow, measurements reveal that the relaxation mechanism occurs with a time scale on the order of  $(1/\dot{\gamma})$ , where  $\dot{\gamma}$  is the typical shear rate involved in

the experiment. This observation allows the identification of a typical time scale and the characterization of mechanisms occurring in steady flow processes, such as extrusion [131].

Basing on the above argument, we surmised that the selection of base relaxation time for the constitutive model is indeed based on numerical investigations and relaxation mechanism encountered in real flow conditions. From the physical point of view, it is worth mentioning that it is difficult to confirm that the typical shear rates in capillary extrusion and the intersection point of  $G'$  and  $G''$  curves are similar as pointed out by Choi and Lyu [37].

#### ***4.10 Relaxation time and relaxation mode***

The relaxation time of 0.0185 s was set as the base relaxation time denoted by  $\lambda_b$ . Thus, the relaxation times were  $(\lambda_b/2)$  and  $(\lambda_b \times 2)$  in single relaxation mode. Under two-mode relaxation, the relaxation times were  $(\lambda_b/3)$  and  $(\lambda_b \times 3)$  as the minimum and maximum relaxation times, respectively. The relaxation time also ranged from  $(\lambda_b/4)$  to  $(\lambda_b \times 4)$  to in the two relaxation modes. Under three relaxation modes, the maximum relaxation time was set to four times the basis  $(\lambda_b \times 4)$ , and the minimum relaxation was set to one-fourth of the basis  $(\lambda_b/4)$ . One-fifth of the basis  $(\lambda_b/5)$  and five times the basis  $(\lambda_b \times 5)$  were also used in the three relaxation modes. In all cases, the range of relaxation time should not exceed two decades [130]. **Table 4-5** displays the relaxation time setup and the parameters of the Giesekus model which were extracted through the fitting of rheological data in **Figure 4.24** using the Ansys Polymat Package. During fitting of experimental data according to Giesekus model some parameters, such as the range of relaxation time and number of mode, are defined, whereas the parameter alpha is left freely adjustable in the range between 0 and 1.

**Table 4-5:** Parameters of Giesekus model for various relaxation time and relaxation mode.

Mode number		Relaxation time $\lambda$ [s]	Giesekus, Model1 Parameter: $\eta, \alpha$	Giesekus, Mode2 Parameter: $\eta, \alpha$	Giesekus, Mode3 Parameter: $\eta, \alpha$
1 Mode	Case1	Min. $\lambda = 0.00925$ ( $\lambda_b \cdot 1/2$ )	$\eta = 282044.2$ $\alpha = 0.211$		
	Case2	Mid. $\lambda = 0.0185$ ( $\lambda_b$ )	$\eta = 226422.8$ $\alpha = 0.190$		
	Case3	Max. $\lambda = 0.037$ ( $\lambda_b \cdot 2$ )	$\eta = 186239.3$ $\alpha = 0.1701$		
2 Mode	Case1	Min. $\lambda = 0.00616$ ( $\lambda_b \cdot 1/3$ ) Max. $\lambda = 0.0555$ ( $\lambda_b \cdot 3$ )	$\eta = 0.2997$ $\alpha = 0.212$	$\eta = 154698$ $\alpha = 0.151$	
	Case2	Min. $\lambda = 0.0046$ ( $\lambda_b \cdot 1/4$ ) Max. $\lambda = 0.074$ ( $\lambda_b \cdot 4$ )	$\eta = 2.896$ $\alpha = 0.211$	$\eta = 144575.6$ $\alpha = 0.145$	
3 Mode	Case1	Min. $\lambda = 0.0046$ ( $\lambda_b \cdot 1/4$ ) Mid. $\lambda = 0.0185$ ( $\lambda_b$ ) Max. $\lambda = 0.074$ ( $\lambda_b \cdot 4$ )	$\eta = 3.982645$ $\alpha = 0.20706$	$\eta = 7.813225$ $\alpha = 0.20706$	$\eta = 106688.2$ $\alpha = 0.31059$
	Case2	Min. $\lambda = 0.0037$ ( $\lambda_b \cdot 1/5$ ) Mid. $\lambda = 0.0185$ ( $\lambda_b$ ) Max. $\lambda = 0.0925$ ( $\lambda_b \cdot 5$ )	$\eta = 5.107388$ $\alpha = 0.201$	$\eta = 14.35975$ $\alpha = 0.203$	$\eta = 138890.3$ $\alpha = 0.134$

#### 4.11 Modelling swell in complex geometry

The extrusion die described previously in **Figure 4.1** are further analysed by adopting the viscoelastic rheological model to predict the swell phenomena and their effect on the final profile geometry. This process is essentially required to verify the proposed die design and necessary correction in the die design in the primary stage of die manufacturing. The same model which was applied to capillary die, namely the Giesekus model was used to investigate the swelling behaviour in the real extrusion die. The extrusion die geometry described in **Figure 4.1** was used with one change represented by the addition of the extrude in the structure of the model. The discretisation by the finite elements was similar to the approach used in the capillary die; therefore, we will only describe the extruded part in this section. The stationary domain, represented by the die region, was discretised using the



tetrahedral finite element mesh as described previously in **Figure 4.16**. The extrude finite element mesh and dimension are presented in **Figure 4.26**.

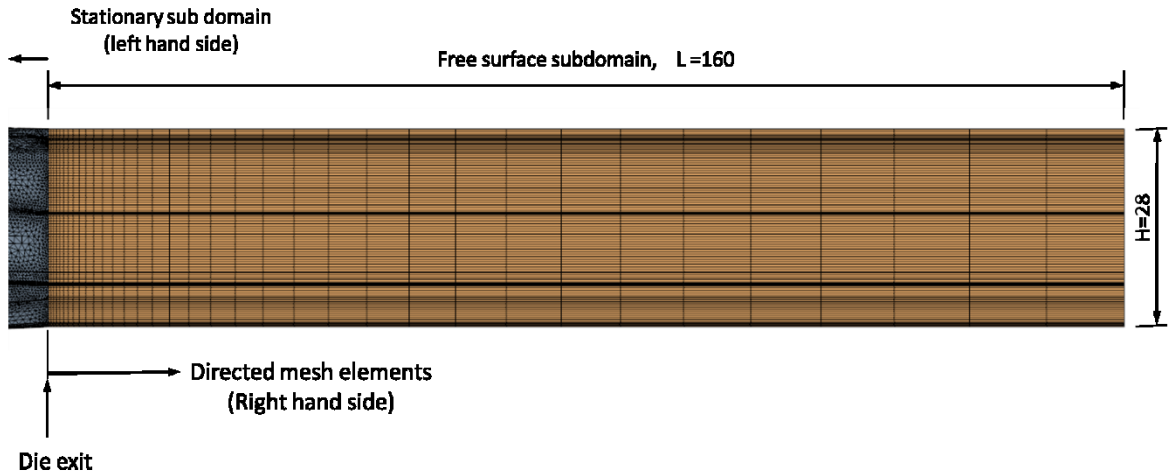


**Figure 4.26:** Extrude Finite elements directed mesh technique.

The extrude extended to 160 mm on the right hand side of the die exit with a total height of about 28 mm. The directed mesh elements were used to discretize this domain by dividing the length into 35 layers. The One Sided Hyperbolic function was used to stretch the layer in the direction of the outlet flow. This is important to increase the mesh resolution near to the die exit and to help reach the convergence solution for the free surface domain. The mesh independency was also performed by increasing the number of the mesh element from 266022 to 349497 elements. It is worthy to mention that the computation cost is very expensive; especially with the increase in the number of the mode for constitutive model adopted in simulation. Therefore, the technique of the local mesh refinement was adopted to reduce computation costs. The boundary condition imposed on the free surface was similar to the boundary described previously for the capillary die extrusion.

## CHAPTER V

### RESULTS OF VISCOUS MODELLING

#### ***5.1 Introduction***

In this chapter, the results of modelling complex flow in an industrial scale extrusion die (stationary domain) are discussed. In the first section of this chapter, the rheological variables in term of pressure and temperature were validated with experimental data. The effect of extruder speed on rheological field variables were discussed and analysed. In the second part the calculated residence time of material flow was compared with experimental scorch time obtained from curing tests. The streamline of flow pattern was also investigated to reveal the stagnation point or circulation flow. Based on these results, a decision was made about optimum extruder speed which can be used without risk of curing inside the die. On the other hand, a validity of die design can be concluded for the suitability of proposed die design or the requirement of die revision (correction in design). The effect of viscous dissipation was discussed and analysed.

#### ***5.2 Temperature field***

The measured temperatures from the local sensors inside the die were compared with the temperatures predicted by the proposed FEM for different extruder speeds as depicted in **Figure 5.1**. The temperature progressively increased with increasing extruder speed. This behavior is attributed to the increase in viscous dissipation due to shearing between the melt layers as well as between the melt layer and the die wall. This remarkable effect of viscous dissipation will introduce modification on other filed variable such as pressure, velocity

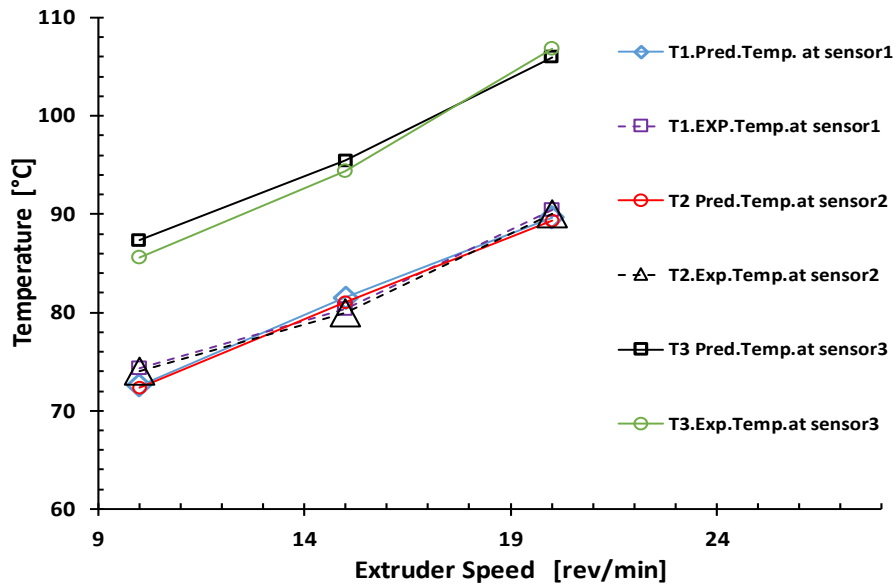


**Figure 5.1:** Measured and predicted temperatures versus extruder speed.

distribution and residence time. The contours of the temperatures predicted by the proposed model in the entire flow domain for different extruder speeds are shown in **Figure 5.2**. The local temperature rise, known as “shoulders,” was observed near the wall and reached the maximum at the die exit.

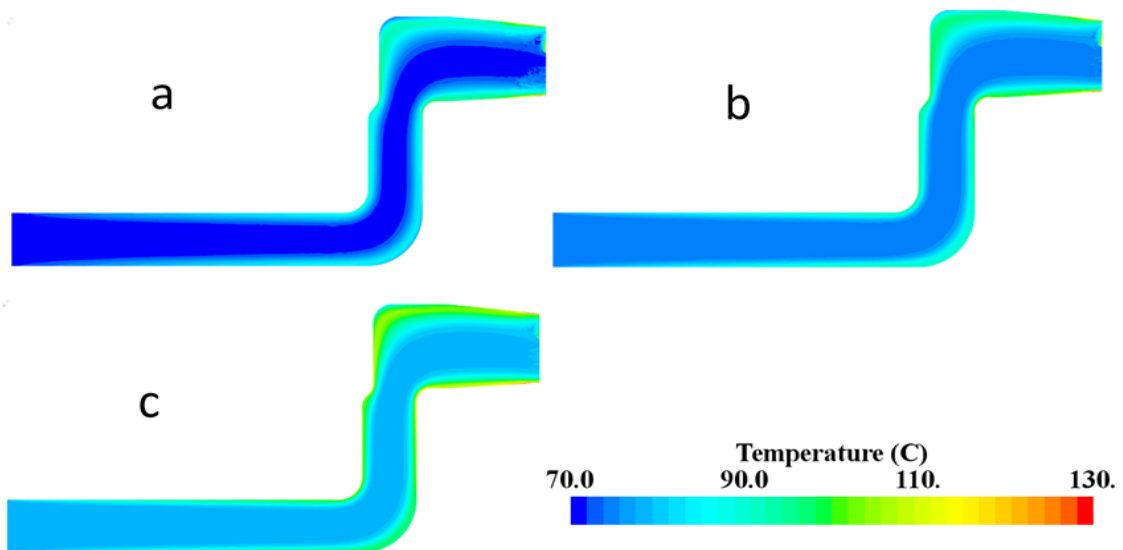


**Figure 5.2:** Contours of temperature distribution in the entire flow domain for different extruder speeds: (a) 10 (b) 15, and (c) 20 rev/min.

The magnitudes of the total predicted temperature rise (difference between mean outlet and inlet temperatures) were 15.7°C, 14.5°C, and 14.3°C for the extruder speeds of 10, 15, and 20 rpm, respectively. The maximum error in the predicted temperature results was less than 1.7%. This typical error is due to certain assumptions during the solution of the heat flow problem in addition to sensor tolerance.

### 5.3 Pressure field

The comparison between the predicted and measured pressure values at the local sensors for various extruder speeds is shown in **Figure 5.3**. The pressure remarkably decreased with increasing extruder speed.

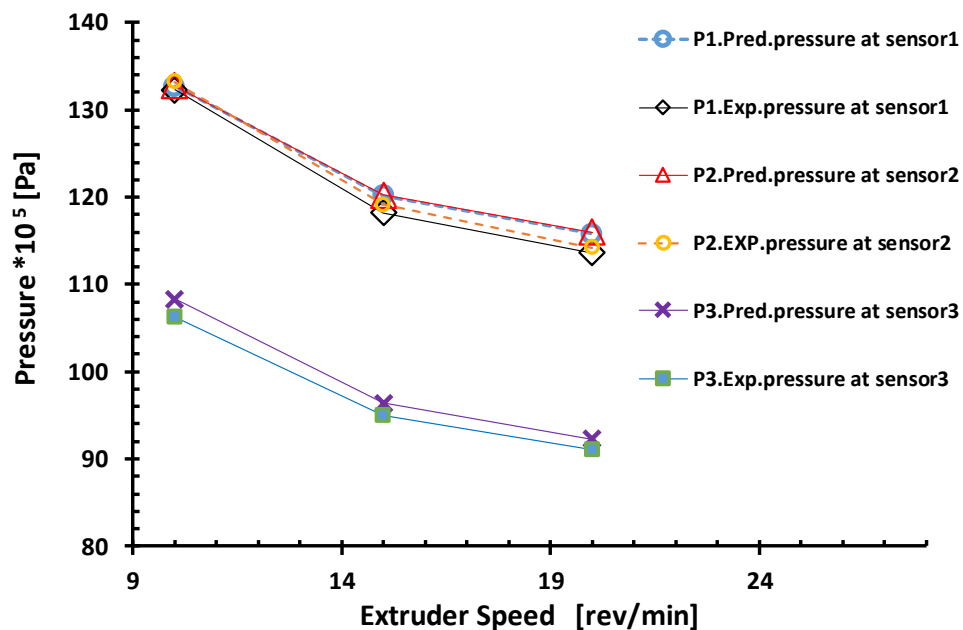


**Figure 5.3:** Measured and predicted pressure versus the extruder speed.

The total pressure drop decreased from  $1.7393 \times 10^5$  to  $1.6049 \times 10^5$  Pa as the extruder speed increased from 10 rpm to 20 rpm. This trend of the pressure drop is attributed to the increase in temperature due to self-heating, which leads to a decrease in viscosity. Moreover, the pressure values in sensors 1 and 2 coincided because of their symmetric locations in the die regime. Thus, the transducer measurements were validated. In addition, the experimental and numerical results showed that the elbow design reduced the pressure by approximately  $25 \times 10^3$  Pa. This reduction is attributed to the increase in the resistance to the flow due to geometric effect and directional change of the flow. The maximum error in the pressure prediction was less than 2%. The contours of the predicted pressure in the entire flow domain for different extruder speeds are depicted in **Figure 5.4**.

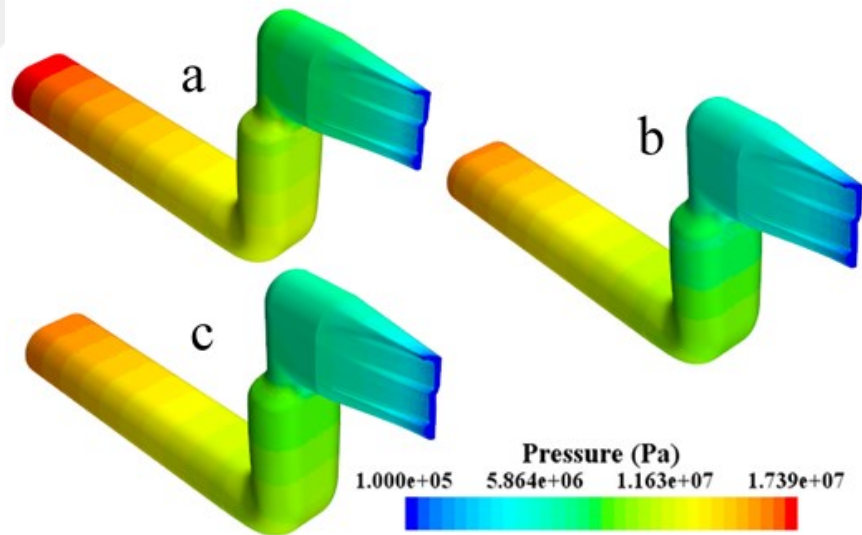


**Figure 5.4:** Contours of predicted pressure distribution in the entire flow domain for different extruder speeds: (a) 10, (b) 15, and (c) 20 rev/min.

## 5.4 Velocity field

The contour of velocity distribution at die exit are shown in **Figure 5.5** for different extruder speeds. The predicted mean velocity increased from 0.16852 [m/s] to 0.32656 [m/s] as the extruder speed increased from 10 rpm to 20 rpm. This increase is due to the increase in mass flow rate in addition to modification occur due to change in temperature field.

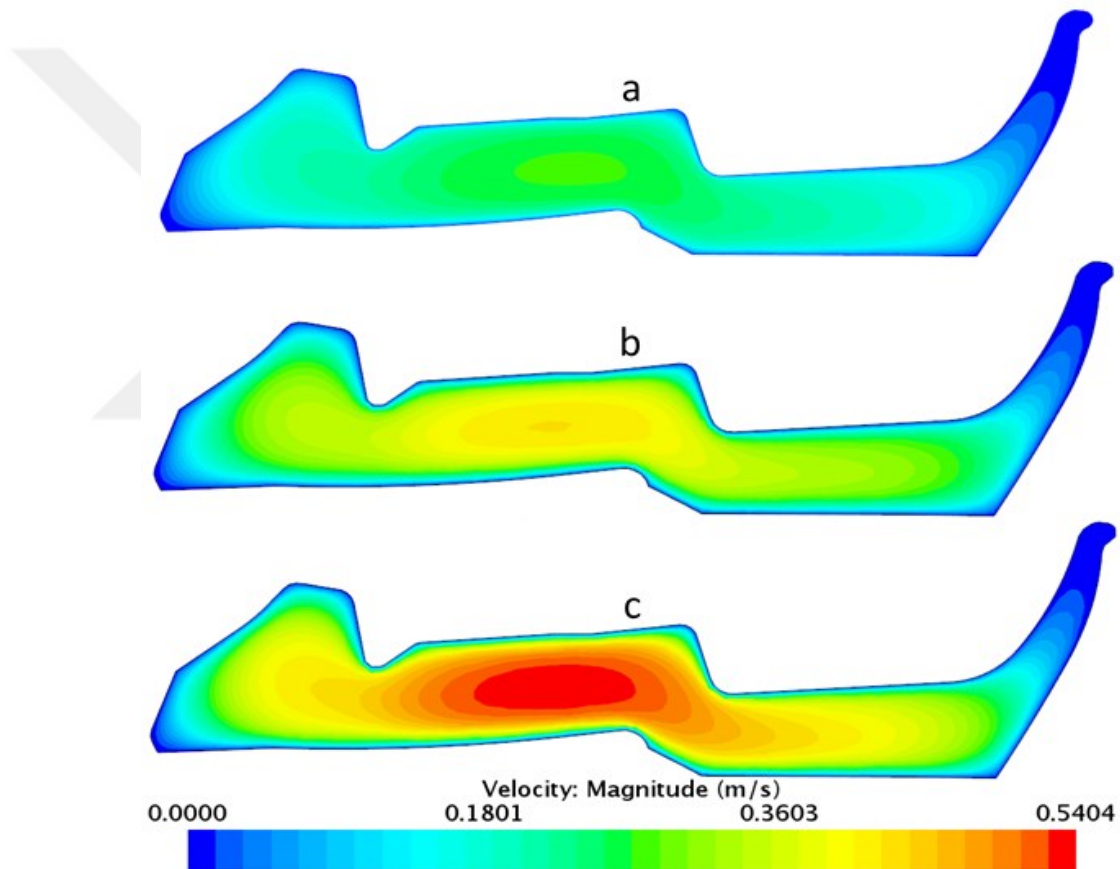


**Figure 5.5:** Contours of velocity distribution at exit section of die for different extruder speeds: (a) 10, (b) 15, and (c) 20 rev/min.

The other important factor in extrusion process is the velocity uniformity at the outlet section of the die which greatly influence on extrudate quality [56]. This factor has accurately described by uniformity index expressed as [71]:

$$V_u = 1 - \frac{\sum_f |V_f - \bar{V}| A_f}{2|\bar{V}| \sum_f A_f}, \quad (5.1)$$

where:  $\bar{V}$  is the average velocity at the outlet surface,  $V_f$  is the velocity at each individual node at the face,  $A_f$  is the area of each individual face of node element.

Uniform velocity distribution is desired at die exit to reduce the defect of distortion but from practical point of view it is difficult to reach a value of 1 which mean complete uniform velocity profile at the outlet surface.

The predicted uniformity index is about 0.8 for all extruder speed which indicates that this property was independent on processing variables or rheological field variable. Indeed, this criterion mostly depend on design parameter of the die. This can be explain by considering the velocity vector at die exit as depicted in **Figure 5.6**. It can be seen that high velocity appears at thick area of die exit while less velocity appears at thin area. Thereby the velocity index mostly covering by design parameters of the die.

The value of predicted velocity uniformity index with reach to about 0.8 imply that the proposed die design is not required for correction. Since this value not show big distortion or deviation in the outlet profile geometry during extrusion experiment. Therefore, this criterion can be helpful to get primary information before die manufacturing and save in time and cost.

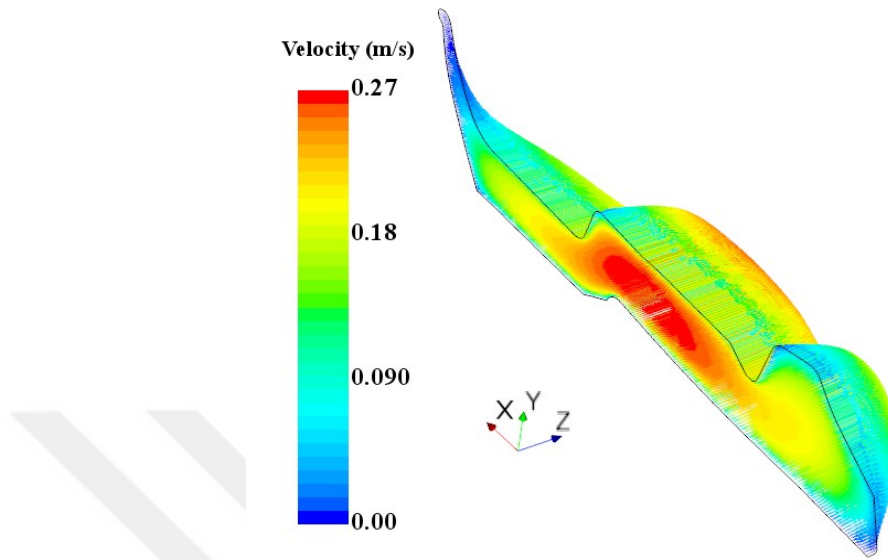


**Figure 5.6:** Velocity vector at die exit at extruder speed 10 rev/min.

## 5.5 Residence time

Residence time ( $t_{res}$ ) was calculated by integrating its convective derivative on velocity field obtained from the simulation by using the following equation [132]:

$$\frac{Dt_{res}}{Dt} = \frac{\partial t_{res}}{\partial t} + v \cdot \nabla t_{res} = 1, \quad (5.2)$$

**Figure 5.7** depicts the contour of residence time distribution calculated for each extruder speed.



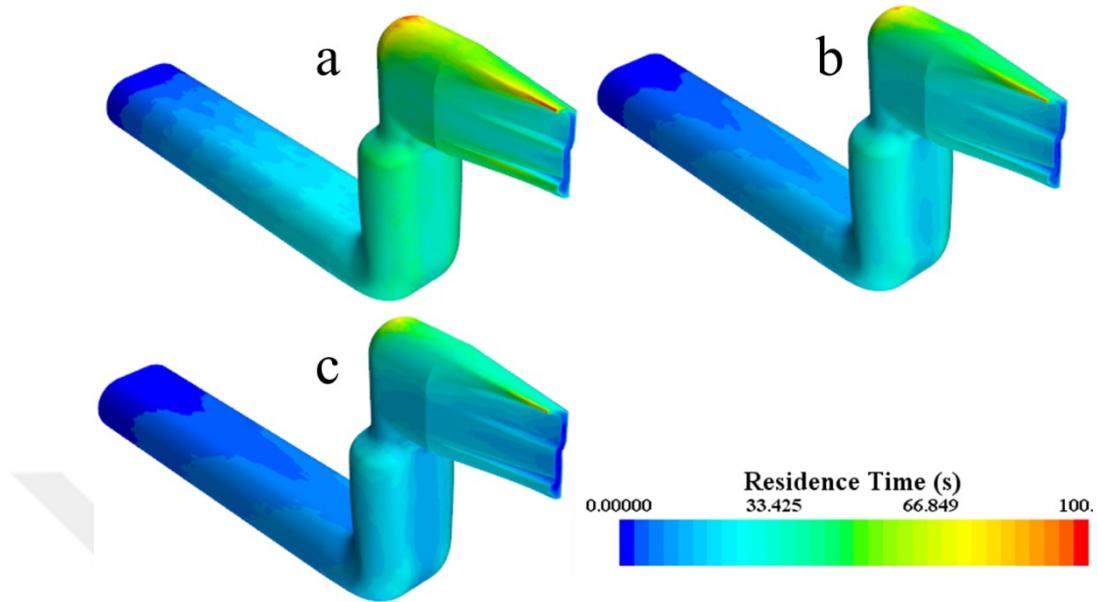


**Figure 5.7:** Contour of residence time distribution at various extrusion speeds: a. 10, b. 15, and c. 20 rev/min

The variation in the maximum residence time versus the extruder speed is plotted in **Figure 5.8**. The residence time remarkably decreased with increasing extruder speed. This decrease in residence time is generally due to the increase in the velocity of the material particle inside the die with increasing mass flow rate; as such, passing through the flow domain requires less time.

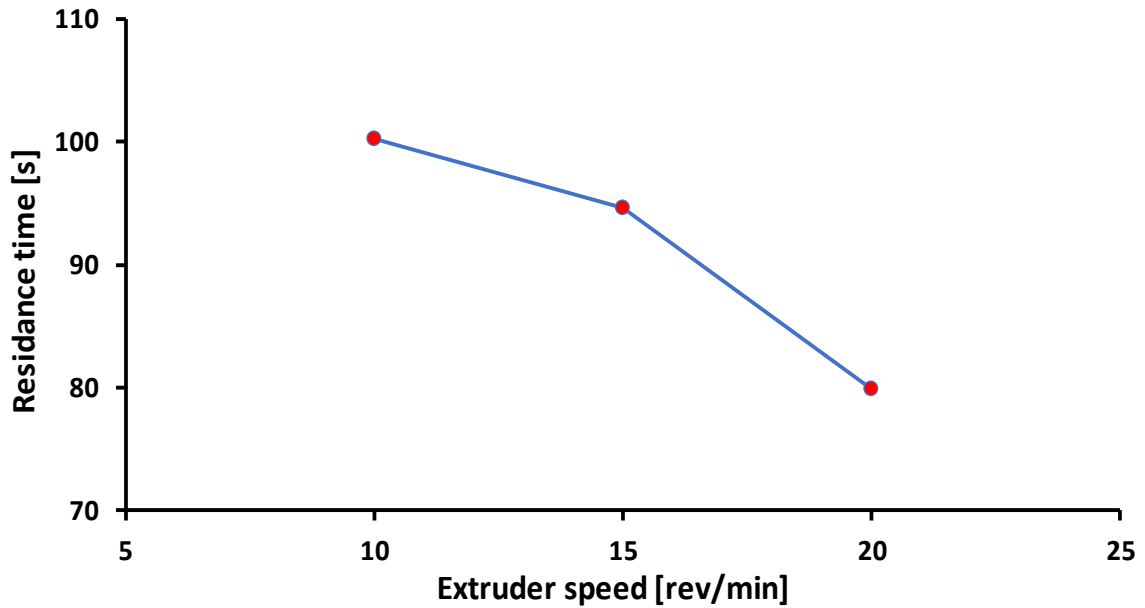


**Figure 5.8:** Variation of maximum residence time with extruder speed.

The calculated scorch time values from the curing tests previously described in **Figure 3.12** (in chapter3) show remarkable reduction in the scorch time with increasing temperature as shown in **Figure 5.9**. Within 120 °C to 140 °C, the scorch time decreased by half with each 10 °C increment in the temperature. However, for high temperature ranges (140 °C to 150 °C), less influence of temperature rise was observed.

From the analysis of residence time presented in **Figure 5.8** for all ranges of the extruder speed, the maximum residence time is approximately 1.67 min. Therefore, all of the studied ranges of screw speed are considered safe processing conditions in terms of curing inside the die. The experiments conducted in the extrusion line confirm this finding due to the absence of curing inside the die. However, this result suggests that the additional increase in the extruder speed is possible to improve productivity. The maximum temperature rise of

approximately 130°C in the third extruder speed has a scorch time about 6.93 min, which is far from max. predicted residence time.

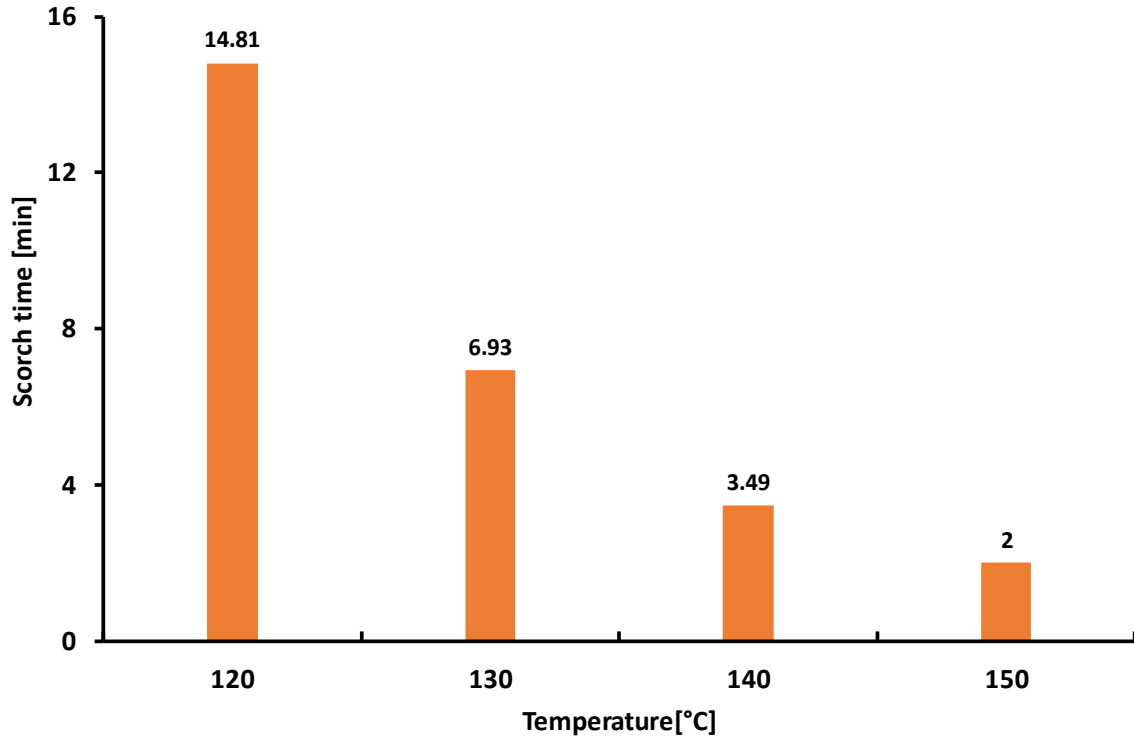


**Figure 5.9:** Variation of scorch time versus temperature for EPDM rubber compound.

## 5.6 *Streamline*

The path of zero mass particle in the three dimensional fluid domain described by streamline as shown in **Figure 5.10** Runge-Kutta method implemented during simulation to calculate this path by integration of velocity vector variable with time step control. The stream line created under the assumption of steady-state flow even with transient simulation and it take considerable amount of memory and time [71].

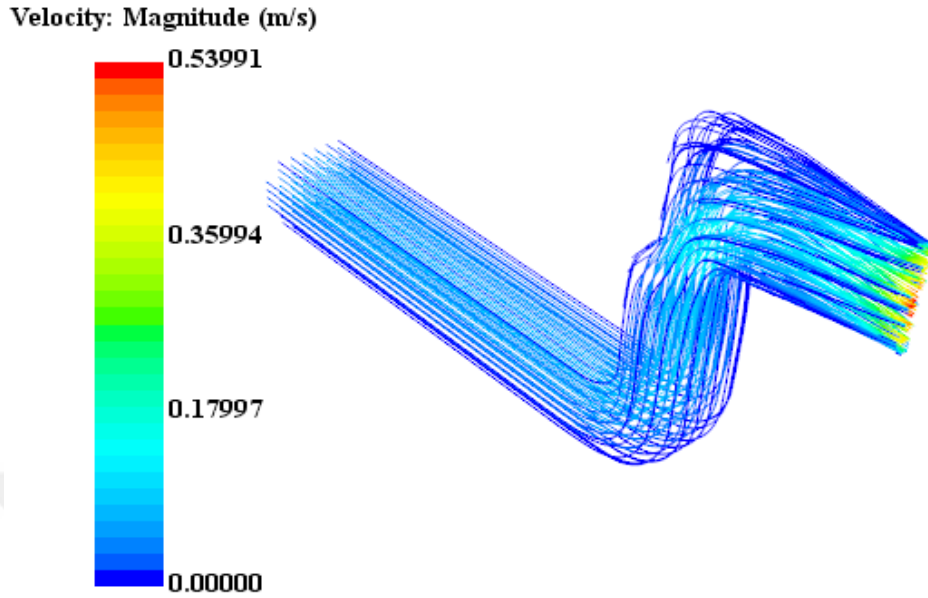


**Figure 5.10:** Streamline in the three dimension flow domain for extruder speed 20 rev/min.

The analysis of streamline in the flow pattern show that there is no circulation flow or overlap between fluid layer inside the die. Moreover, no terminated line appears in the flow pattern which indicate to the absence of stagnation region in the entire flow domain [71]. Therefore, from this point of view the proposed die design not need to correction and can directly put in work without running-in experiments.

From the above analysis of rheological field variable and their effect on product quality one can choose the optimum operating conditions together with monitor and control of these variable.

# CHAPTER VI

## RESULTS OF VISCOELASTIC MODELLING

### **6.1 Introduction**

In this chapter, the result of adopting viscoelastic rheological model namely, Giesekus model was presented. The first part described the result of swelling of 10% Butadiene rubber BR and 90% Styrene rubber SR in simple geometry represented by capillary die taken as benchmark problem. The result of swelling compares with experimental data available elsewhere [37] for validation of computational results obtained. The effect of relaxation time, number of mode and mass flowrate on swelling behaviour and circulation flow were discussed and analysed. In addition, the flow field variables velocity pressure was calculated and discussed. In the second section, viscoelastic modelling was applied to more complex geometry represented by industrial scale extrusion die. EPDM rubber for weather strip application was used as extruded material. The result of swelling was discussed and analyses.

### **6.2 Extrudate swell of rubber compound**

Two elastic mechanisms associated with memory effect and elastic relaxation contribute to extrudate swell in polymer flow. These mechanisms can be explained from molecular stand point. The flexible polymer chain has a random coil conformation in un deformed state. As this material deformed by shear field, it has oriented in the direction close to the flow field. When the polymer emerges from the die exit, all external stresses are released, so the polymer chain returns to its preferred original conformation shape. This causes the swelling in travers direction as well as contraction in axial direction [133].

The predicted swelling results were compared with the experimental data of [37] in **Figure 6.1**. The predicted results were calculated by applying the Giesekus model with various relaxation time ranges and relaxation modes over a range of flow rate. Results reveal that die swell generally increases with the increase in the range of relaxation time for all the simulation results. This trend can be attributed to the high elasticity of the material which exhibits a wide range of relaxation time [63]. With regard to the single relaxation mode, the slope of the final profile shows a slight increase with increased relaxation time.

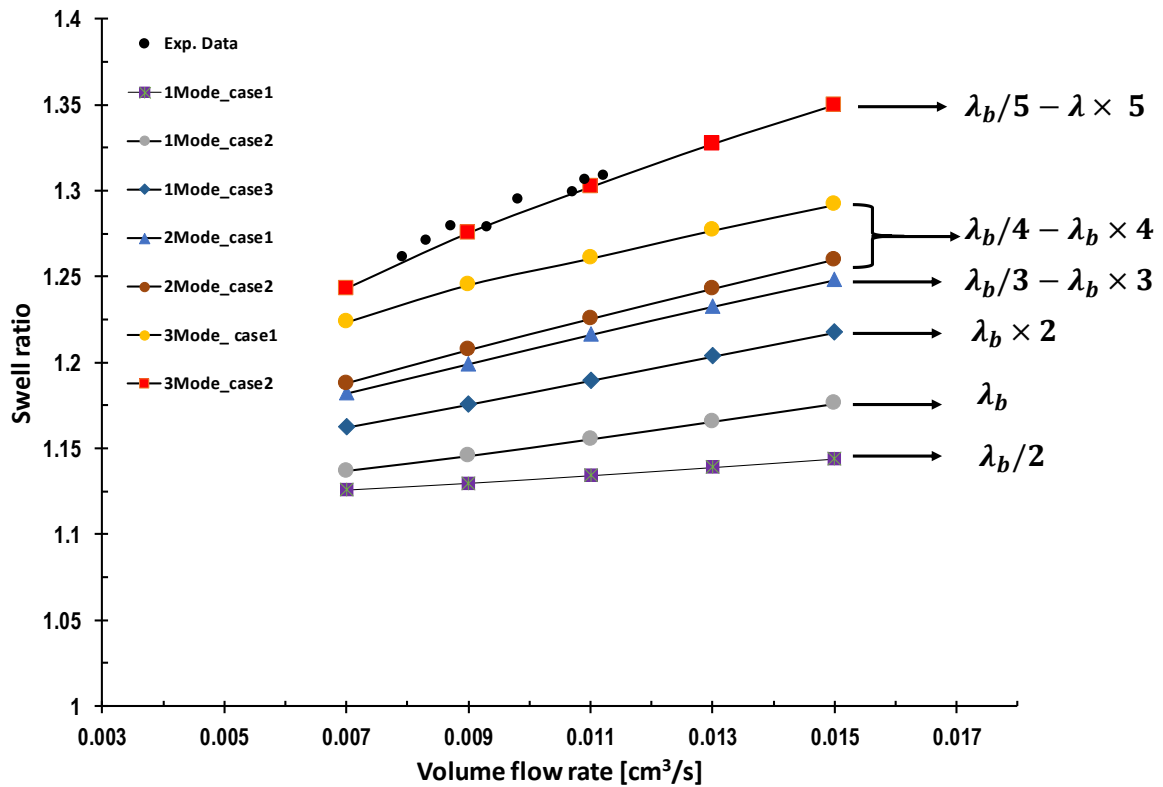


**Figure 6.1:** Comparison of predicted die swell adopting various relaxation time and relaxation mode with experimental data given by Choi and Lyu [37].

When two relaxation modes are used, swelling increases with the increased flow rate, with approximately equal slope for both relaxation times. The use of one mode and two

modes with all relaxation times shows results deviating from the experimental data. The simulations converge to the experimental data with the increased number of modes. Three relaxation modes with a wide range of relaxation time in case two show a sharper increase in swelling than those in other cases. In addition, the experimental results of the extrudate swells presented by Choi and Lyu [37] show an increase in the range of 1.26–1.3. The predicted extrudate swells using three relaxation modes with the range of relaxation time of  $(\lambda_b/5 - \lambda_b \times 5)$  are close to the experimental results. The three relaxation modes using the parameter in case one with the relaxation time range of  $(\lambda_b/4 - \lambda_b \times 4)$  underestimate the measured swelling data.

### ***6.3 Velocity and pressure field***

The predicted velocity distributions under three relaxation modes for the same mass flow rate and different relaxation times are depicted in **Figure 6.2**. Fluid velocity is considerably slow in the entrance of the reservoir, and it starts to increase promptly when the material approaches the die regime because of the large contraction in the flow area; it finally reaches the maximum level at the die center. Moreover, for the three-mode viscoelastic simulation, the velocity in the extrudate region is slightly low when a wide range of relaxation time is adopted because of the region's high cross-sectional area due to high swelling.

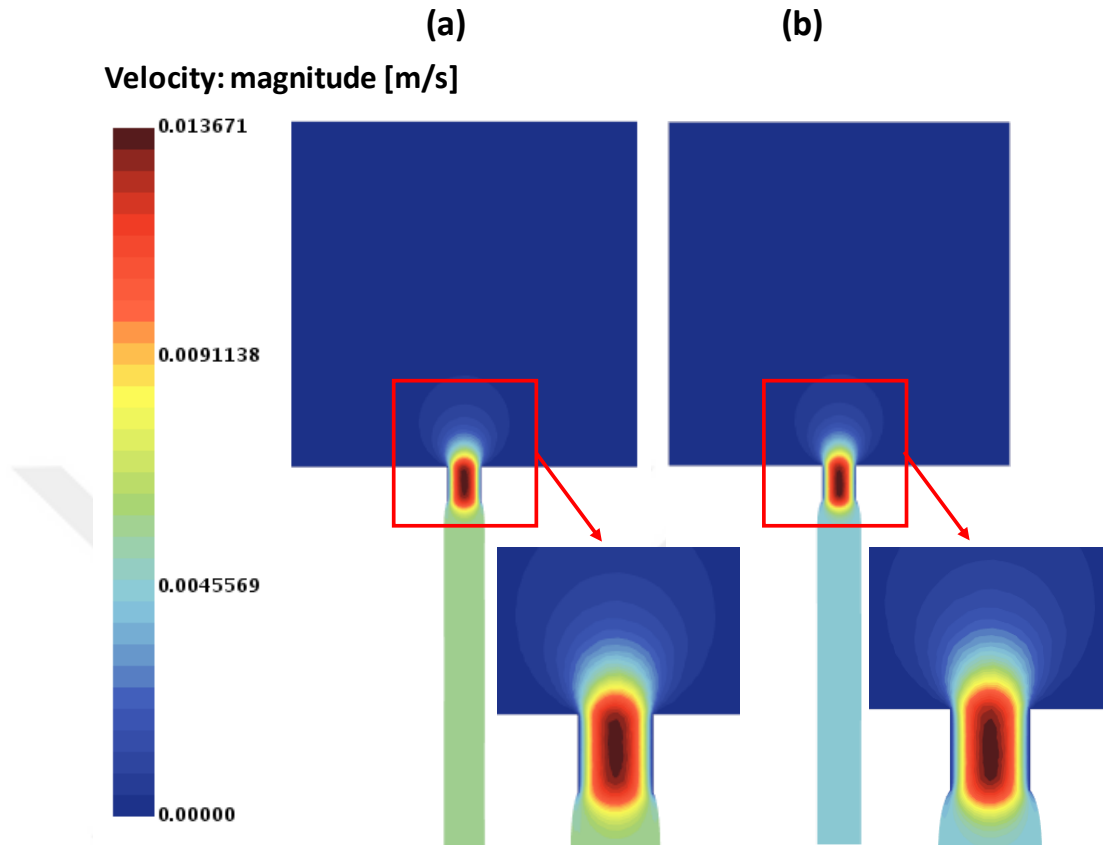


**Figure 6.2:** Velocity distributions (m/s) in a capillary die for three relaxation mode simulation and constant flow rate = 0.011 cm<sup>3</sup>/s. a)  $\lambda = (\lambda_b/4 - \lambda_b x 4)$  , b)  $\lambda = (\lambda_b/5 - \lambda_b x 5)$ .

**Figure 6.3** displays the pressure distributions using three relaxation modes. The maximum pressure in the flow domain observed near the capillary die entry corner progressively decreases and reaches the minimum when the material passes the die exit. For the three relaxation modes, the pressure drops increase with increased relaxation time. A high range of relaxation time indicates high elasticity and consequently high resistance to flow. The pressure drop is high when a wide range of relaxation time is adopted.



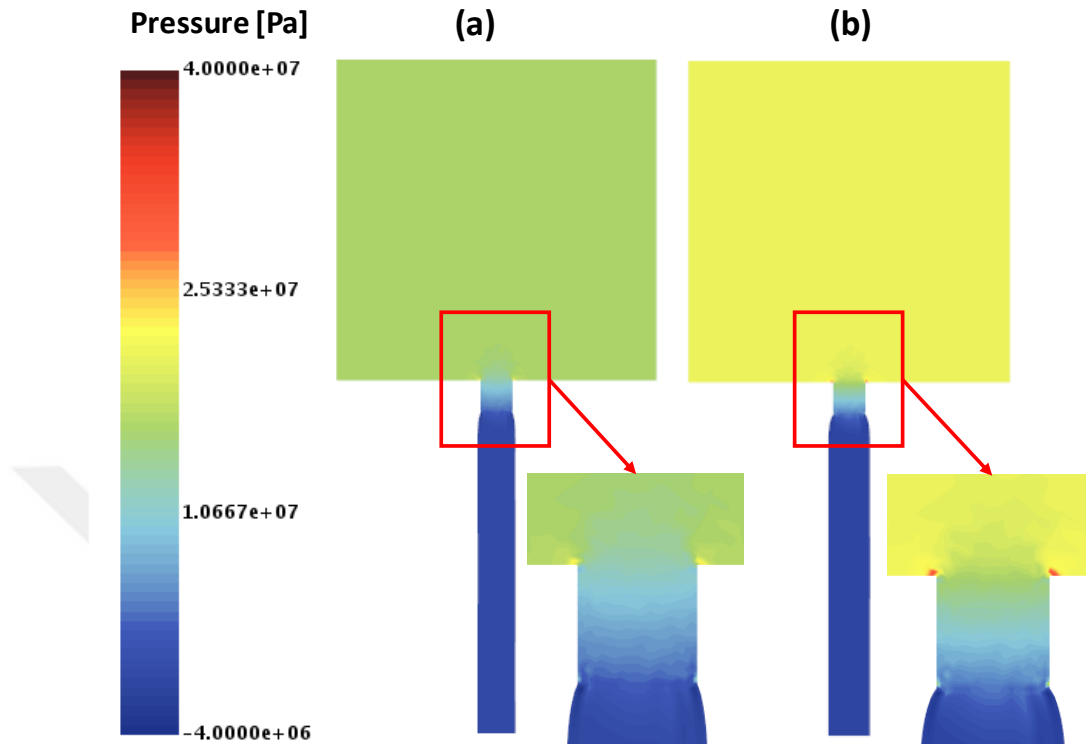


**Figure 6.3:** Contour of pressure distributions in a capillary die for three relaxation mode simulation and constant flow rate=0.011cm<sup>3</sup>/s .a)  $\lambda = (\lambda_b/4 - \lambda_b \times 4)$ , b)  $\lambda = (\lambda_b/5 - \lambda_b \times 5)$ .

## 6.4 Shear rate and dynamic viscosity

Figure 6.4 illustrates the shear rate and dynamic viscosity using three relaxation modes. The maximum shear rate in the flow domain is observed in the entrance of the capillary die and on the die wall as a result of the high contraction area. Consequently, the minimum dynamic viscosity is observed on the die wall due to the shear thinning behaviour of the rubber compound. There no change in dynamic viscosity observed in the reservoir region due to low shear rate.

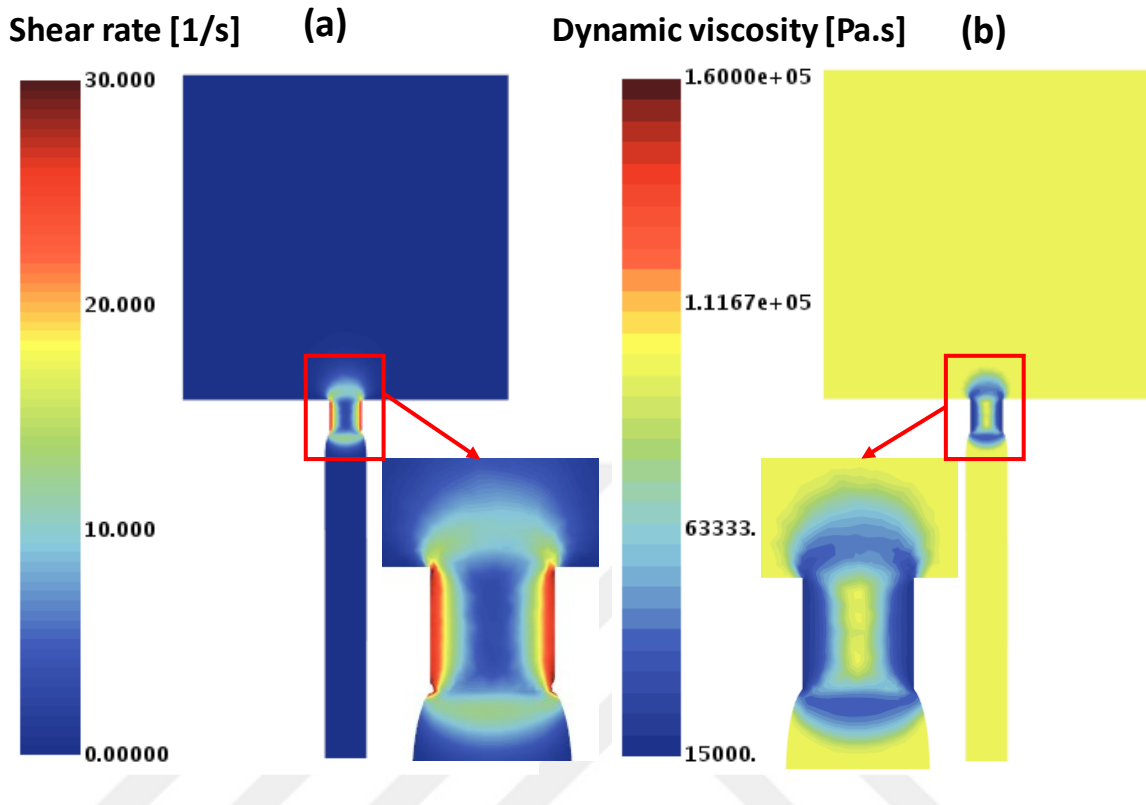


**Figure 6.4:** Contour of a- Shear rate distribution b-Dynamic viscosity distributions in a capillary die for three relaxation mode simulation case2,  $\lambda = (\lambda_b/5 - \lambda_b \times 5)$ .

## 6.5 Circulation flows

To visualize the vortices, the line integral convolution is applied on all velocity vectors in the flow domain[134,135].The vortices adopting three relaxation modes and different relaxation times are depicted in **Figure 6.5** . Results reveal that the wide relaxation time range shows larger vortices at the corner than those with narrow relaxation time range. This result is attributed to the increase in elasticity with the increased relaxation time[136]. The same trend is observed using two relaxation modes.

Circulation flow or vortex formation can be considered the main viscoelastic behaviour of polymeric fluid, and it mainly depends on the degree of elasticity in a material.

The degree of elasticity for a viscoelastic fluid is characterized by a dimensionless parameter, namely, the Deborah number, which is the ratio between the relaxation time of a fluid and the characteristic time of flow. In the case of capillary die contraction flow, the Deborah number can be expressed as follows [137].

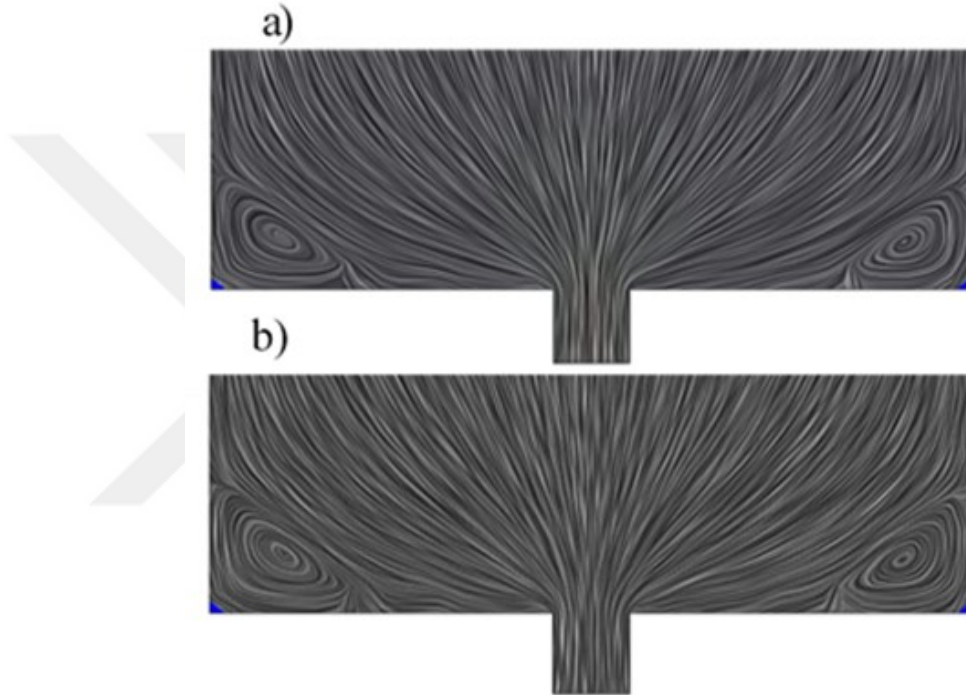


**Figure 6.5:** Core vortices at the corner of reservoir for three relaxation mode, a) Case1  $\lambda = (\lambda_b/4 - \lambda_b \times 4)$ , b) Case2  $\lambda = (\lambda_b/5 - \lambda_b \times 5)$ . (Flowrate=0.011 cm<sup>3</sup>/s).

$$D_e = \frac{\lambda \dot{V}}{d/2} \quad (6.1)$$

where  $\dot{V}$  and  $d$  are the average velocity and diameter in the downstream region, respectively. The trend in Figure 6.5 is consistent with experimental and numerical findings of Sousa et al.[137], who investigated the flow pattern of shear thinning viscoelastic fluid in a contraction flow. They found that vortex size increases with increasing Deborah number. Given that Deborah number is a function that increases with relaxation time and mean velocity, as stated

in Equation 6, vortex is enhanced at increased relaxation time and mass flowrate. This finding proves that vortex formation and growth are directly linked to fluid elasticity. Moreover, when the elastic behaviour predominates the viscous behaviour in a viscoelastic fluid, the system is becoming increasingly energetically conservative, hence promoting circulation flow. By contrast, a viscous-dominated flow is energetically dissipative and thus reduces vortex activity. **Figure 6.6** shows the evolution of vortices for one, two and three relaxation modes.

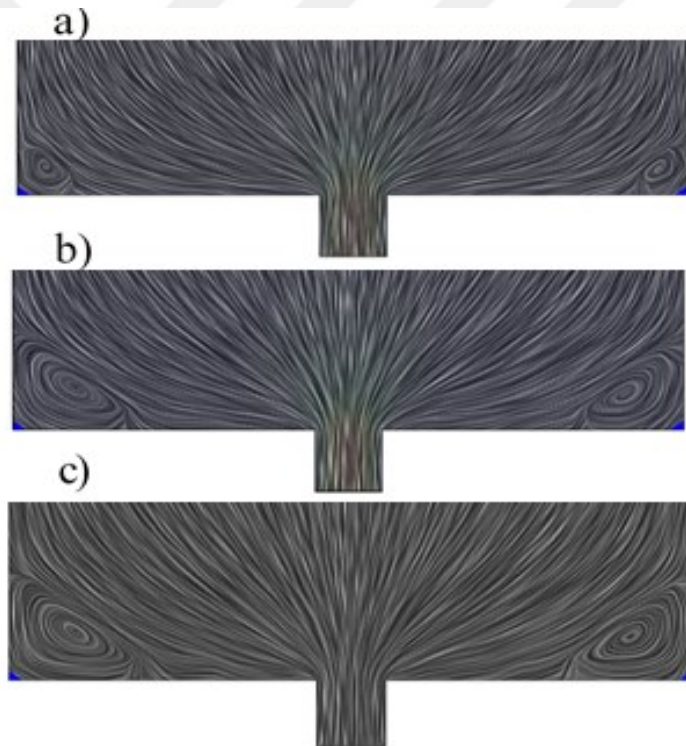


**Figure 6.6:** Core vortices at the corner of reservoir for various relaxation modes, a) One relaxation mode simulation case1  $\lambda = (\lambda_b/2)$ , b) Two relaxation modes case1  $\lambda = (\lambda_b/4 - \lambda_b \times 4)$ , c) Three relaxation modes simulation case2  $\lambda = (\lambda_b/5 - \lambda_b \times 5)$  (Flowrate=0.011 cm<sup>3</sup>/s).

The trend in **Figure 6.6** shows the increase in vortex size with increasing number of relaxation mode in the simulation. This behaviour may be attributed to the increase in

maximum relaxation time at increased number of mode, which also lead to increase in elasticity. Moreover, from the prospective of molecular weight and molecular weight distribution in a polymeric system, a direct link exists between the molecular weight of a structural element in a polymeric material and relaxation time[138]. Adopting a high relaxation mode apparently allows the coverage of expected various molecular weight distributions, leading to vortex enhancement.

The effects of flow rate on vortex enhancement are presented in **Figure 6.7**. Circulation flow (vortex size) increases with increased flow rate because a high flow rate combines with the high shear rate. The trend of circulation flow under the studied parameters shows good agreement with that of circulation flow with the PTT model given by Choi and Lyu [37].

In addition to relaxation time, vortex size is dependent on the ratio of elongational properties versus shear properties. For large shearing, the shearing viscosity is proportional to  $((1 - \alpha)/\alpha)^{0.5}$ . Hence the ratio of elongational viscosity/ shear viscosity is proportional to  $1/((1 - \alpha)\alpha)^{0.5}$ . In this regard, the value of mobility factor  $\alpha$  is relevant to the vortex enhancement, and the ratio  $1/((1 - \alpha)\alpha)^{0.5}$  controls the value of vortex enhancement [117]. This ratio will increase by decreasing the value of  $\alpha$  from 0.5. For instance, depending on the value  $\alpha$  (in Table 4.5), this ratio equal to 2.161 for three relaxation mode case 1. While, this ratio increase to 2.935 for three relaxation mode case 2.

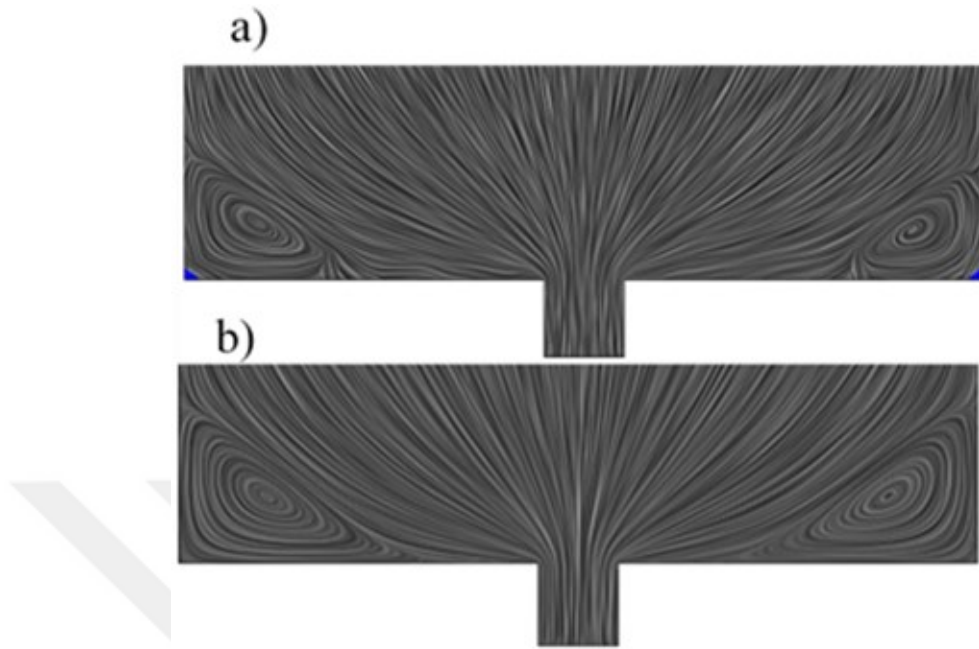


**Figure 6.7:** Core vortices at the corner for various flowrate adopting three relaxation mode

## 6.6 Swelling of EPDM rubber in capillary die

The previously validated proposed model was utilized to investigate the swelling behaviour of EPDM rubber compound in capillary die. The swell ratio in capillary die is calculated from the ratio of fully relaxed extrudate diameter to the diameter of die at exit flow. A comparison between swelling of Butadiene rubber and EPDM rubber presented in **Figure 6.8**. The trend of swelling in Figure 6.8 show increase in swelling ratio from 1.1 to 1.14 upon increase in volume flow rate from 0.007 to 0.015 cm<sup>3</sup>/ s. This swelling has very low as compared by swelling behaviour of (SBR) rubber studied by Choi and Lyu [37]. From physical point of view, this considerable change in swelling behaviour can attribute to high additive content which primary used in EPDM rubber compound.

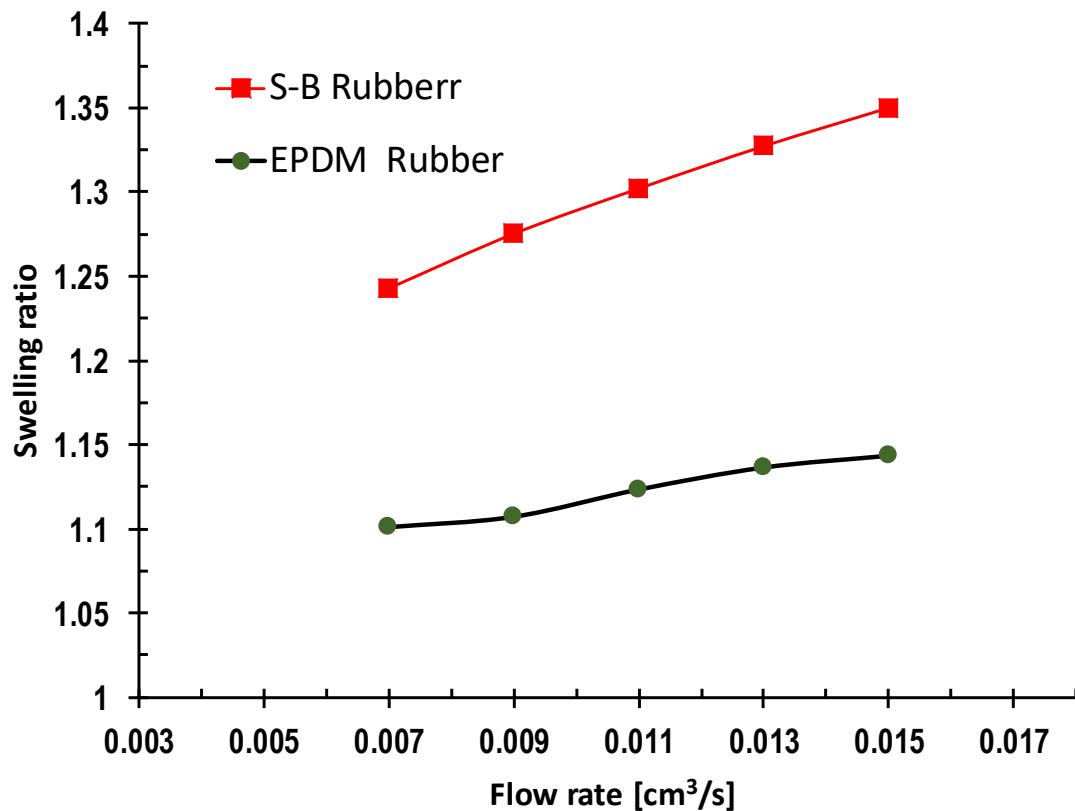


**Figure 6.8:** Comparison of swelling for Styrene-Butadiene rubber and EPDM rubber.

Therefore, the typical viscoelasticity of the polymer phase is suppressed with the generous amounts of fillers and reinforcements that are generally used [51]. This finding indicate that the reinforcing filler used with EPDM rubber make a big change in viscoelastic properties. This finding approved the assumption which applied firstly in modelling fluid flow adopting purely viscous model such as power law. This will reduce computation time and memory cost of expensive finite element computation.

We also should point out that the finite element analysis in industrial scale extrusion die will arise the difficulty in computer memory and time cost required in the case of adopting complex rheological model such as viscoelastic model. For instance, adopting simple model

(inelastic model) the computation time has been done on High performance computer (HPC) with 2 nodes and 28 parallel processor take a time about 24 hours for one numerical experiments. Meanwhile computation cost will increase extensively in the case of adopting complex rheological model.

### 6.7 Stress evolution in capillary die

During fluid flow in extrusion die, the material experiences deformation and strained thereby stress generated and reach its maximum at region of maximum strain. Through the simulation the three stress components are calculated from each mode. It is widely known that swelling occurs dominantly along the principle shearing axis [133]. Therefore, the contributions of principle stress from each individual mode is mostly responsible for swelling after the material leave the die exit. The three principle stress calculated from the first mode depicted in **Figures** (6.9,6.10 and 6.11) bellow.

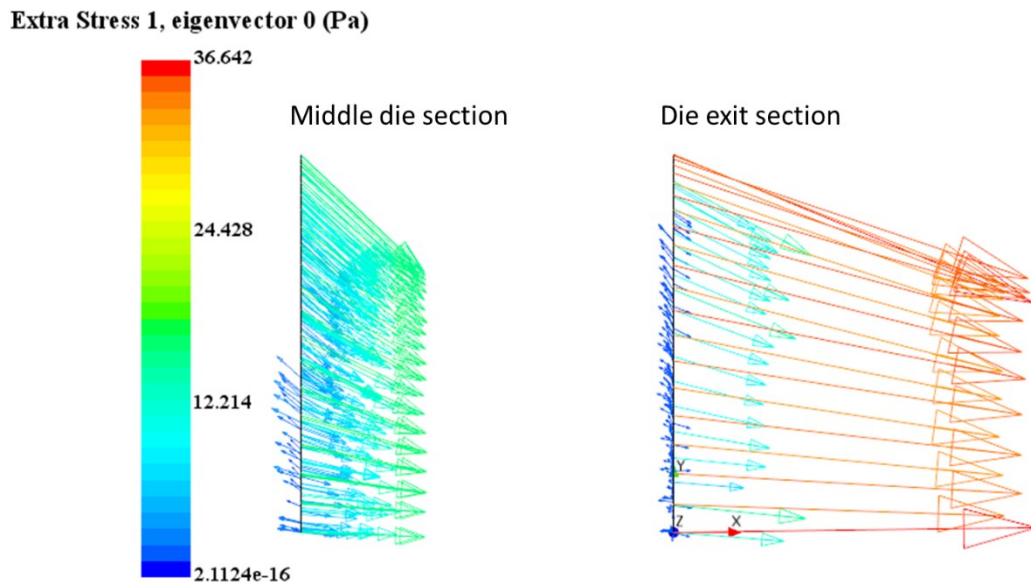


**Figure 6.9:** Stress vectors evolution at die exit and middle die section from the first mode in x-direction.



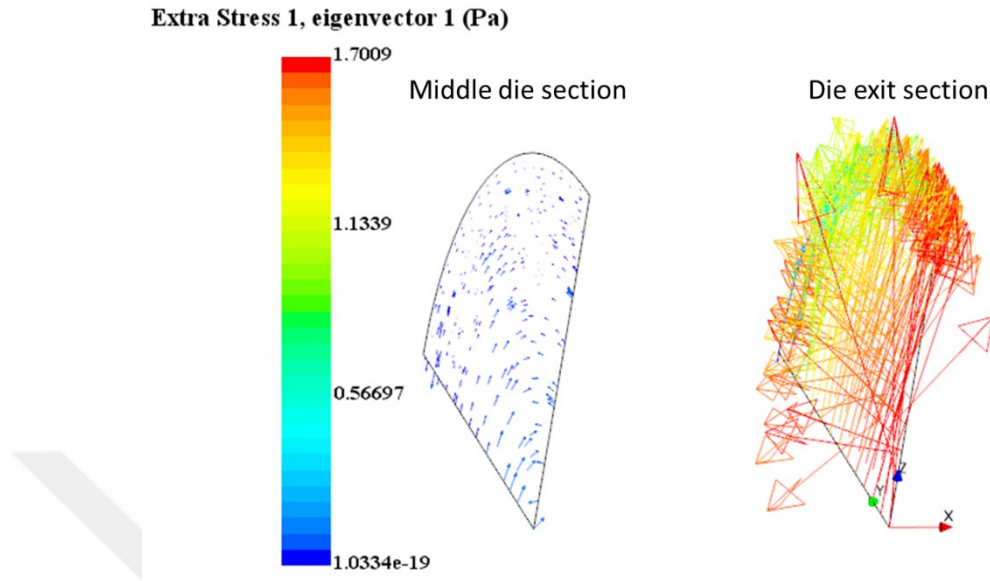


**Figure 6.10:** Stress vectors evolution at die exit and middle section plan from the first mode in y-direction.

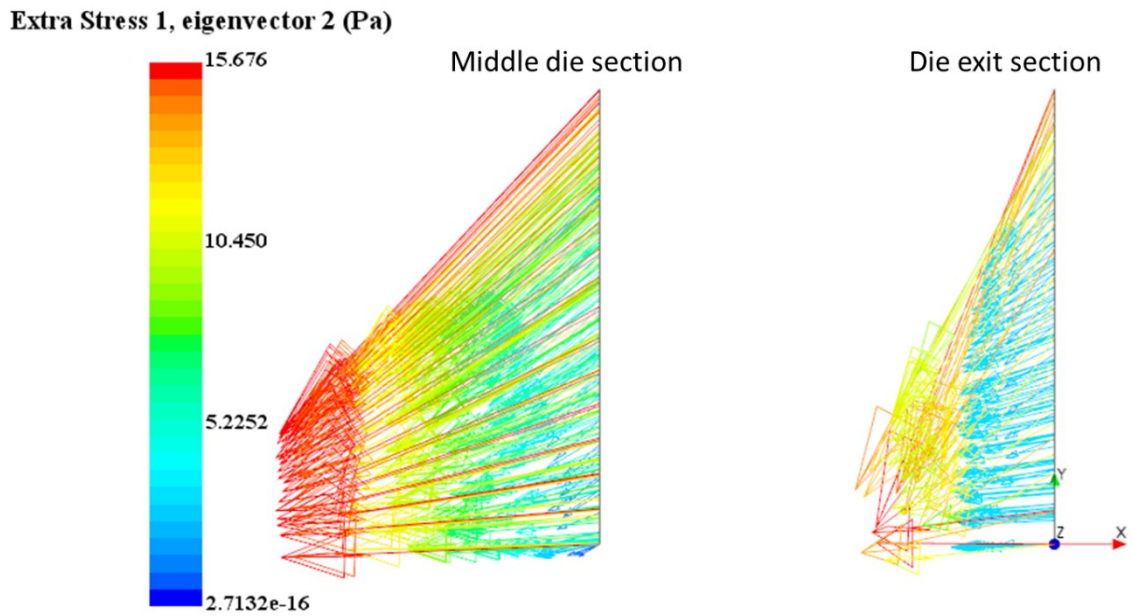


**Figure 6.11:** Stress vectors evolution at die exit and middle section plan from the first mode in Z-direction.

The analyses of stress vector from first mode represented by eigenvector on different projection show that maximum normal stress is about 15.6 Pa as presented in **Figure 6.11**.

While the maximum normal stress in y-direction reach about 1.7 Pa at die exit section as shown in **Figure 6.10**. However, the total normal stress difference from three mode which adopted in the simulation is responsible for swelling phenomena in extrusion process [71].

## **6.8 Effect of design parameters**

The die length is one of design parameters of capillary die. To investigate the influence of this parameter on extrudate swell, extrusion simulation experiments were conducted with die lengths range of 1mm, 2.5mm and 4 mm to determine die swell ratio. It has been reported by Huneault et al.[133] that swell ratio is a function of residence time R (time scale of observation) and relaxation time of material. Therefore, the length of the die plays a rule in extrudate swell since the change in die length will modify the value of residence time. When the die length changed from 1 to 2.5 mm there is very slight change in swelling. This observation implies that the residence time is still below the range of material relaxation time. While with increase in die length to 4 mm there is a remarkable change in swell ratio. This observation suggest that the residence time exceed the critical limit of material relaxation time which give the opportunity for material to relax.

The results obtained presented in **Figure 6.12** agree with the results previously reported by Huneault et. al.[133]. This trend is explained by the fact that with long die, material have longer residence time thereby it can be relaxed more and decrease the memory effect [139]. In other word, increase residence time in polymer melt flow will reduce elastic characteristic and thus reduced swelling [133].

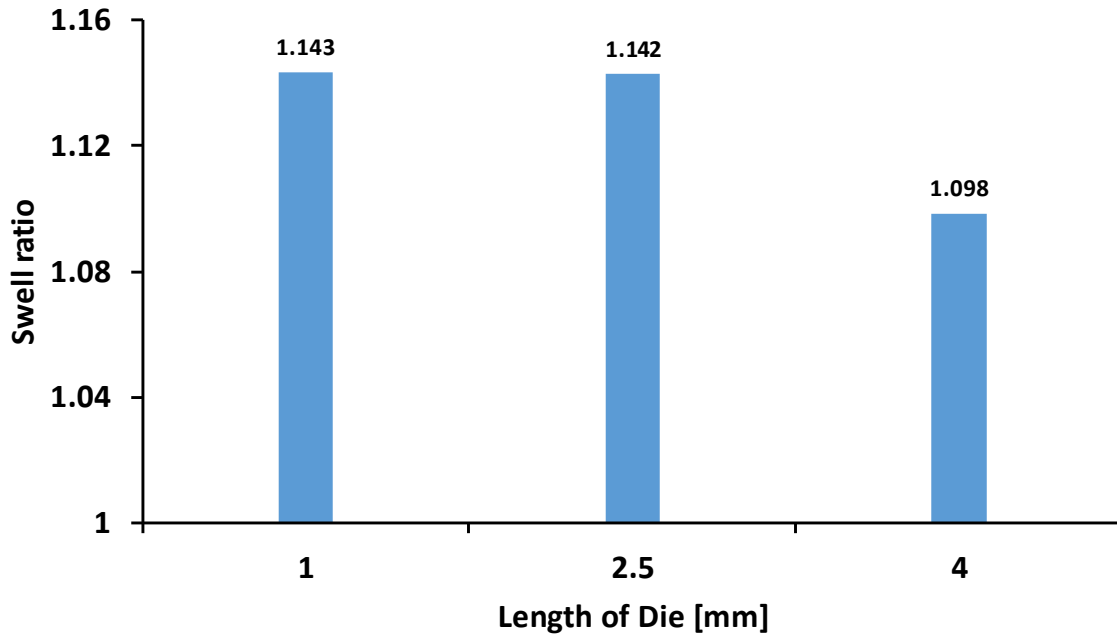


**Figure 6.12:** Swell ratio versus different die length of die for EPDM rubber compound.

## 6.9 Effect of slip

It has been reported by Yang and Li [140] that reinforcing filler, such as silica and carbon black, tends to promote slippage at the wall of die. Unfortunately, the experimental data of slip coefficient for capillary extrusion die was not available. Therefore, Numerical experiment based finite element simulation was utilised to analyse the influence of wall slip on swell in capillary extrusion.

Star CCM uses Navier slip law to model the present of slip on the walls which imposed as boundary conditions. This slip model relate the shear stress per unit surface  $f_s$  to the slip velocity  $v_s$  as expressed below.

$$p = f_s = -k_s v_s^{n_s} \quad (6.2)$$

where  $k_s$ ,  $n_s$  are the slip coefficient and slip exponent, respectively.

Comparison of swell ratio in capillary die for various value of slip coefficient and No-slip condition is depicted in **Figure 6.13**. As revealed by the predicted swelling results, the no-slip condition produce swell is higher than all the swell ratio predicted with imposing slip condition. However, the swell under slip condition show slight decrease in swell with decrease the value of slip coefficient. This is because the amount of shear rate at the wall show low value with imposing slip condition on the die wall. Thereby the velocity profile and generated stress field will be effected by the amount of shear rate. Therefore, those modifications will contribute to change the amount of swell at die exit.

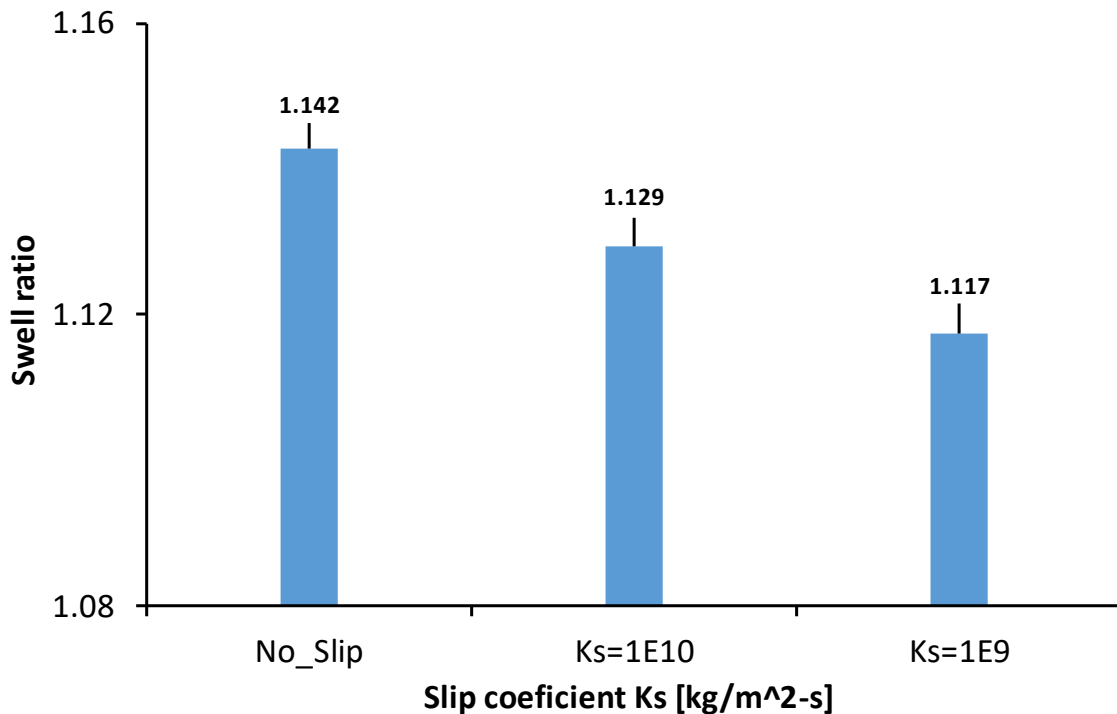


**Figure 6.13:** Swell ratio of EPDM rubber for various slip conditions.

## 6.10 Swelling of EPDM rubber in complex geometry

A comparison between predicted extrude profile and die profile presented in **Figure 6.14**. The trend of swell in complex geometry show a very slight deviation in extrudate profile from the original die profile. The results obtained from the analysis of extrudate profile suggest that the primary computational analysis for the proposed design of die not required a correction. Therefore, this die can be used in extrusion line with known processing variable without running-in experiments to produce the required product geometry. The swelling behaviour for EPDM rubber agree with swell behavior of the same material in capillary die. The experimental work conducted in extrusion line also show acceptance of final profile dimension with respect to designed die.

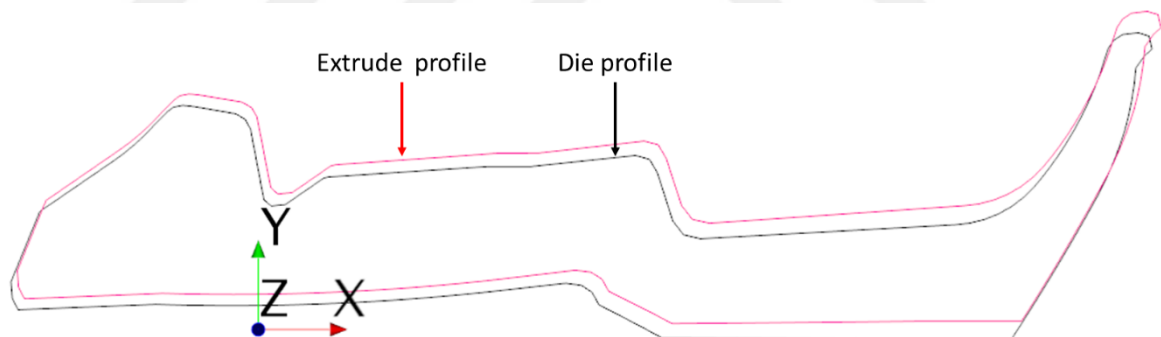


**Figure 6.14:** Die exit profile and final predicted extrude profile in complex geometry

## 6.11 Stress evolution in complex geometry

During extrusion process, the melt flow leaves the die lips with different velocity over cross section area at die exit. This will lead to accelerate the velocity of material near the die wall to reach the maximum velocity of extrudate. Thereby tensile stress likely to generate at the surface area of extrude. This tensile should not exceeds the tensile strength of melt

material otherwise surface rupture can appear and make surface defect such as sharkskin or surface fracture.

The analysis of stresses at die exit shows maximum contribution of stresses from third elastic mode as depicted in **Figure 6.15**.

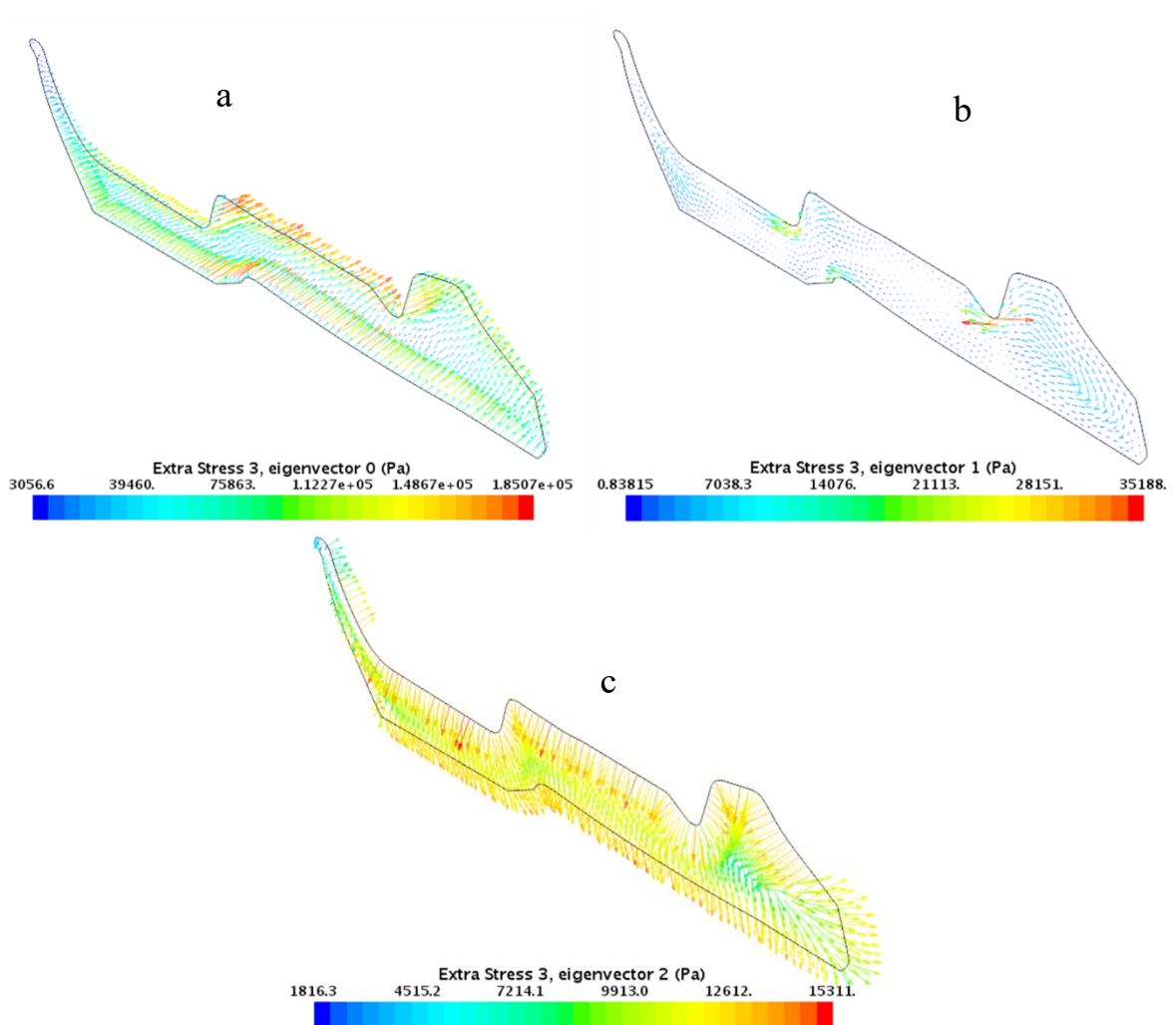


**Figure 6.15:** Evolution of stress vector at die exit from third elastic mode a.x-direction component, b.y-direction component, c.z- direction component.

The total stresses predicted from simulation which contributed from all mode adopted in three Cartesian coordinate were 190621.23 Pa, 36103.261 Pa and 17666.519 Pa in X, Y

and Z direction, respectively. This indicate that the maximum tensile stress generated in the direction of extrusion (Z-direction) was 17.6665 MPa which should not exceed to avoid surface defect. Unfortunately, there is no available data about the tensile strength of melt material to compare. Whoever, extrusion surface defects were not observed during extrusion experiments which indicate that the tensile strength of used material is above the predicted limit.



## CHAPTER VII

### CONCLUSION AND FUTURE WORK

#### *7.1 Conclusions*

Profile extrusion of rubber compound in especially design extrusion die is studied by modelling rheological flow based on finite element method. For this purpose, a schematic frame work for modelling non-isothermal flow with viscous dissipation in industrial scale extrusion die was presented and explained.

The variations in the rheological properties (i.e., pressure temperature, velocity field and residence time versus different extruder speeds) of the rubber melts during extrusion in an industrial scale extrusion die were investigated by experiments and FE numerical simulation. Stable numerical results were achieved by adopting SUPG technique in the solution scheme and PSPG method. The experimental and numerical results showed the remarkable effects of viscous dissipation on temperature and pressure field during the flow inside the die. The comparison between the simulated and experimental results in terms of temperature and pressure confirmed the ability of the proposed model to predict flow field variables.

The analyses of the temperature field in the entire flow domain together with the predicted residence time confirm the production ability without risk of premature vulcanisation or 'scorch' for all studied ranges of the extruder speed. Therefore, high extrusion speed should be chosen to obtain the maximum productivity. The rheological properties measured in this work provide a helpful reference for processing of rubber



compounds in the rubber industry to determine the suitable extruder speed and ensure thermal stability. Furthermore, the results can provide guidance to avoid some problems in rubber extrusion, such as the emergence of a stagnation zone near the wall. These zones are induced by the temperature rise due to viscous dissipation and can restrict flow and promote the curing effect inside flow domain. Hence, productivity enhancement by increasing the extruder speed could be achieved by elaborate modification in both residence time and temperature field inside flow domain. Thus, for highly reactive materials, such as elastomers, non-Newtonian simulations that consider self-heating are important to investigate and monitor flow in the extrusion die.

The experimental results did not enable the quantification of the relative influence of self-heating on the total entire flow domain. The proposed model can thus be used to predict rheological field variables and viscous dissipation in the entire flow domain and can be extended to different materials or die geometries. Furthermore, information about pressure drop and velocity field in a real extrusion die is useful in extruder design engineering and die design engineering to make necessary design modification and development for product quality enhancement. This work can be extended to investigate higher range of extruder speed or incorporating the effect of slip on the studied variable.

The viscoelastic flow of a rubber compound in capillary extrusion was simulated using a nonlinear differential viscoelastic model, that is, the Giesekus model. The swelling prediction ability of the Giesekus model was analysed systematically. The method involving the reciprocal number of the average shear rate in the capillary die was used as basis for the determination of relaxation time.

The predicted results showed an increase in die swelling with the increased range of relaxation time and number of modes for all relaxation modes under study. Applying three relaxation modes with a wide range of relaxation time was the most suitable way to obtain experimental results. The predicted pressure drop showed a direct dependency on the range of relaxation time. By contrast, the velocity distribution range showed a slight change in velocity with the increased relaxation time. The circulation flow results showed the direct dependency of vortex size on the studied parameters, including relaxation time, number of modes and flow rate.

The present results revealed that the multi-mode version of the Giesekus differential viscoelastic model can predict the complex viscoelastic behaviour of rubber compounds, with the capillary die as benchmark problem. This work can be extended to complex geometries and different viscoelastic materials.

The main outcome from analysis of flow of rubber compound in extrusion die can be summarised as follows.

- 1- The proposed finite element model can be used for modelling and analysing flow behaviour in different die geometry or for different extruded material.
- 2- From the analyses of profile swell and flow field variable in an industrial-scale extrusion die, no correction is required in die design and the proposed die can be put in service without running-in experiments.
- 3- It is shown that Giesekus viscoelastic model can be used as an alternative model to PTT or K-BKZ models to predict swell behavior in polymer extrusion.

- 4- We have shown that viscoelastic model parameters are very important to improve the ability of viscoelastic model for prediction of swelling and viscoelastic flow behaviour of material in the die. Therefore, setting up relaxation time and relaxation mode should be depending on the properties of used material and the suitable choice of this parameters should be based on experimental validation of proposed model. In other words, swelling of the materials has to be tested in a capillary extrusion or similar extrusion experiment in which the generated stress is similar to those in real extrusion process.
- 5- In modelling large scale extrusion problem, pure viscous model can be successfully used for modelling the flow in the die, instead of viscoelastic model. Additionally, the most important phenomenon is to analyse the effect of viscous dissipation in the total flow domain of the die. This phenomenon promotes scorching due to temperature rise. In this study, it is shown that pure viscous model is capable of capturing viscous heating.

## ***7.2 Future Work***

The outcomes of the first topic show that there is no risk of scorch inside the proposed die design with all range of studied extruder speed. This results suggest that extended the range of extruder speed is possible to improve productivity. Therefore, further analyses can be done for higher range of extruder speed to find optimum value in term of productivity.

Relating to viscoelastic modelling more intensive study can extended by adopting different rheological model such as Pom-Pom rheological model which show good predictive capability in both steady and transient flow [97]. In addition, the effect of slip on wall boundary is not consider in this study. Therefore, more rigorous investigation for extrusion of rubber compound can extended to incorporate slippage effect. On the other hand, addition

investigation using more complex profile can be done to study the extrusion process intensively.

To decrease the computational demand of adopting viscoelastic model in large scale problem, more advance strategies can be implemented in future work. For instance, using pure viscous model for modelling flow in the stationary domain (die regime) and the calculated results of flow field at die exit can be then imposed on the second domain of extrudate (moving boundary domain) and adopting viscoelastic model. This strategy can decrease the computational cost accompanied using complex viscoelastic model.

Furthermore, co-extrusion modelling can be implemented on more complex problem for modelling extrusion of multi-phase material which is necessary for production multi-layer products.

# APPENDIX

## ANALYTICAL SOLUTION OF HEAT FLUX ACROSS EXTERNAL BOUNDARY

The analytical solution based on empirical equations for calculating natural convection of horizontal hot cylinder and vertical plate. The following assumption is implied.

Considering the heat flow from internal melted rubber flow to outer boundary of steel die as illustrated in **Figure 7.1**.

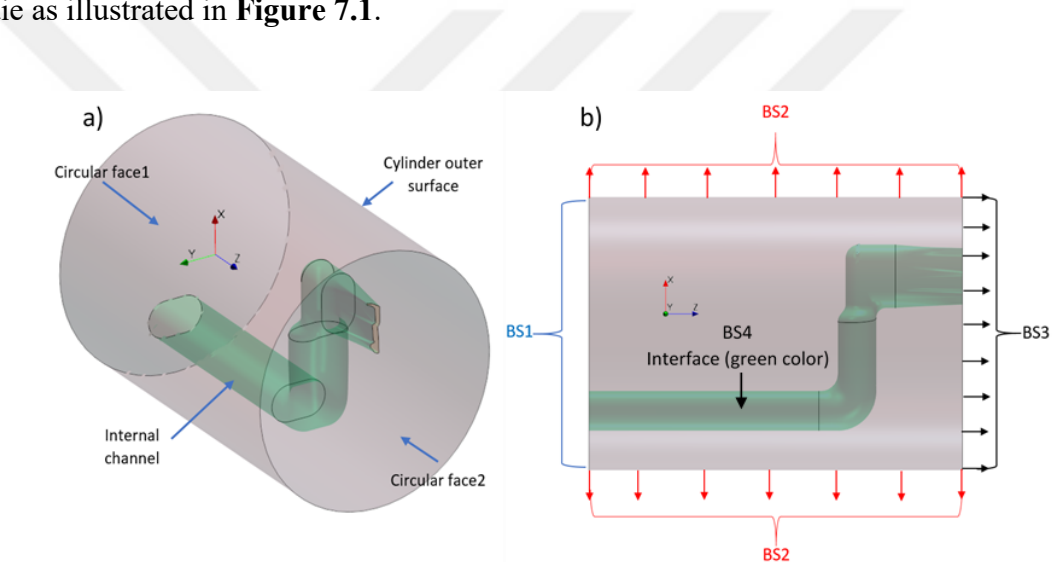


**Figure 7.1:** a-3-D View of internal channel with external steel die. b. 2-D View of internal channel with steel die with imposed thermal boundary conditions.

The left hand circular face(BS1) is considered under adiabatic condition since this surface is in contact with extruder head surface and no heat flow is assumed through this boundary. On the outer surface boundaries (BS2 and BS3) as shown in **Figure 7.1**, the heat is assumed to transfer by natural convection to surrounding air. In the present case, the contribution of radiant heat transfer is negligible as verified by the work of M. Fernando et al. [141]. So it is required to calculate the two local heat transfer coefficient for each boundary as follows.

**a- Local convection heat transfers on boundary BS2.**

The die simplified to horizontal hot cylinder with internal flow and the temperature is measured at three point on the outer surface.

$$T_{average} = \frac{(T_1 + T_2 + T_3)}{3} = \frac{74.5 + 75 + 77}{3} = 75.5 \text{ }^\circ\text{C} = T_s \quad (\text{A.1})$$

The properties of air at the film temperature  $T_f$

$$T_f = (T_s + T_\infty)/2 \quad (\text{A.2})$$

$$T_f = \frac{(75.5 + 15)}{2} = 45.25 \text{ }^\circ\text{C} \quad (\text{A.3})$$

where  $T_\infty$  is the surrounding air temperature ,  $T_f$  is the film temperature ,  $T_s$  Is the surface temperature at boundary BS2 (see Figure7.1).

Then from properties table in appendix at given temperature (Table A-15) [115] we can find the properties of air at film temperature.

$$Pr = 0.724035 , \quad \nu = 1.7524 * 10^{-5} \text{ m}^2/\text{s} , k = 0.027008 \text{ W/m. K}$$

$$\beta = \frac{1}{T_f} = \frac{1}{318.4}$$

where:  $T_f$  is the temperature in kelvin,  $Pr$  is the Prandtl number,  $\nu$  is kinematic viscosity ,  $k$  is the thermal conductivity.

The characteristic length in this case is the outer diameter of the steel cylinder,  $L_c = D = 0.138 \text{ m}$ . Then the **Rayleigh number** calculated as follows [115].

$$Ra_D = \frac{g \beta (T_s - T_\infty) D^3}{\nu^2} Pr \quad (A.4)$$

$$Ra_D = \frac{(9.81) (1/318.4) (75.5 - 15)(0.138)^3}{(1.7524 * 10^{-5})^2} (0.724035) = 11549991$$

where: D is the outer diameter of the cylindrical die.

The natural convection Nusselt number in this case can be determined from Equation as follows.

$$Nu = \left\{ 0.6 + \frac{0.387(Ra_D)^{1/6}}{[1 + (0.559/Pr)^{(9/16)}]^{(8/27)}} \right\}^2 \quad (A.5)$$

$$Nu = \left\{ 0.6 + \frac{0.387(11549991)^{1/6}}{[1 + (0.559/0.724035)^{(9/16)}]^{(8/27)}} \right\}^2 = 29.56820928$$

Then the convective heat transfer coefficient  $h_{BS2}$  for cylindrical surface is calculated from the following equation.

$$h_{BS2} = \frac{k}{D} Nu = \frac{0.027008}{0.138} * 29.56820928 = 5.786798523 \frac{W}{m^2 \cdot K} \quad (A.6)$$

$$A_{BS2} = \pi DL = \pi(0.138)(0.1952) = 0.084661029 m^2$$

The heat out of cylindrical surface  $Q_{BS2}$  (loss from boundary BS2), see **Figure 7.1**

$$Q_{BS2} = h_{BS2} \cdot A_{BS2} (T_s - T_\infty) \quad (A.7)$$

$$Q_{BS2} = 5.786798523 * (0.084661029)(75.5 - 15) = 29.63993706 W$$

Where  $A_{BS2}$  is the surface area of boundary  $BS2$  and  $Q_{BS2}$  is the heat transfer from the surface boundary  $BS2$ .

**b- The local convective heat transfer coefficient on boundary BS3 (see Figure 7.1).**

The local convective heat transfer coefficient  $h_{BS3}$  is calculated by simplifying the boundary  $BS2$  to vertical plate and assuming the surface temperature equal to average temperature measured at the surface. The vertical plate with height equal to the diameter of cylinder is depicted in **Figure 7.2**. The value of  $h_{BS3}$  is calculated by applying the empirical equations for calculating natural convective heat transfer coefficient for vertical plate as follows.

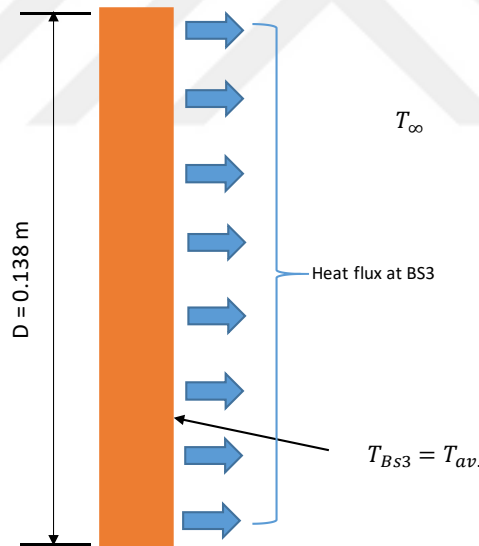


**Figure 7.2:** Vertical hot plat ( $T_{BS3}$  is the surface temperature at boundary BS3,  $T_{\infty}$  is surrounding air temperature, D diameter of cylinder).

The average temperature ( $T_{av.}$ ) is calculated from measuring temperature at three point on the surface as used in previous approach.



The characteristic length in this case is the outer diameter of the steel cylinder,  $L_c = D = 0.138$  m. Then the **Rayleigh number** calculated as follows.

$$Ra_L = \frac{g \beta (T_s - T_\infty) L^3}{\nu^2} Pr \quad (A.8)$$

$$Ra_L = \frac{(9.81) \left(\frac{1}{318.4}\right) (75.5 - 15)(0.138)^3}{(1.7524 * 10^{-5})^2} (0.724035)$$

$$\therefore Ra_L = 11549991.21$$

The natural convection Nusselt number in this case can be determined from Equation below.

$$Nu = \left\{ 0.825 + \frac{0.387(Ra_L)^{1/6}}{[1 + (0.492/Pr)^{(9/16)}]^{(8/27)}} \right\}^2 \quad (A.9)$$

$$\therefore Nu = 32.60074893$$

Then the convective heat transfer coefficient  $h_{BS3}$  for circular surface (boundary  $BS3$  in Figure 7.1) is calculated from the following equation.

$$h_{BS3} = \frac{k}{L} Nu = \frac{0.027008}{0.138} * 32.60074893 = 6.380297297 \frac{W}{m^2 \cdot K} \quad (A.10)$$

Then the heat out of boundary  $BS3$ ,  $Q_{BS3}$  (see Figure 7.1) can be determined.

$$Q_{BS3} = h_{BS3} \cdot A_{BS3} (T_s - T_\infty) \quad (A.11)$$

$$Q_{BS3} = 6.380297297 \cdot (0.014963143) (75.5 - 15) = 6.775892646 \text{ W}$$

$$A_{BS3} = \pi r^2 = \pi \left( \frac{0.138}{2} \right)^2 = 0.014963143 \text{ m}^2 \quad (\text{A.12})$$

Where  $A_{BS3}$  is the surface area of boundary  $BS3$  and  $Q_{BS3}$  is the heat transfer from this surface boundary.

Now, the total heat loss by natural convection outside the steel die  $Q_T$  is determined as follows.

$$Q_T = Q_{BS2} + Q_{BS3} = 29.63993706 + 6.775892646 \quad (\text{A.13})$$

$$Q_T = 35.41582971 \text{ W}$$

The same approach is used to calculate the convective heat transfer coefficient and total heat flow out of external boundary ( $BS2$  and  $BS3$ ) for each extruder speed.

By applied energy balance equation which imply that the heat transfers from melted rubber through the interface boundary  $BS4$  (See **Figure 7.3**) to the steel die is equal to heat loss from the external boundaries ( $BS2$ ,  $BS3$ ) of steel die.

$$\text{This mean } Q_T = Q_{BS4} = 35.41582971 \text{ W}$$

Where  $Q_{BS4}$  is the total heat transfer through the interface surface ( $BS4$  in Figure 7.3),  $Q_T$  is total heat loss from external boundary ( $BS2$ ,  $BS3$ ) of steel die.

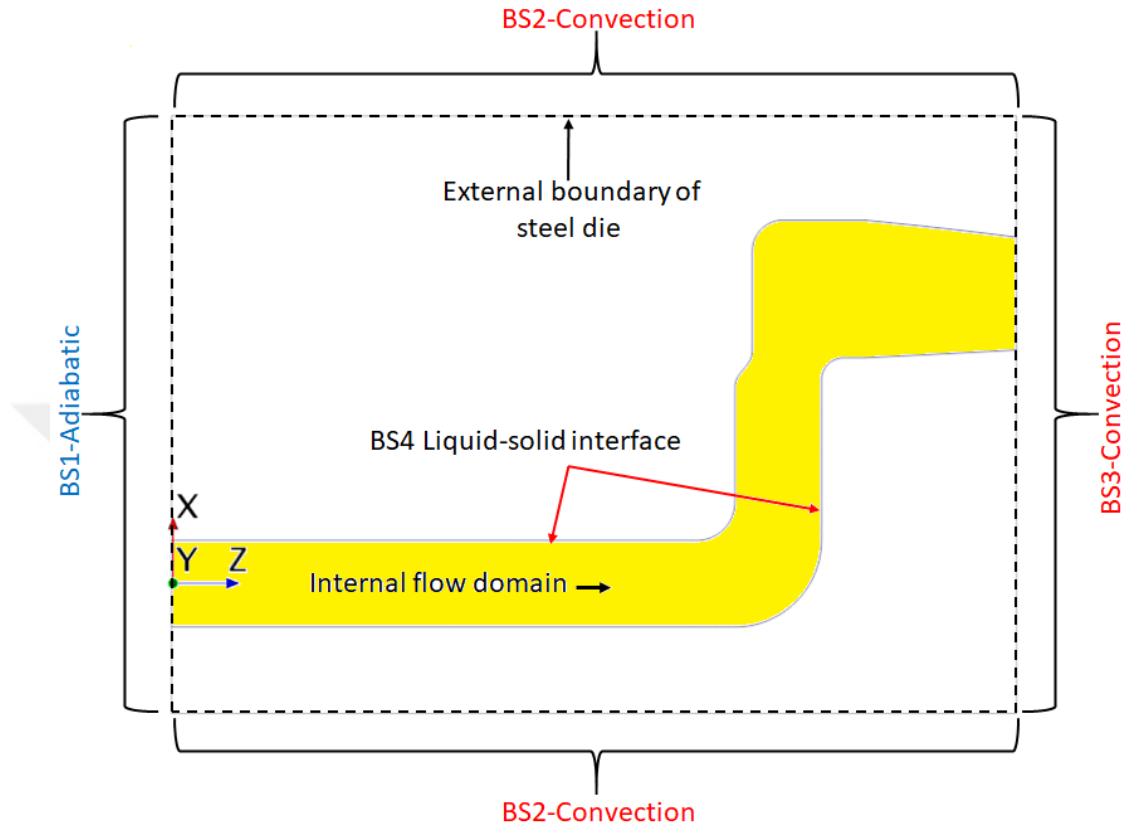


**Figure 7.3:** Section view of fluid-solid interface domain.

Therefore, in our finite element simulation the total heat flux  $q_{BS4}$  is imposed on the surface boundary (BS4) of flow domain. The total heat flux  $q_{BS4}$  is calculated as follows.

$$q_{BS4} = \frac{Q_{BS4}}{A_{BS4}} = \frac{35.41582971}{0.0213642} = 1657.718506 \text{ W/m}^2 \quad (\text{A.14})$$

Where  $A_{BS4}$  is the interface surface area (boundary BS4 in Figure 7.3) which is equal to  $0.0213642 \text{ m}^2$  (this non-regular area calculated from the software).

## References

- [1] J. J. Shea, "Handbook of elastomers, second edition [Book Reviews]," *IEEE Electr. Insul. Mag.*, vol. 17, no. 6, Nov. 2001.
- [2] C. M. Roland, *Encyclopedia of Polymeric Nanomaterials*. Berlin, Heidelberg: Springer Berlin Heidelberg, 2015.
- [3] J. L. Leblanc, "Rubber- filler interactions and rheological properties in filled compounds," *Prog. Polym.*, vol. 27, pp. 627–687, 2002.
- [4] Y. Mu, G. Zhao, X. Wu, and J. Zhai, "Finite-Element Simulation of Polymer Flow and Extrudate Swell Through Hollow Profile Extrusion Die with the Multimode Differential Viscoelastic Model," *Adv. Polym. Technol.*, vol. 32, no. S1, pp. E1–E19, Mar. 2012.
- [5] W.-S. Lee and H.-Y. Ho, "Experimental study on extrudate swell and die geometry of profile extrusion," *Polym. Eng. Sci.*, vol. 40, no. 5, pp. 1085–1094, May 2000.
- [6] J. M. N. Carneiro, Olga S, *Design of Extrusion Forming Tools Edited by Forming Tools*. UK: Smithers Rapra Technology Ltd, 2012.
- [7] J. Aho, "Rheological Characterization of Polymer Melts in Shear and Extension: Measurement Reliability and Data for Practical Processing," Tampere University of Technology, 2011.
- [8] R. G. Owens and T. N. Phillips, *Computational Rheology*. Imperial College Press, 2002.
- [9] A. Lozinski, R. G. Owens, and T. N. Phillips, "The Langevin and Fokker–Planck Equations in Polymer Rheology," in *Handbook of Numerical Analysis*, vol. 16, no. C, P. G. Ciarle, Ed. Elsevier B.V., pp. 211–303, 2011.
- [10] F. C. W. . K. M. J.L.White, Y.Wang, A.I.Isayev, N.N.JIMA, "Modelling shear viscosity behaviour for rubber compound.," *Rubber Chem. Technol.*, vol. 60, pp. 337–360, 1986.

- [11] C. Barrès, A. Mongruel, M. Cartault, and J. L. Leblanc, “Linear and nonlinear viscoelasticity of carbon black filled elastomers: Use of complementary rheological characterizations,” *J. Appl. Polym. Sci.*, vol. 87, no. 1 SPEC., pp. 31–41, 2003.
- [12] A. Kaye, “Non-Newtonian flow in incompressible fluids,” College of Aeronautics Cranfield, CoA Note No. 134, 1962.
- [13] K. S. Cho, K. Hyun, K. H. Ahn, and S. J. Lee, “A geometrical interpretation of large amplitude oscillatory shear response,” *J. Rheol. (N. Y.)*, vol. 49, no. 3, pp. 747–758, May 2005.
- [14] S. Kallus *et al.*, “Characterization of polymer dispersions by Fourier transform rheology,” *Rheol. Acta*, vol. 40, no. 6, pp. 552–559, Nov. 2001.
- [15] J. L. Leblanc, “Fourier Transform rheometry : a new tool to investigate intrinsically non-linear viscoelastic materials.,” *J. Appl. Polym. Sc.*, vol. 13, no. Paris 6, pp. 1–19, 2005.
- [16] A. Calin, M. Wilhelm, and C. Balan, “Determination of the non-linear parameter (mobility factor) of the Giesekus constitutive model using LAOS procedure,” *J. Nonnewton. Fluid Mech.*, vol. 165, no. 23–24, pp. 1564–1577, 2010.
- [17] A. Calin, C. Balan, and M. Wilhelm, “A New Approach to Determine the Nonlinear Parameter of the Giesekus Constitutive Model,” *XV Int. Congr. Rheol. Soc. Rheol. 80th Annu. Meet.*, vol. 1027, no. 2008, pp. 1372–1374, 2008.
- [18] J.-E. Bae and K. S. Cho, “Semianalytical methods for the determination of the nonlinear parameter of nonlinear viscoelastic constitutive equations from LAOS data,” *J. Rheol. (N. Y. N. Y.)*, vol. 59, no. 2, pp. 525–555, 2015.
- [19] P. J. Cable and D. V Boger, “A comprehensive experimental investigation of tubular entry flow of viscoelastic fluids: Part I. Vortex characteristics in stable flow,” *AIChE J.*, vol. 24, no. 5, pp. 869–879, 1978.
- [20] R. E. Evans and K. Walters, “Flow characteristics associated with abrupt changes in

- geometry in the case of highly elastic liquids,” *J. Nonnewton. Fluid Mech.*, vol. 20, no. C, pp. 11–29, 1986.
- [21] R. Keunings, “On the high Weissenberg number problem,” *J. Nonnewton. Fluid Mech.*, vol. 20, no. C, pp. 209–226, 1986.
- [22] D. Rajagopalan, R. C. Armstrong, and R. A. Brown, “Finite element methods for calculation of steady, viscoelastic flow using constitutive equations with a Newtonian viscosity,” *J. Nonnewton. Fluid Mech.*, vol. 36, no. C, pp. 159–192, 1990.
- [23] M. A. Alves, F. T. Pinho, and P. J. Oliveira, “Effect of a high-resolution differencing scheme on finite-volume predictions of viscoelastic flows,” *J. Nonnewton. Fluid Mech.*, vol. 93, no. 2–3, pp. 287–314, 2000.
- [24] R. Guenette and M. Fortin, “A new mixed finite element method for computing viscoelastic flows,” *J. Nonnewton. Fluid Mech.*, vol. 60, no. 1, pp. 27–52, 1995.
- [25] J. M. Marchal and M. J. Crochet, “Hermitian finite elements for calculating viscoelastic flow,” *J. Nonnewton. Fluid Mech.*, vol. 20, no. C, pp. 187–207, 1986.
- [26] J. M. Marchal and M. J. Crochet, “A new mixed finite element for calculating viscoelastic flow,” *J. Nonnewton. Fluid Mech.*, vol. 26, no. 1, pp. 77–114, 1987.
- [27] L. A. Utracki, Z. Bakerdjian, and M. R. Kamal, “A method for the measurement of the true die swell of polymer melts,” *J. Appl. Polym. Sci.*, vol. 19, no. 2, pp. 481–501, 1975.
- [28] C. D. Han, “A Method for the Determination of Polymer,” vol. 218, no. 1970, pp. 213–218, 1970.
- [29] C. D. M. C. Han, “Rheological Implications of the Exit Pressure and Die Swell in Steady Capillary Flow of Polymer Melts. I. The Primary Normal Stress Difference and the Effect of  $L/D$  Ratio on Elastic Properties,” *J. Rheol. (N. Y. N. Y.)*, vol. 14, no. 3, p. 393, 1970.
- [30] H. J. Song, J. L. White, K. Min, N. Nakajima, and F. C. Weissert, “Rheological

- properties, extrudate swell, and die entry extrusion flow marker experiments for rubber–carbon black compounds,” *Adv. Polym. Technol.*, vol. 8, no. 4, pp. 431–449, 1988.
- [31] D. C. Huang and J. L. White, “Extrudate swell from slit and capillary dies: An experimental and theoretical study,” *Polym. Eng. Sci.*, vol. 19, no. 9, pp. 609–616, 1979.
- [32] N. Sombatsompop and S. Sergsiri, “Die swell ratio of polystyrene melt from an electro-magnetized capillary die in an extrusion rheometer: Effects of barrel diameter, shear rate and die temperature,” *Polym. Adv. Technol.*, vol. 15, no. 8, pp. 472–480, 2004.
- [33] J. C. Huang and Z. Tao, “Melt fracture, melt viscosities, and die swell of polypropylene resin in capillary flow,” *J. Appl. Polym. Sci.*, vol. 87, no. 10, pp. 1587–1594, 2002.
- [34] J. C. Huang and K. S. Leong, “Shear viscosity, extensional viscosity, and die swell of polypropylene in capillary flow with pressure dependency,” *J. Appl. Polym. Sci.*, vol. 84, no. 6, pp. 1269–1276, 2002.
- [35] H. W. Mullner, J. Eberhardsteiner, and W. Fidi, “Rheological characterization of the die swell phenomenon of rubber compounds,” *Polym. Test.*, vol. 26, no. 8, pp. 1041–1048, 2007.
- [36] H. Uematsu, N. Horisawa, T. Horikida, S. Tanoue, and Y. Iemoto, “Effect of carbon fiber on the capillary extrusion behaviors of high-density polyethylene,” *Polym. J.*, vol. 45, no. 4, pp. 449–456, 2013.
- [37] S. H. Choi and M. Y. Lyu, “Application of the PTT model for capillary extrusion of rubber compounds,” *Int. Polym. Process.*, vol. 24, no. 4, pp. 326–333, 2009.
- [38] J. H. Kim and M. . Lyu, “Predictions of flow behaviors and entrance pressure drop characteristics of a rubber compound in a capillary die using various rheological models,” *Polym. Eng. Sci.*, vol. 54, no. 10, pp. 2441–2448, Oct. 2014.

- [39] M. Javadi, E. Alizadeh, B. Rahimi, and A. Hosseini, "Experimental and Numerical Investigation of Rubber Extrusion Forming for Multi Material Automobile Weather Strip," *Fract. Strength Solids VII, Pts 1 2*, vol. 462–463, pp. 831–836, 2011.
- [40] R. Pohorecki, J. Bridgewater, M. Molzahn, R. Gani, and C. Gallegos, *Constitutive Modeling of Viscoelastic Fluids*, vol. 1. USA: EOLSS, 2010.
- [41] Y. Dai, H. Zheng, C. Zhou, and W. Yu, "Quick Profile Die Balancing of Automotive Rubber Seal Extrusion by CAE Technology," *J. Macromol. Sci. Part A*, vol. 45, no. 12, pp. 1028–1036, 2008.
- [42] O. S. Carneiro, J. M. Nóbrega, F. T. Pinho, and P. J. Oliveira, "Computer aided rheological design of extrusion dies for profiles," *J. Mater. Process. Technol.*, vol. 114, no. 1, pp. 75–86, 2001.
- [43] Y. K. Dai, C. X. Zhou, and W. Yu, "Inverse designing simulation of extrusion die of auto rubber seal and verifications," *Plast. Rubber Compos.*, vol. 36, no. 4, pp. 141–148, 2007.
- [44] Adnan Saeed, "Modeling Dies for Rubber Parts," U.S.A, 2007.
- [45] J. . White, H. Potente, and U. Berghaus, *Screw Extrusion*, Second Edi. USA: Hanser Gardner Publications, Inc, 2003.
- [46] Dr. Chris Rauwendaal, *Polymer Extrusion*, 5th Ed. USA: Hanser Publishers, Munich, 2014.
- [47] H. W. Cox and C. W. Macosko, "Viscous dissipation in die flows," *AIChE J.*, vol. 20, no. 4, pp. 785–795, 1974.
- [48] J. L. White and Z. Chen, "Simulation of non-isothermal flow in modular co-rotating twin screw extrusion," *Polym. Eng. Sci.*, vol. 34, no. 3, pp. 229–237, 1994.
- [49] Y. Wang, "3-D Non-Isothermal Die Flow of Power-Law Fluids with Viscous Heating," vol. 1, no. 2, pp. 175–182, 1994.



- [50] G. A. Campbell, C. Wang, H. Cheng, M. Bullwinkel, and M. A. te-Riele, "Investigation of flow rate and viscous dissipation in a single screw pump-extruder," *Int. Polym. Proc.*, vol. 16, no. 4, pp. 323–333, 2001.
- [51] H. Zheng, G. Wang, C. Zhou, W. Yu, and H. Zhang, "Computer-aided optimization of the extrusion process of automobile rubber seal," *J. Macromol. Sci. Part A Pure Appl. Chem.*, vol. 44, no. 5, pp. 509–516, 2007.
- [52] D. M. Kalyon, A. Lawal, R. Yazici, P. Yaras, and S. Railkar, "Mathematical modeling and experimental studies of twin-screw extrusion of filled polymers," *Polym. Eng. Sci.*, vol. 39, no. 6, pp. 1139–1151, Jun. 1999.
- [53] A. Limper and D. Schramm, "Process Description for the Extrusion of Rubber Compounds – Development and Evaluation of a Screw Design Software," *Macromol. Mater. Eng.*, vol. 287, no. 11, pp. 824–835, 2002.
- [54] J. J. de. C. Díaz, P. J. G. Nieto, A. B. García, J. G. Muñoz, and J. O. Meré, "Finite volume modeling of the non-isothermal flow of a non-Newtonian fluid in a rubber's extrusion die," *J. Non. Cryst. Solids*, vol. 354, no. 47–51, pp. 5334–5336, 2008.
- [55] Y. S. Ha, J. R. Cho, T. H. Kim, and J. H. Kim, "Finite element analysis of rubber extrusion forming process for automobile weather strip," *J. Mater. Process. Technol.*, vol. 201, no. 1–3, pp. 168–173, 2008.
- [56] S. Elgeti, M. Probst, C. Windeck, M. Behr, W. Michaeli, and C. Hopmann, "Numerical shape optimization as an approach to extrusion die design," *Finite Elem. Anal. Des.*, vol. 61, pp. 35–43, 2012.
- [57] J. Launay, N. Allanic, P. Mousseau, R. Muller, and R. Deterre, "Scorch arisen prediction through elastomer flow in extrusion die," *Int. J. Mater. Form.*, vol. 7, no. 2, pp. 197–205, Jun. 2014.
- [58] C. Abeykoon, A. L. Kelly, P. J. Martin, and K. Li, "Dynamic modelling of die melt temperature profile in polymer extrusion," *Proc. IEEE Conf. Decis. Control*, vol. 38, no. 4, pp. 2550–2555, 2013.

- [59] E. I. Borzenko and G. R. Shrager, “Effect of viscous dissipation on temperature, viscosity, and flow parameters while filling a channel,” *Thermophys. Aeromechanics*, vol. 21, no. 2, pp. 211–221, 2014.
- [60] S. Brockhaus and V. Schöppner, “Influence of barrel and screw heating in rubber extrusion,” no. 7, pp. 470–474, 2015.
- [61] H. Nishizawa, “Heat controls and rubber flow behaviour in screw of extruder and injection machine and the problems occurring in these processes,” *Int. Polym. Sci. Technol.*, vol. 43, no. 4, pp. T41–T50, 2016.
- [62] C. Barrès, A. Mongruel, M. Cartault, and J. L. Leblanc, “Linear and nonlinear viscoelasticity of carbon black filled elastomers: Use of complementary rheological characterizations,” *J. Appl. Polym. Sci.*, vol. 87, no. 1, pp. 31–41, Jan. 2003.
- [63] C. D. Han, *Rheology and Processing of Polymeric Materials, Volume 1: Polymer Rheology*. New York: Oxford University Press, Inc., 2007.
- [64] J. Z. Liang, “Effects of extrusion rate, temperature, and die diameter on melt flow properties during capillary flow of low-density-polyethylen,” *Polym. - Plast. Technol. Eng.*, vol. 46, no. 3, pp. 245–249, 2007.
- [65] S. Montes and J. L. White, “Rheological models of rubber-carbon black compounds: low interaction viscoelastic models and high interaction thixotropic - plastic - viscoelastic models,” *J. Nonnewton. Fluid Mech.*, vol. 49, no. 2–3, pp. 277–298, 1993.
- [66] L. Gast and W. Ellingson, “Die swell measurements of second-order fluids: Numerical experiments,” *Int. J. Numer. Methods Fluids*, vol. 29, no. 1, pp. 1–18, 1999.
- [67] M. Catalysts, “Polymer Rheology for Melt Processing: Molecular Modeling,” *Rheology*, no. Ottinger, pp. 1–4, 2000.
- [68] E. Mitsoulis and S. G. Hatzikiriakos, “Bagley correction: The effect of contraction angle and its prediction,” *Rheol. Acta*, vol. 42, no. 4, pp. 309–320, 2003.
- [69] V. K. Konaganti, M. Ansari, E. Mitsoulis, and S. G. Hatzikiriakos, “Extrudate swell

of a high-density polyethylene melt: II. Modeling using integral and differential constitutive equations,” *J. Nonnewton. Fluid Mech.*, vol. 225, pp. 94–105, 2015.

- [70] P. Peltola, “Rubber Extrusion Parameter Optimization.” Tampereen ammattikorkeakoulu, 2013.
- [71] C D adapco, *STAR CCM+ documentation and user guide , Version 12.04.011-R8, Melville, USA*. Siemens PLM Software, 2017.
- [72] F. A. Morrison, “Constitutive modeling of viscoelastic fluids,” *Rheology*, vol. 1, pp. 180–204, 2010.
- [73] Faith A. Morrison, *Understanding rheology*, vol. 11, no. 200203. New York, USA: Oxford University Press s, Inc, 2001.
- [74] O. H. R.B. Bird, R.C. Armstrong, *Dynamics of Polymer Liquids*, Second Edi. USA: John wiley and Sons,Inc, 1987.
- [75] O. Catherine, “Polymer melt rheology and flow simulations applied to cast film extrusion die design: An industrial perspective,” *AIP Conf. Proc.*, vol. 1843, 2017.
- [76] C. W.Macosko, D. C. Huang, and J. L. White, *Rheology: Principles, Measurements and Applications*, vol. 19, no. 9. USA: John wiley and Sons,Inc, 1994.
- [77] X. Chen, “Numerical Modeling of Fluid-Structure Interaction with Rheologically Complex Fluids,” Darmstadt University / China, 2014.
- [78] R. B. Bird, C. F. Curtiss, R. C. Armstrong, and O. Hassager, *Dynamics of Polymeric Liquids, Kinetic Theory*, Second edi. John wiley and Sons,Inc, 1987.
- [79] S. N. Elgeti, “Free-surface flows in shape optimization of extrusion dies,” P.h.D. Thesis . Aachen University, 2011.
- [80] B. Bernstein, E. . Kearsley, and L. J. Zapas, “A Study of Stress Relaxation with Finite Strain,” *Trans. Soc. Rheol.*, vol. 7, pp. 391–410, 1963.
- [81] M. H. Wagner, “Analysis of stress-growth data for simple extension of a low-density

- branched polyethylene melt,” *Rheo.Acta*, vol. 135, no. 15, pp. 133–134, 1976.
- [82] M.H.Wanger, “Zur Netzwerktheorie von Polymer-Schmelzen,” *Rheo. Acta*, vol. 82, no. 18, pp. 33–50, 1979.
- [83] C.W.Maacosko, *Rheology: Principles, Measurements and Applications*. New York, USA: Wiley-VCH, 1994.
- [84] J. G. Oldroyd, “On the Formulation of Rheological Equations of State,” *Proc. R. Soc. A Math. Phys. Eng. Sci.*, vol. 200, no. 1063, pp. 523–541, Feb. 1950.
- [85] M. J. Crochet and R. Keunings, “Finite element analysis of die swell of a highly elastic fluid,” *J. Nonnewton. Fluid Mech.*, vol. 10, no. 3–4, pp. 339–356, 1982.
- [86] N. P. Thien and R. I. Tanner, “A new constitutive equation derived from network theory,” *J. Nonnewton. Fluid Mech.*, vol. 2, no. 4, pp. 353–365, 1977.
- [87] H. Giesekus, “A simple constitutive equation for polymer fluids based on the concept of deformation-dependent tensorial mobility,” *J. Nonnewton. Fluid Mech.*, vol. 11, no. 1–2, pp. 69–109, Jan. 1982.
- [88] L. Pauli, “Simulating die swell in the context of profile extrusion,” Master Thesis. Rwthachen University, 2011.
- [89] R. Darby, *Viscoelastic Fluids: An Introduction to Their Properties and Behavior*. New York, Basel: Marcel Dekker, Inc., 1977.
- [90] N. Phan-Thien, *Understanding Viscoelasticity*, Second Edi. Berlin, Heidelberg: Springer Berlin Heidelberg, 2013.
- [91] Y. Mu, G. Zhao, A. Chen, and X. Wu, “Modeling and simulation of polymer melts flow in the extrusion process of plastic profile with metal insert,” *Int. J. Adv. Manuf. Technol.*, vol. 67, no. 1–4, pp. 629–646, Jul. 2013.
- [92] F. A. Morrison, *Understanding Rheology, Topics in Chemical Engineering*. Oxford University Press, New York, 2001.

- [93] A. Calin *et al.*, “A New Approach to Determine the Nonlinear Parameter of the Giesekus Constitutive Model,” in *AIP Conference Proceedings*, 2008, vol. 1027, no. 1372, pp. 1372–1374.
- [94] H. Giesekus, “A unified approach to a variety of constitutive models for polymer fluids based on the concept of configuration-dependent molecular mobility,” *Rheol. Acta*, vol. 21, no. 4–5, pp. 366–375, Jul. 1982.
- [95] R.G.Larson, *The structure and rheology of complex fluids*. New York: Oxford University Press, Inc, 1999.
- [96] T. C. B. McLeish and R. G. Larson, “Molecular constitutive equations for a class of branched polymers: The pom-pom polymer,” *J. Rheol. (N. Y. N. Y.)*, vol. 42, no. 1, pp. 81–110, 1998.
- [97] B. Debbaut and T. Marchal, “Numerical simulation of extrusion process and die design for industrial profile, using multimode pom–pom model,” *Plast. Rubber Compos.*, vol. 37, no. 2–4, pp. 142–150, 2008.
- [98] J. D.Ferry, *Viscoelastic Properties of Polymer*. John Wiley and sons, inc., 1980.
- [99] Bayram ALAKUŞ, “Efficient and fast finite element viscoelastic fluid flow simulation efforts,” *D.P.Ü. Fen Bilim. Enstitüsü*, vol. 17, p. 14, 2008.
- [100] A. N. Brooks and T. J. R. Hughes, “Streamline upwind/Petrov-Galerkin formulations for convection dominated flows with particular emphasis on the incompressible Navier-Stokes equations,” *Comput. Methods Appl. Mech. Eng.*, vol. 32, no. 1–3, pp. 199–259, 1982.
- [101] R. C. King, M. R. Apelian, R. C. Armstrong, and R. A. Brown, “Numerically stable finite element techniques for viscoelastic calculations in smooth and singular geometries,” *J. Nonnewton. Fluid Mech.*, vol. 29, no. C, pp. 147–216, 1988.
- [102] S. F. Krar, A. R. Gill, and J. C. Cahall, *Exploring advanced manufacturing technologies*, First Edit. New York, NY: Industrial Press Inc., 2003.

- [103] I. Manual and Mode, “testo 925 Temperature measuring instrument,” 2017.
- [104] E. B. Bagley, “End corrections in the capillary flow of polyethylene,” *J. Appl. Phys.*, vol. 28, no. 5, pp. 624–627, 1957.
- [105] B. Rabinowitsch, “Über die Viskosität und Elastizität von Solen,” *Z Phys Chem*, vol. 145, no. 1, p. 1–26: in German, Jan. 1929.
- [106] J. M. Dealy and K. F. Wissbrun, *Melt Rheology and Its Role in Plastics Processing*, vol. 49. Dordrecht: Springer Netherlands, 1990.
- [107] P. S. Gill, S. R. Sauerbrunn, and M. Reading, “Modulated differential scanning calorimetry,” *J. Therm. Anal.*, vol. 40, no. 3, pp. 931–939, 1993.
- [108] Z. Cheheb, P. Mousseau, A. Sarda, and R. Deterre, “Thermal conductivity of rubber compounds versus the state of cure,” *Macromol. Mater. Eng.*, vol. 297, no. 3, pp. 228–236, 2012.
- [109] T. Gao, R. Xie, L. Zhang, H. Gui, and M. Huang, “Use of Rubber Process Analyzer for Characterizing the Molecular Weight Parameters of Natural Rubber,” *Int. J. Polym. Sci.*, vol. 2015, 2015.
- [110] R. H. Moore, R. K. Zeigler, and L. A. R. La, “RPA 2000 Servic Manual,” vol. M0377(2B), Alpha Technologies U.S., pp. 1–116, 2000.
- [111] ASTM, “Standard test method for rubber-Measurment of unvalcanized rheological properties using rotless shear rheometer,” no. D 6204 – 99, pp. 1–5, 2014.
- [112] M. Karrabi and S. Mohammadian-Gezaz, “Study of the cure characteristics and viscoelastic behavior of styrene-butadiene rubber compounds by using a rubber process analyzer,” *J. Vinyl Addit. Technol.*, vol. 21, no. 2, p. n/a-n/a, Jul. 2010.
- [113] J. S. Dick, *Rubber technology: compounding and testing for performance*, 2nd Editio. Carl Hanser Verlag GmbH Co KG, 2014.
- [114] I. ANSYS, *ANSYS POLYFLOW User ’ s Guide*, no. Release 15.0. U.S.A: SAS IP, Inc,

2013.

- [115] Y. A. Cengel, *Heat Transfer*, 1 st editi. McGraw-Hill Science, 2002.
- [116] Rajendra P. Chhabra, *Rheology of Complex Fluids*. New York, NY: Springer New York, 2010.
- [117] M. A. Hulsen and J. van der Zanden, “Numerical simulation of contraction flows using a multi-mode Giesekus model,” *J. Nonnewton. Fluid Mech.*, vol. 38, no. 2–3, pp. 183–221, 1991.
- [118] M. Mostafaiyan, K. Khodabandehlou, and F. Sharif, “Analysis of a viscoelastic fluid in an annulus using Giesekus model,” *J. Nonnewton. Fluid Mech.*, vol. 118, no. 1, pp. 49–55, 2004.
- [119] J. Étienne, E. J. Hinch, and J. Li, “A Lagrangian-Eulerian approach for the numerical simulation of free-surface flow of a viscoelastic material,” *J. Nonnewton. Fluid Mech.*, vol. 136, no. 2–3, pp. 157–166, 2006.
- [120] V. Ganvir *et al.*, “Extrudate swell of linear and branched polyethylenes: ALE simulations and comparison with experiments,” *J. Nonnewton. Fluid Mech.*, vol. 166, no. 1–2, pp. 12–24, 2011.
- [121] D. Boffi, F. Brezzi, and M. Fortin, *Mixed Finite Element Methods and Applications*, vol. 44. 2013.
- [122] J. Donea and A. Huerta, *Finite Element Methods for Flow Problems*. 2003.
- [123] M. Fortin and F. Brezzi, *Mixed and Hybrid Finite Element Methods*. New York: Springer, 1991.
- [124] T. J. R. Hughes, L. P. Franca, and M. Balestra, “A new finite element formulation for computational fluid dynamics: V. Circumventing the babuška-brezzi condition: a stable Petrov-Galerkin formulation of the stokes problem accommodating equal-order interpolations,” *Comput. Methods Appl. Mech. Eng.*, vol. 59, no. 1, pp. 85–99, Nov. 1986.

- [125] D. Z. Turner, K. B. Nakshatrala, and K. D. Hjelmstad, “On the stability of bubble functions and a stabilized mixed finite element formulation for the Stokes problem,” *Int. J. Numer. Methods Fluids*, vol. 60, no. 12, pp. 1291–1314, 2009.
- [126] F. P. T. Baaijens, “Mixed finite element methods for viscoelastic flow analysis: A review,” *J. Nonnewton. Fluid Mech.*, vol. 79, no. 2–3, pp. 361–385, 1998.
- [127] T. E. Tezduyar, “Some Interesting Issues in Incompressible Fluid Dynamics, Both in the Continuum and in Numerical Simulation,” in *Advances in Applied Mechanics*, vol. 28, Academic Press, Inc, 1991, pp. 45–140.
- [128] R. Guénette and M. Fortin, “A new mixed finite element method for computing viscoelastic flows,” *J. Nonnewton. Fluid Mech.*, vol. 60, no. 1, pp. 27–52, 1995.
- [129] C. W. Macosko, *Rheology: Principles, Measurements and Applications*. USA: John Wiley and Sons, Inc, 1994.
- [130] T. D. Canonsburg, “ANSYS Polyflow Tutorial Guide,” vol. 15317, no. November. pp. 724–746, 2013.
- [131] T. D. Canonsburg, *ANSYS POLYMAT User ’ s Guide*. ANSYS, Inc., 2013.
- [132] M. R. Barone *et al.*, *Fundamentals of computer modeling for polymer processing*, Third Edit. Hanser Verlag, Munich, 1989.
- [133] M. Huneault, “Extrudate Swell and Drawdown in Profile Extrusion,” *Plast. Eng.*, vol. 45, no. 9, pp. 39–42, 1989.
- [134] R. Peikert and M. Roth, “The ‘Parallel Vectors’ operator—a vector field visualization primitive,” *Proc. Vis. ’99 (Cat. No.99CB37067)*, pp. 263–532, 1999.
- [135] B. Cabral and L. C. Leedom, “Imaging vector fields using line integral convolution,” *Proc. SIGGRAPH*, pp. 263–270, 1993.
- [136] J. L. Favero, N. S. M. Cardozo, A. R. Secchi, and H. Jasak, *Simulation of free surface viscoelastic fluid flow using the viscoelasticinterFoam solver*, vol. 28, no. C. Elsevier



B.V., 2010.

- [137] P. C. Sousa, P. M. Coelho, M. S. N. Oliveira, and M. A. Alves, “Effect of the contraction ratio upon viscoelastic fluid flow in three-dimensional square-square contractions,” *Chem. Eng. Sci.*, vol. 66, no. 5, pp. 998–1009, 2011.
- [138] P. Sunthar, “Polymer Rheology,” in *Rheology of Complex Fluids*, New York, NY: Springer New York, 2010, pp. 171–191.
- [139] N. Sombatsompop and R. Dantongee, “Flow visualization and extrudate swell of natural rubber in a capillary rheometer: Effect of die/barrel system,” *J. Appl. Polym. Sci.*, vol. 82, no. 10, pp. 2525–2533, 2001.
- [140] C. Yang and Z. Li, “A study of wall slip in the capillary flow of a filled rubber compound,” *Polym. Test.*, vol. 37, pp. 45–50, 2014.
- [141] M. Fernando, W. H. Fei, and C. Hull, “Cure Simulation of Large Rubber Components: a Comparison of Compression and Extrusion Molding,” *Rubber Chem. Technol.*, vol. 85, no. 4, pp. 495–512, 2012.

## VITA

Nayyef Ahmed Talib was born on January 1, 1969, in Diyala, Iraq. He joint University of Technology in Bagdad, Iraq in 1988. He received his Bachelor and M.SC in Mechanical engineering department from University of Technology, Bagdad, Iraq in 1993 and 2001 respectively. After that, he worked as an instructor at the same university, teaching a variety of courses and achieving several academic ranks; the last one, in 2011, was lecturer. In February 2013, he jointed to Ozyegin university in Istanbul, Turkey. He started with English Preparatory School in Ozyegin University. In February 2014, he joined to study Ph.D. IN Mechanical Engineering Department, Graduate School of Engineering and Science with Assistance Professor Özgür Ertunç at the Ozyegin University, Istanbul, Turkey.

His previous research interests include manufacturing process and Neural network optimization of frictional wear in automotive industries. His current research interests include extrusion die design and computational analysis based finite element modelling (F.E.M) of extrusion in rubber industries. He has one accepted paper in journal and one journal paper was submitted and get acceptance with minor revision as shown below:

No	Paper title	Paper status	Journal name	Data
1	Application of Giesekus Model for Capillary Extrusion of Rubber Compound.	accepted	J. of Chemical Engineering of Japan	02-Jul-2018
2	Experimental and numerical study of rubber flow in the extrusion die of a weather strip	Under Minor revision	J. of Chemical Engineering of Japan	17-Oct-2018